Petrographic and geochemical characterisation of a layered garnetite-pyroxenite xenolith and of garnet in the Breaksea Orthogneiss, Fiordland New Zealand

by Daniel Miescher

Geoscience research project GEOS 899
Presented to the Department of Earth and Planetary Science
In partial fulfilment of the requirements for the degree of
Master of Geoscience

Macquarie University, Sydney

June, 2010

To Petra, Samuel, Delia and Adrian

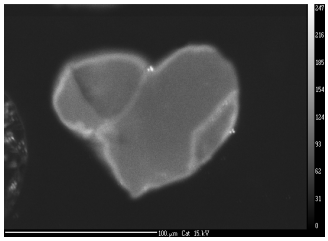

Acknowledgments

Several people have contributed to this work by supporting me technically and by sharing their professional knowledge and skills with me. I thank the two rock preparation technicians Steve Craven and Manal Bebbington. Steve assisted me in the extensive process of zircon analysing from separating zircons up to laser analyses. He always was happy to discuss any matter with me and to give me a hand whenever I was in need of anything. Manal from the rock preparation laboratory helped me in producing polished thin sections. All technical procedures of zircon separation would have been futile without the experience of Dr. Elena Belousova who showed me how to recognize the tiny mineral grains under the binocular and how to finally pick them. Furthermore I thank Dr. Norman Pearson who gave me access to the equipment of the Australian National Key Centre for Geochemical Evolution and Metallogeny of Continents (GEMOC) and who contributed to this work with his valuable critical comments in several discussions. Thanks to Dr. Kevin Grant who introduced me and assisted me in the use of the EMP and to Rosanna Murphy who was of great help with the ICP-MS analyses of U/Pb and Hf**.** Furthermore my thanks go to Prof. Geoffrey Clarke from the University of Sydney and Dr. Nathan Daczko for their hospitality and company and their many explanations on the field trip to Fiordland New Zealand. My biggest gratitude deserves Dr. Nathan Daczko who as my supervisor encouraged me, challenged me and gave me direction when necessary. I'm grateful for the uncountable hours and many days that he spent with me in the field in laboratory and in his office to work out and discuss the questions that came up along the track. I thank him for generously letting me participate in his enthusiasm and mastery.

Abstract

The Breaksea Orthogneiss (BOG) represents the deepest pluton of the Western Fiordland Orthogneiss (WFO) suite. It has been emplaced and recrystallized at P-T conditions around 1.8GPa and 850°C and shows structural and compositional properties characteristic for the transition zone of granulite and eclogite facies. Extensive parts of the BOG are composed of plagioclase, garnet and omphacite.

This study presents an investigation of one xenolith in BOG which is a layered garnetite-pyroxenite and the examination of garnet in different textural settings in the surrounding host rock, which is an omphacite-granulite. Polished thin sections produced from samples collected on a fieldtrip in February 2010 have been examined by the petrographic microscope and by electron microprobe (EMP). The results have been compared to measurements from previous workers, which also include trace element data. For reasons of comparison a data base has been produced. This contains data of comparable rocks found in the literature and includes a selection of related literature. It is added on a CD to this work.

Three texturally different kinds of garnet have been recognized. Geochemical and petrographic properties indicate that two of them may be metamorphic. One cannot definitely be assigned to either an igneous or metamorphic process but from the textural arrangement an igneous origin is conceivable. From the tectonic, petrographic and geochemical context it seems also likely that the layered garnetite-pyroxenite is igneous and cognate. But evidence for that remains ambiguous. Based on these analyses an interpretation of the origin of different garnets in the omphacite-granulite and a hypothetical model for the origin of the layered garnetite-pyroxenite xenolith is presented.

In addition to that, density measurements of diverse rock types of the BOG which were collected on a fieldtrip in February 2009 have been carried out. Furthermore, zircon mineral grains have been separated from one sample of omphacite-granulite and U-Pb as well as Hf-isotope analyses have been made by inductively coupled plasma mass spectrometry (ICP-MS) in order to date the host rock. The achieved Pb206/U238 age of 116 Ma might be too young and probably results from Pb-loss and metamorphic neo-crystallisation of zircon.

Table of contents

Acknowledgments 3

Abstract 4

1. Introduction 7

2. Geological setting 8

2.1 Regional geological history – from Gondwana margin to New Zealand 8

2.2 Regional geology – The Median Batholith 9

2.3 The Western Fiordland Orthogneiss and the Breaksea Orthogneiss 10

2.3.1 Tectonic relation 10

2.3.2 Petrographic overview of the Breaksea Orthogneiss 13

3. Garnet and garnetite-pyroxenite in the Breaksea Orthogneiss 16

3.1 Garnet in omphacite granulite 17

3.1.1 Field observations 17

3.1.2 Garnet in omphacite-granulite in thin section 20

3.2 Xenolith of layered garnetite-pyroxenite 25

3.2.1 Field observations 25

3.2.2 Garnetite-pyroxenite in thin section 28

3.3 Geochemistry 34

3.3.1 Major element whole rock composition 34

3.3.2 Major elements mineral composition 34

3.3.3 Trace elements 41

3.3.4 Liquids recalculated by partition coefficients 45

4. Determining the age of the Breaksea Orthogneiss 47

4.1 Zircon separation 47

4.2 U/Pb analyses 48

4.3 Hf analyses 49

5. Density measurements 51

6. Discussion 52

6.1 Interpretation of field observations and thin sections 52

6.1.1 Garnet in omphacite-granulite 52

6.1.2 Xenolith of layered garnetite and pyroxenite 53

6.2 Interpretation of geochemical data 54

6.2.1 Comparison with other ultramafic rocks 54

6.2.2 Mineral major element composition 57

6.2.3 Rare earth elements in garnet 59

6.2.4 Recalculated Liquid 60

6.3 Interpretation of Pb/U and Hf data 61

6.4 Hypothesis on the origin of different garnets in the BOG and of the xenolith of layered pyroxenite-garnetite 62

6.4.1 Garnet in omphacite-granulite 63

6.4.2 Layered garnetite-pyroxenite 64

7. Conclusion 68

References 69

Appendix

Appendix 1 – EMP data garnet 72

Appendix 2 – EMP data clinopyroxene 83

Appendix 3 – rock densities of BOG 89

Appendix 4 – Zircon pictures 91

Appendix 5 – U/Pb data 94

Appendix 6 – Hf data 98

Appendix 7 - Zircon composition 99

Appendix 8 – CIPW norms of Snake River basalt and BOG 100

Appendix 9 – List of abbreviations 101

List of figures and tables 102

Statement of originality 104

1. Introduction

The lowest parts of the continental crust and its transition to the mantle are exhumed at only a few places on Earth. They appear either as complete magmatic sequence like the Himalayan Kohistan sequence, or as ultramafic xenoliths in plutonic or volcanic rocks like in South African Kimberlites, to name two end members of the spectrum.

The Breaksea Orthogneiss (BOG) in western Fiordland of South Island, New Zealand has been recognized as one of these rare occurrences. It can be described as a meta-diorite to meta-gabbro which has been emplaced at a depth of at least 60 km and has been crystallized under P-T conditions at the transition of granulite and eclogite facies. Thus it represents the deepest and probably one of the younger parts of the Western Fiordland Orthogneiss (WFO). Therefore this study can help us to extend our knowledge on magmatic and metamorphic processes in deep parts of an active continental margin.

More than that, the BOG is the host rock of a variety of ultramafic xenoliths. A common feature of many amongst them is a high mode of clinopyroxene and garnet. This property appears impressively in one pod of layered garnetite-pyroxenite, which is not only distinctive for its composition but also for the banded structure (Fig. 14).

This work contains a petrographic and geochemical characterisation of this layered garnetite-pyroxenite as well as a closer look at different types of garnet in the host rock, the Breaksea omphacite-granulite (omp-granulite). In addition to that, zircon from one sample of omp-granulite has been separated and analysed in order to determine a U/Pb-age.

This work shall help to create a model for the origin of the layered xenolith and to improve the knowledge about the history of the BOG. The statements in this work are based on field observations, the investigation of thin sections, geochemical data from own analyses as well as from other workers and on a comparison with data from other locations with a similar tectonic setting.

During the process of this work a data base has been created which is added on a CD in the jacket of this paper. The measurements made in this study are printed in the appendix.

2. Geological setting

2.1 Regional geological history – from Gondwana margin to New Zealand

According to Mortimer (2004) the islands of New Zealand represent a mere 10% of the submerged continent Zealandia (Fig. 1), which became separated from Gondwana during the Late Cretaceous. Before its drift to the east, present New Zealand was part of a magmatic continental margin of Andean style. This was active from the Cambrian until the Early Cretaceous and according to De Paoli et al. (2009) had a crustal thickness of more than 60 km.

Parts of the arc probably were formed in an outboard location to Gondwana's margin during the Triassic and Jurassic (247-131 Ma). In the Early Cretaceous (130-105 Ma) they got accreted to the continent (De Paoli et al., 2009).

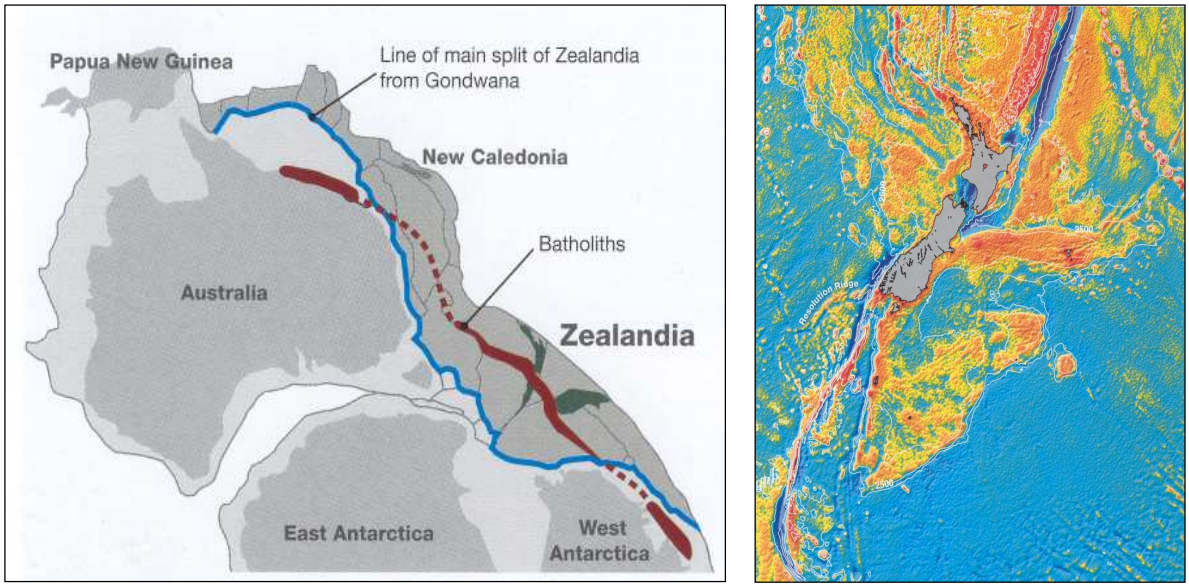

Fig. 1: The continent of Zealandia. Left: restored to its former position in Gondwana 90 Ma ago (Mortimer and Bradshaw, in Graham [chief editor], 2008). Right: Gravity anomaly map of offshore New Zealand, reds and yellows represent thick continental crust and mark the extension of present Zealandia (Wright and Wood, in Graham [chief editor], 2008).

Triggered by the collision of the Ontong-Java plateau with the subduction zone (Watton, 2009) or by subduction rollback of Gondwana margin caused from buoyant uplift of the mantle wedge (Rey and Müller, 2010), movement direction eventually changed in the Late

Cretaceous (105-83 Ma) and became divergent. Sea-floor spreading began in the Tasman Sea at 84 Ma (Clarke, 2002) and resulted in the separation of Zealandia from Gondwana and in sea floor spreading with opening of the Tasman Sea and finally in the formation of the Cenozoic Australian-Pacific plate boundary (Mortimer, 2004).

Convergent motion at the present plate boundary, which crosses the South Island and forms the Alpine Fault (see Fig. 2) led to the uplift and exhumation of intrusions of the former magmatic continental margin. In addition to these plutons, extensive parts of the South Island are built by terranes of volcanic and volcaniclastics composition which represent Palaeozoic and Mesozoic fore-arc and back-arc basins. In overview (Fig. 2) the tectonic structure of the South Island of New Zealand can be subdivided into three parts: the Western Province (two terranes) and the Eastern Province (seven terranes), separated by the intrusive zone dominated by the Median Batholith.

2.2 Regional geology – The Median Batholith

The plutonic zone of New Zealand's South Island is divided into three major batholiths, the Karamea-Paparoa, the Hohonu and the Median Batholith (Fig.2).

The Karamea-Paparoa batholith lies entirely within the Buller Terrane of the Western Province. It is mostly composed of Devonian to Carboniferous S- and I-type granites, comparable to those of the Lachlan Fold Belt in Eastern Australia.

The Hohonu Batholith results from plutonic events prior to Late Cretaceous-Cenozoic sea floor spreading and Cenozoic plate boundary deformations. It preserves the transition from subduction to extension on the Gondwana margin.

The most extensive of the three intrusive complexes is the Median Batholith. It best represents the long existing cordilleran-style Gondwana margin and is made of dozens of plutons from 1 km up to 10 km in diameter. The ages range from Devonian to Early Cretaceous (375-110 Ma), the composition is of gabbroic to granitic sub-alkaline, I-type and A-type magmatism.

Three zones within the Median Batholith can be recognized: The eastern edge with the Permian gabbroids of the Brook Street terrane, the central zone of diorites ranging in age

from Triassic to Early Cretaceous and the western edge composed of adakitic granitoids from the Early Cretaceous. The latter includes the youngest suite of the Median Batholith, called the Separation Point Suite.

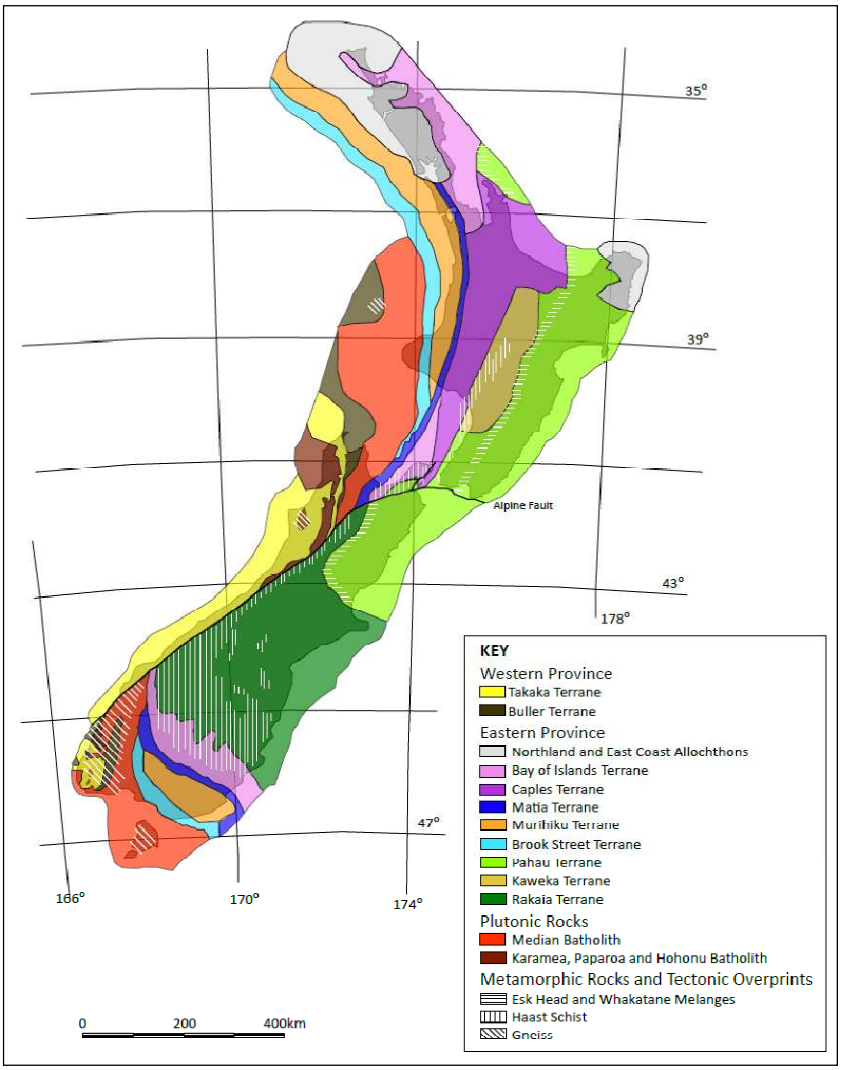

Fig. 2: Tectonic map of South Island New Zealand (Mortimer, 2004)

2.3 The Western Fiordland Orthogneiss and the Breaksea Orthogneiss

2.3.1 Tectonic relation

The Median Batholith is dominated by the Western Fiordland Orthogneiss (WFO). Investigations by the New Zealand geologic mapping program (QMAP) have shown that the WFO is made of seven separate plutons (Fig.3). These are: the Worsley Pluton, the McKerr Intrusives, the Lake Wade Diorite, the Misty Pluton, the Malaspina Pluton, the Breaksea

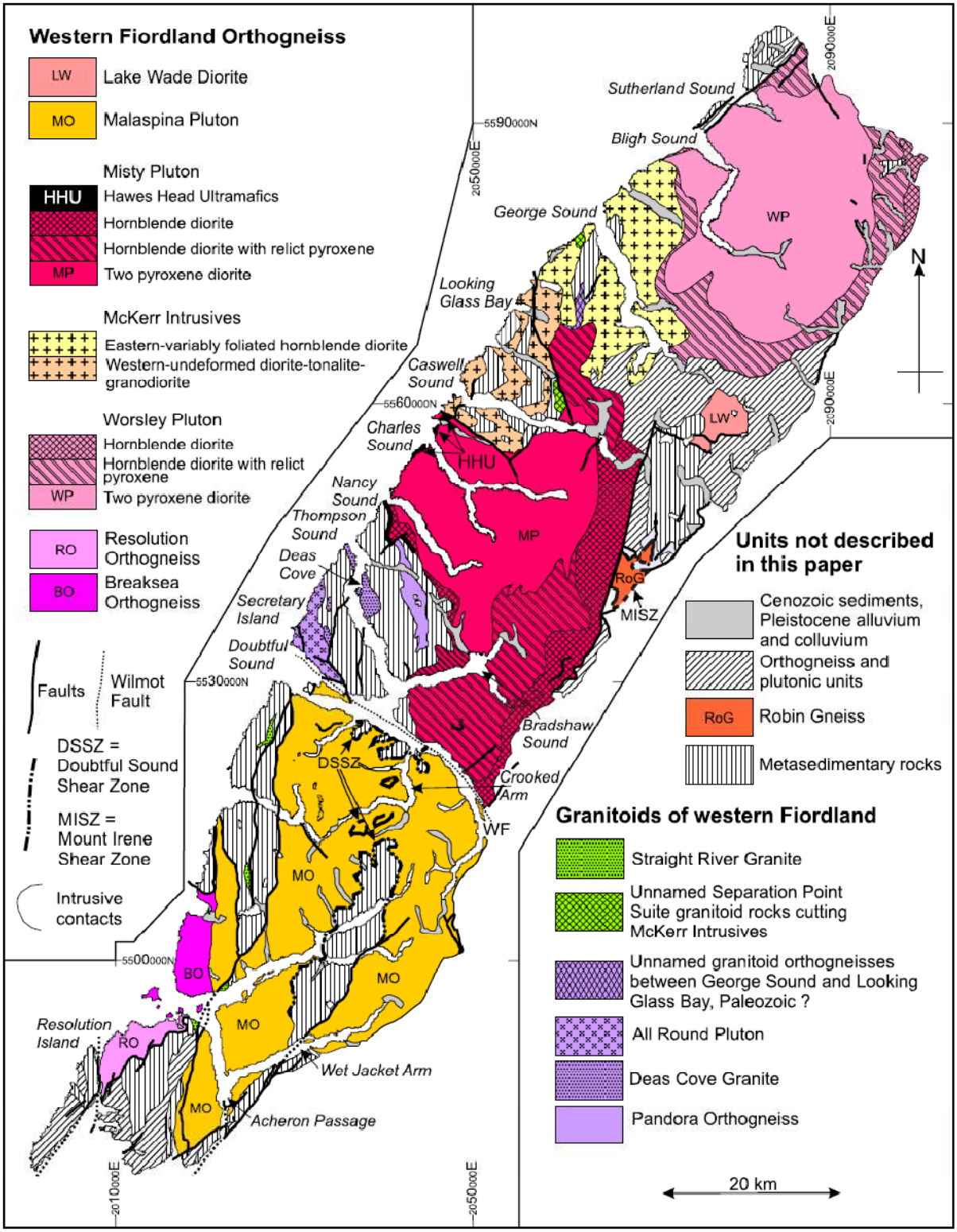

Fig. 3: Geologic map of the Western Fiordland Orthogneiss. (Alibone et al. 2009)

Orthogneiss and the Resolution Orthogneiss. The latter two are amongst the youngest intrusions within the magmatic arc (Allibone et al., 2009).

The petrologic compositions of the WFO range from felsic diorites to monzodiorites and minor gabbros. Together with adjacent units they were emplaced or buried at depths of between 30 and 70 km (see Fig. 4, for the Breaksea Orthogneiss). Consequently they have been variably recrystallized to eclogite, omphacite-granulite, garnet-granulite, two-pyroxene granulite, and hornblende granulite as well as hornblende amphibolite facies which represent different P-T conditions during metamorphism of each separate body (Allibone et al, 2009).

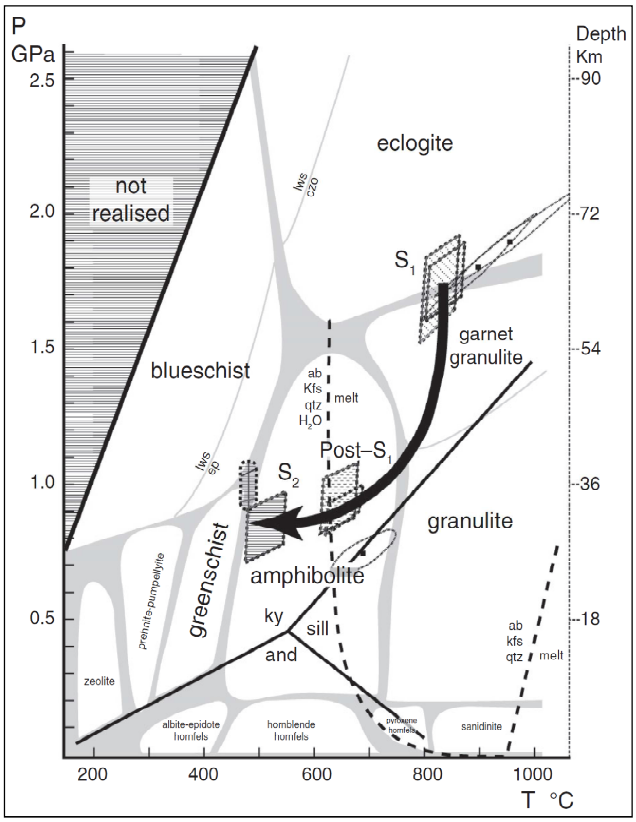

Fig. 4: P-T path of the Breaksea Orthogneiss (De Paoli et al. 2009)

Exposures of the WFO therefore provide an opportunity to study the nature of magmatic processes such as partial melting, fluid flow and crystallization as well as deformation near the base of a Phanaerozoic continental margin arc.

Within that context the BOG represents “an unusual natural example of the eclogite-granulite transition”, which is valuable since “natural examples that record the high pressure granulite to eclogite transition are rare”, as De Paoli et al (2009) emphasize.

According to geographic descriptions by De Paoli et al. (2009) and Alibone et al. (2009) the BOG covers the area around the mouth of Breaksea Sound, Breaksea Island, Entry and Hawea Islands. Several of the Gilbert Islands, small parts of Resolution Island and mountains to the north as far as Coal River are underlain by coarse grained layered orthogneiss with garnet-granulite and eclogite facies assemblages. In the words of Allibone et al. (2009): "These rocks are referred to as Breaksea Orthogneiss and Breaksea Island is nominated as the reference area, with the best exposures on the south west shore."

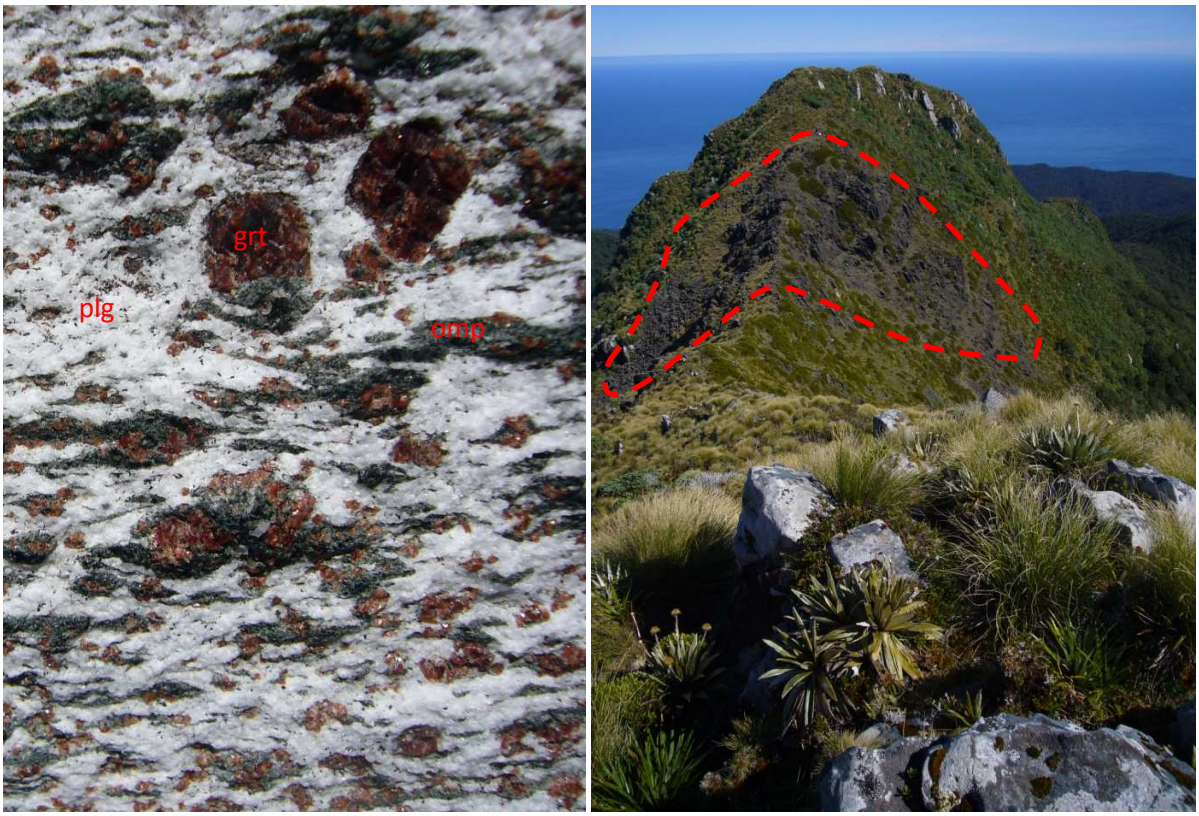

Fig. 5: a) Typical outcrop of omphacite granulite (base of picture 4cm). b) Ultramafic pod within the omp-granulite.

2.3.2 Petrographic overview of the Breaksea Orthogneiss

Detailed petrographic descriptions of all rock types within the BOG, carried out by previous workers such as De Paoli et al. (2009), Alibone et al. (2009) and Watton (2009) do not need to be repeated here. However, an overview of the major and most important compositional properties is given in Table 1. It shows that in large parts of the BOG clinopyroxene is omphacite. This jadeite bearing clinopyroxene normally occurs in eclogites at P-T conditions

Rock type	Major minerals				accessory
	Pyroxene	**Garnet** (core-rim)	**Plagioclase** (core-rim)	**others**	**minerals**
Omphacite granulite	Omp (25-45%)	Alm_{43-46} Pyr_{38-28} Grs_{18-23} Sps_{1-2} (4-25%)	Ab_{75-82} An_{25-16} Or_{2-2} (50%)	___	rutile, hematite, apatite, kyanite, (symplectites : paragasite, biotite, diopside, enstatite, epidote)
Two-pyroxene-granulite	opx, omp	____	Ab_{75-82} An_{25-16} Or_{2-2}	___	K-feldspar, rutile, kyanite, quartz, apatite plagioclase inclusions in garnet and as symplectites
Opx-eclogite component (m-scale)	Opx, omp	$Alm_{(44-52)-(45-55)}$ $Pyr_{(33-43)-(30-41)}$ $Grs_{(5-7)-(6-7)}$ $And_{(5-8)-(5)}$	$Ab_{85\ (core)}$ $An_{14\ (core)}$ $Or_{1\ (core)}$	___	Ilmenite, rutile, apatite
Eclogite	Omp (45-50%)	Alm_{38-44} Pyr_{43-31} Grs_{20-24} Sps_{1-1} (45-50%)	___	___	rutile (symplectites : diopside, paragasite, biotite, epidote, ilmenite) plg inclusions in grt
Garnetite-layer	Diopside (15-20%)	Alm_{38-44} Pyr_{43-31} Grs_{20-24} Sps_{1-1} (80-85%)	___	___	rutile, (symplectites: pargasite, biotite), plagioclase inclusions in garnet
Pyroxenite-layer	Diopside (95%)	Alm_{38-45} Pyr_{38-31} Grs_{18-24} Sps_{1-2} (5%)	___	___	rutile, (symplectites: pargasite, biotite)
Hornblende peridotite	Diopside (10-15%) Enstatite (5%)	Alm_{38-42} Pyr_{44-40} Grs_{16-16} Sps_{2-2}	___	Olivine (35%) Pargasite (40%)	ilmanite, spinel, (symplectites: enststite, ilmenite, pargasite, diopside, enstatite)

Tab. 1: Overview of compositions and basic mineral chemistry data of different lithologies of BOG, after data from Watton, (2009) and De Paoli et al. (2009).

where plagioclase is unstable. Because of its unusual coexistence with plagioclase in the granulite the rock has been called an omphacite bearing granulite or simply an omphacite-granulite by other workers such as De Paoli et al. (2009) and Watton (2009).

The major minerals in the omp-granulite (outcrop see Fig. 5a) are plagioclase, omphacite and garnet (modes and compositions see Tab. 1). Omphacite and plagioclase form xenoblastic crystals of 0.1-0.5mm in size. Both also occur as inclusions in garnet.

Garnet can be found in diverse structural settings: in equi-granular clusters with omphacite or forming replacement structures in coronae between omphacite and plagioclase or as idioblastic large grains lined up along plagioclase rich veins (see Chapters 3.1 and 3.2). Symplectites of pargasite (0-10%) and minor biotite document alteration during uplift and exhumation (Watton, 2009). Accessory plagioclase, orthopyroxene, diopside, hornblende, rutile and ilmenite have been described by De Paoli et al. (2009) as symplectites and as inclusions stemming from S_2 deformation (see Fig. 4 and Tab. 1).

Ultramafic xenoliths occur as small pods of centimetre to metre size (Fig. 8c) and as large units encompassing tens of metres (e.g. the olivine-rich pyroxenite in Fig. 5b). The overview of the minerals in common xenoliths within the BOG (Tab. 1) shows how much these can vary in composition. They occur as peridotite, eclogite, garnetite and pyroxenite, with or without considerable amounts of hornblende. But according to P-T estimates by De Paoli et al. (2009), all of them share the same retrogressive metamorphic path with the host rock, the omp-granulite.

3. Garnets and garnetite-pyroxenite in the Breaksea Orthogneiss

The area shown in Fig. 6, mostly consists of omp-granulite which hosts xenoliths of different size, texture and composition. An additional property of the BOG in this area is the variety of modes of the main minerals omphacite, garnet, plagioclase and orthopyroxene as well as the appearance of garnet in diverse textural settings. This Chapter contains petrographic and geochemical descriptions of garnet in the host rock and of one ultramafic xenolith of layered garnetite and pyroxenite.

Fig. 6: Field aspect of the layered xenolith. The boundary of the layered garnetite-pyroxenite xenolith (Samples BS1010A-F) within the omp-granulite is marked by the dashed red line. Outcrops of omp-granulite are indicated by a green arrow. Modified picture from Watton (2009).

3.1 Garnet in omphacite-granulite

3.1.1 Field observations

In outcrop garnet in omp-granulite occurs in the following three textural settings (Fig. 7): Outstanding bigger garnet mineral grains of 3-4mm in diameter are lined up along plagioclase rich vein-like lines. The boundaries of these vein structures with the surrounding omp-granulite are gradational. Garnet minerals in the surrounding rock are smaller and in many cases assembled with omphacite. These assemblages occur in two different patterns with garnet either forming coronae around omphacite grains or in equi-granular clusters of equal mode, order and structure with omphacite.

Furthermore there may be a compositional layering (blue dotted line, Fig. 7) which runs oblique to the foliation of the rock. This feature, already described by Watton (2009), could also be interpreted as the reaction zone (100 mm wide) of a vein which can be recognized by the chain of large garnet grains.

The mineral modes of garnet, clinopyroxene and plagioclase in omphacite-granulite, given in Tab. 1, can change considerably. Granulites with less plagioclase and more enriched in omphacite and garnet can be met in the field. Also the compositions of pyroxenes and garnet can vary. Thus the BOG shows variants containing omphacite and orthopyroxene along with garnet as well as of two-pyroxene granulite which doesn't bear any garnet at all (see Fig. 8).

Field observations show that ultramafic units within the granulite are not only bound to the relatively confined appearance of xenoliths. Ultramafic rocks can also form layers within the omp-granulite (Fig. 9) as seen on Mt. Richards at (2018500 E/5497150 S) in the New Zealand coordinate grid. The surrounding rock at this site has been recognised as typical omp-granulite and has been sampled as BS1003A. Geochemical analyses of an ultramafic layer (sample BS1003B) confirm its eclogitic composition made of garnet and omphacite (see appendix-2). The structure of this rock is different from eclogite which occurs as non-layered and non-foliated xenoliths and according to Watton (2009) are imbedded in the host rock by a podiform or lenticular shape with a width to length ratio of 1:4 (Fig. 8c). The mode shown in Tab. 1 of both garnet and omphacite in eclogite is 45% to 55%.

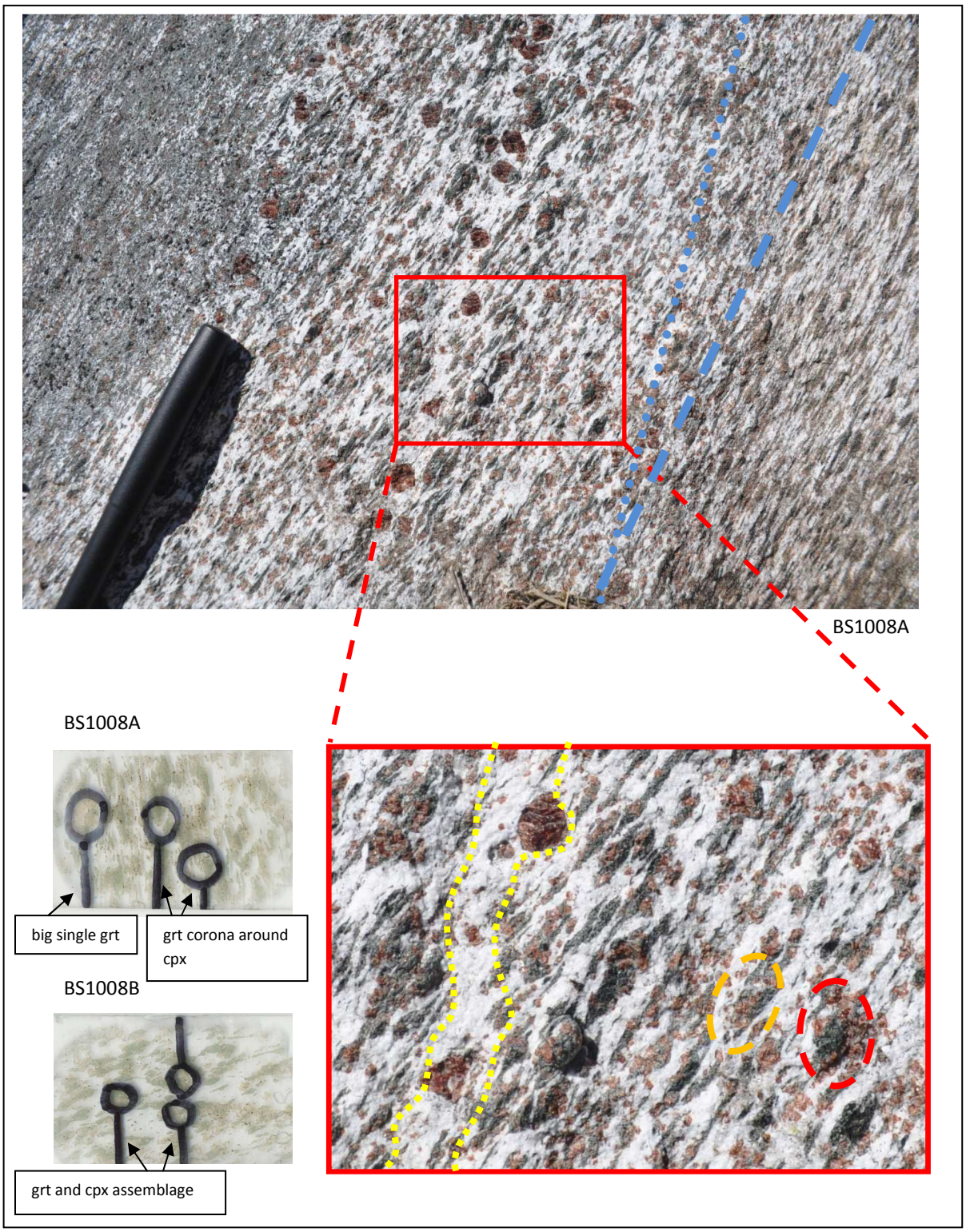

Fig. 7: Garnet in different structural settings in outcrop. Upper picture: Compositional layering and foliation (Blue dotted line: compositional layering. Blue dashed line: foliation). The close-up below shows three different textural settings of grt in omp-granulite: large grains along veins with gradational boundary (dotted yellow line), coronae of small grains around omp grains (within red dashed circle) and equi-granular clusters of grt and omp (within orange dashed circle). The thin sections include grt which has been chosen for EMP analyses.

Two-pyroxene granulite (Sample BS1009)

Omp-granulite with low mode of mafic minerals.

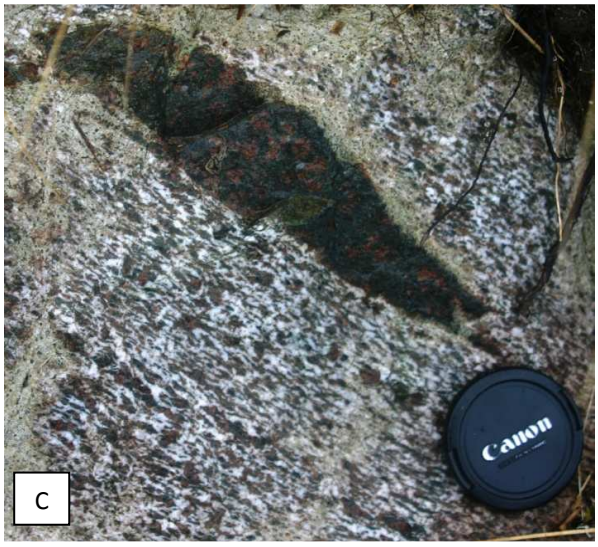

Omp-granulite with high mode of mafic minerals and a lenticular eclogite-pod.

Fig. 8: Field aspects of different modes of feldspar, pyroxene and garnet. a) Hand sample of two-pyroxene granulite, lacking garnet. b) Omp-granulite with relatively low mode of mafic minerals, c) Omp-granulite with relatively high mode of mafic minerals and containing a lenticular eclogite-pod. (Photo c) by Watton, 2009)

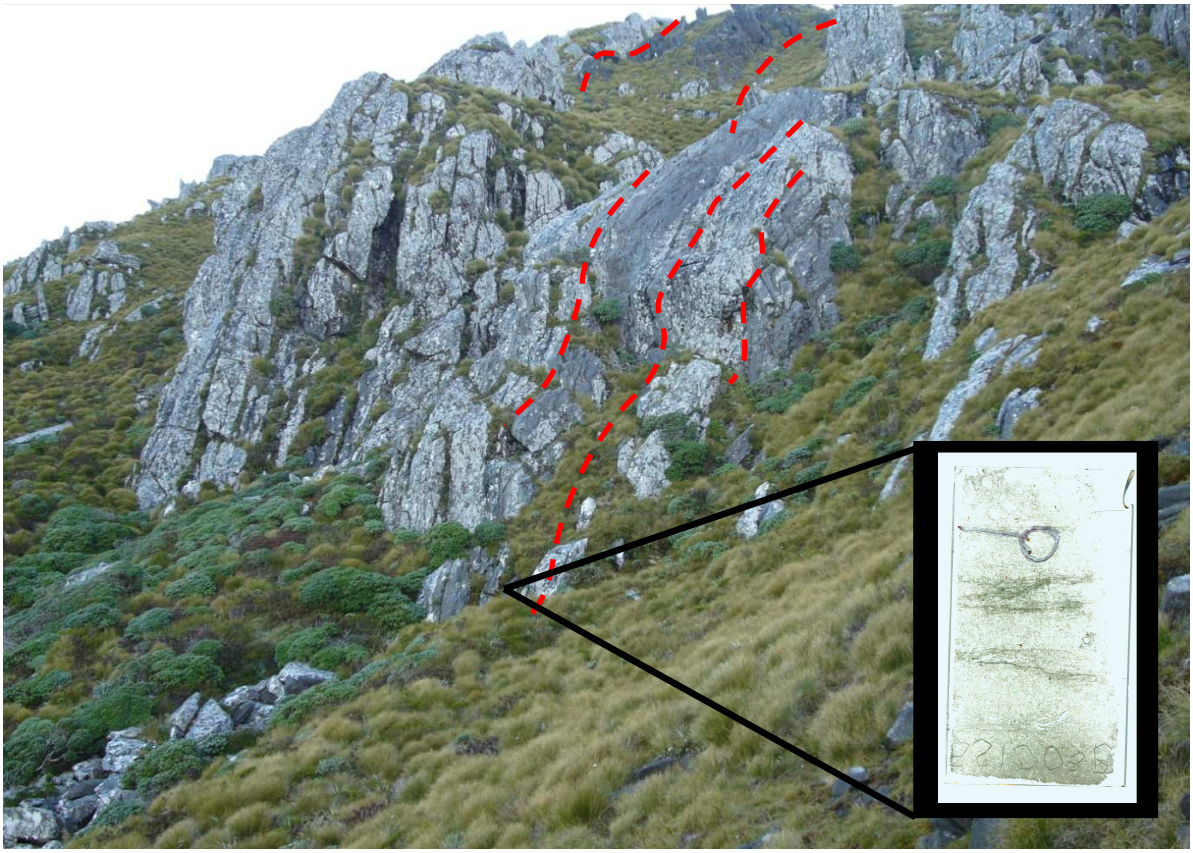

Fig. 9: Field aspect of dark ultramafic layers of eclogitic composition within omp-granulite (outcrop of sample BS1003B). For a microscopic view of the encircled area on the polished thin section see Fig. 13. The black arrow indicates the origin of the sample.

3.1.2 Garnet in omphacite-granulite in thin section

The three textural occurrences of garnet found in host rock samples BS1008A-B are displayed in microscopic view in Figs. 10-13. Fig. 10 shows idioblastic garnet arranged in a corona around an assemblage of xenoblastic omphacite grains and forming a boundary to an assemblage of xenoblastic plagioclase. Garnet grains contain vermicular quartz inclusions. A similar arrangement and comparable inclusions are neither found in the larger garnet grains along the veins (Fig. 11) nor in the equi-granular garnet-omphacite clusters in sample 1008B (Fig. 12). Fig. 11 displays a porphyroblastic garnet grain which in outcrop can be found along the vein-like structures presented in Fig. 7. The mineral grain measures 2mm in diameter and is surrounded by xenoblastic plagioclase. It is in contact with surrounding omphacite and plagioclase which both grow into the grain. Rutile exsolution follows the three crystallographic axes of garnet.

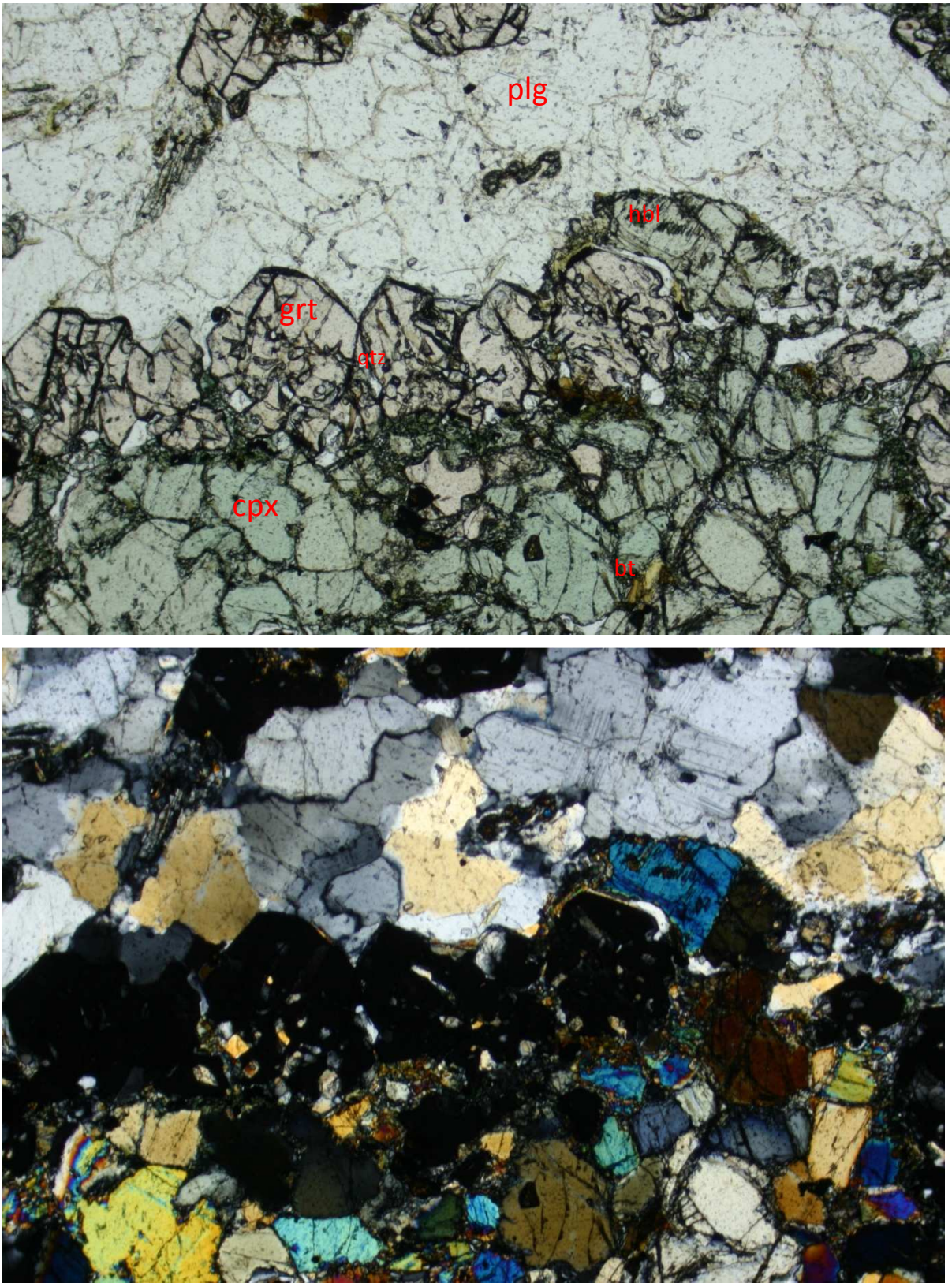

Fig. 10: A grt corona at the edge of omp. Poikiloblastic grt grains containing quartz (qtz). Upper picture plane polarized light lower picture under crossed polars. Base of picture: 2.5mm. Sample BS1008A

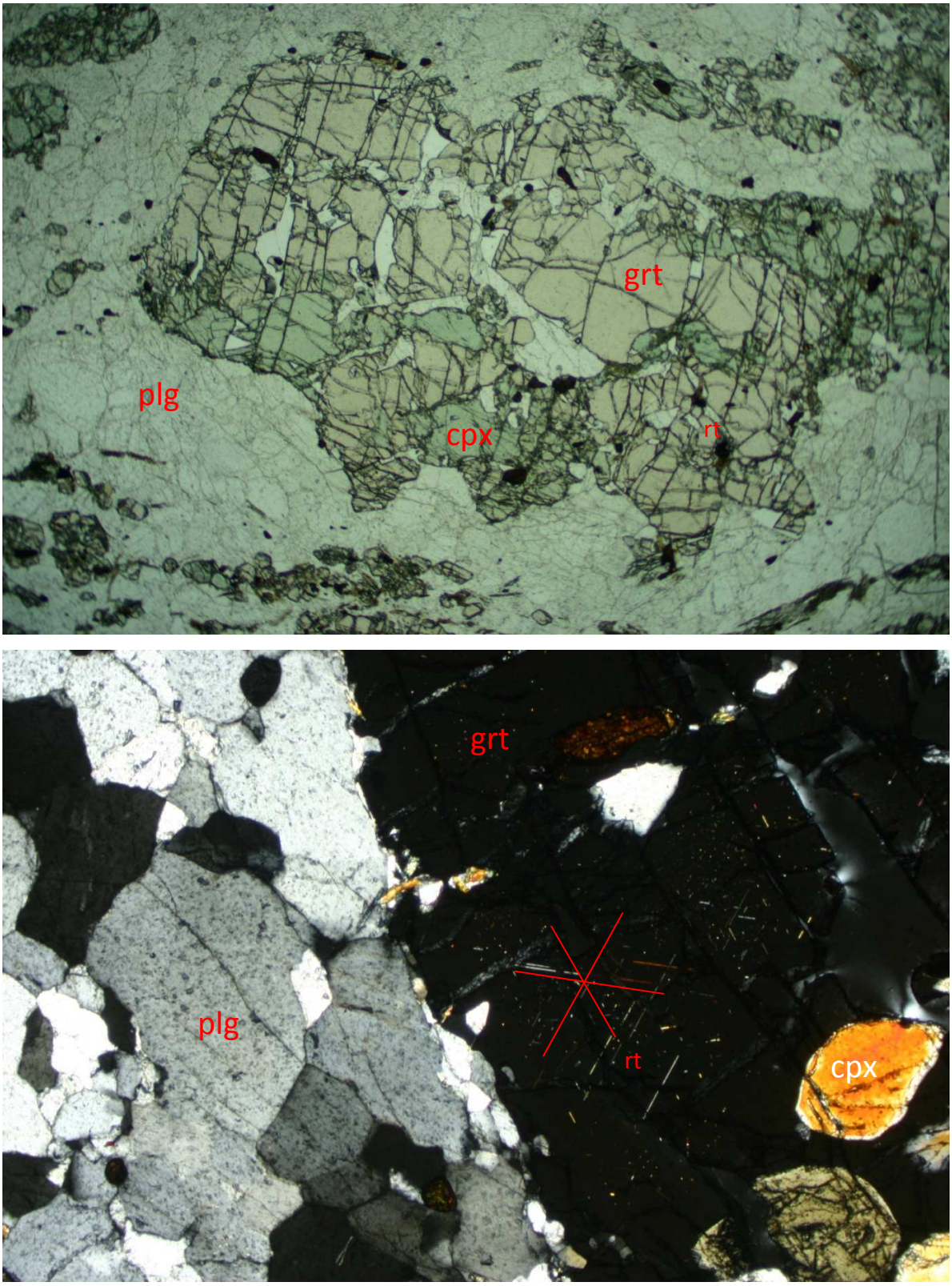

Fig. 11: A single grt grain along a feldspathic vein. Upper picture plane polarized light. Base of picture: 2.5mm. The lower picture, under crossed polars, displays a section of the grain above. Note the rutile (rt) exsolution. Base of picture 1mm. Sample BS1008A

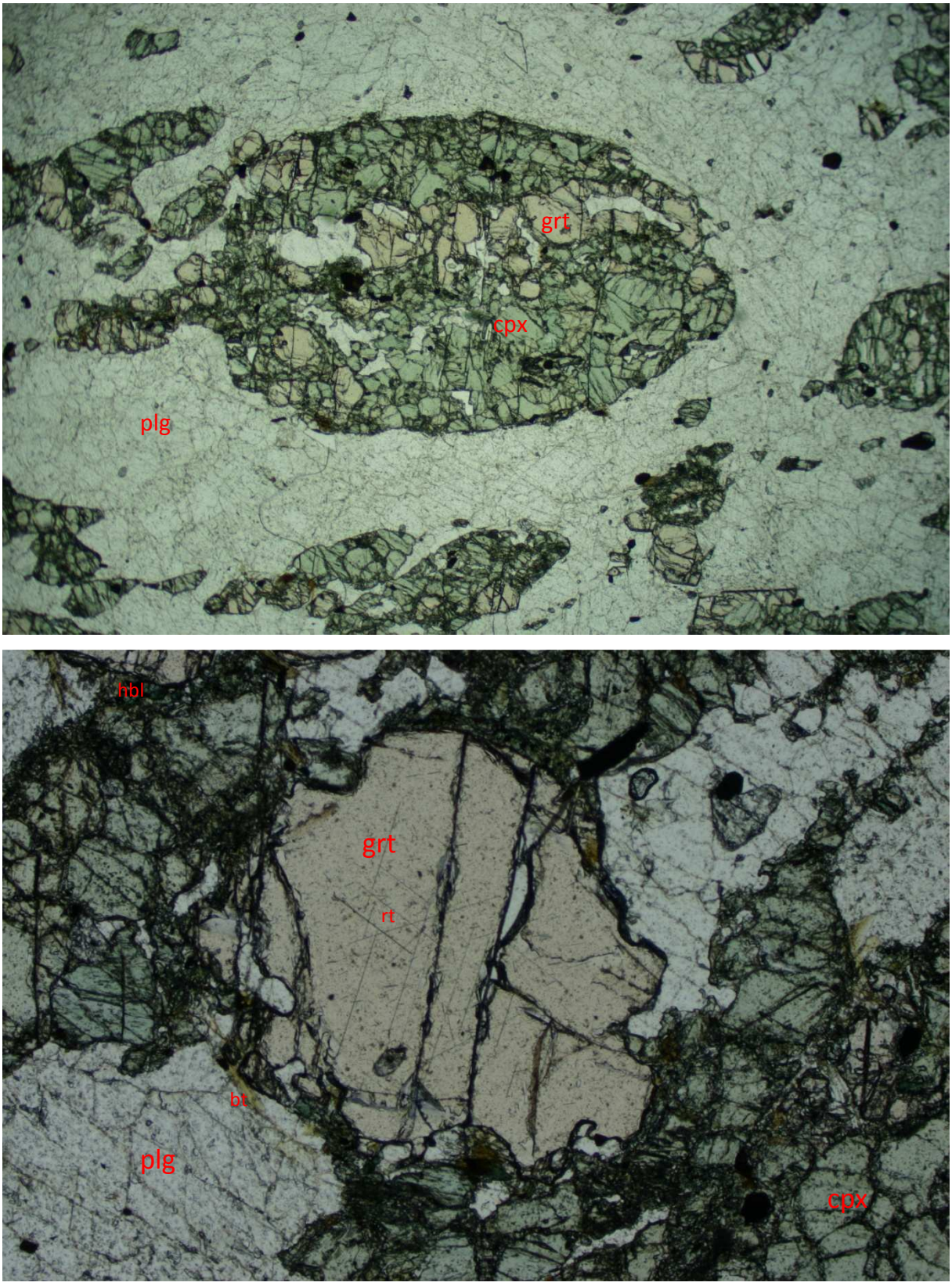

Fig. 12: Grt and omp in equi-granular cluster lacking replacement textures. Base of upper picture 2.5mm. Lower picture: close up on grt showing rutile (rt) exsolution along crystallographic axes. Base of picture: 1mm. Sample BS1008B.

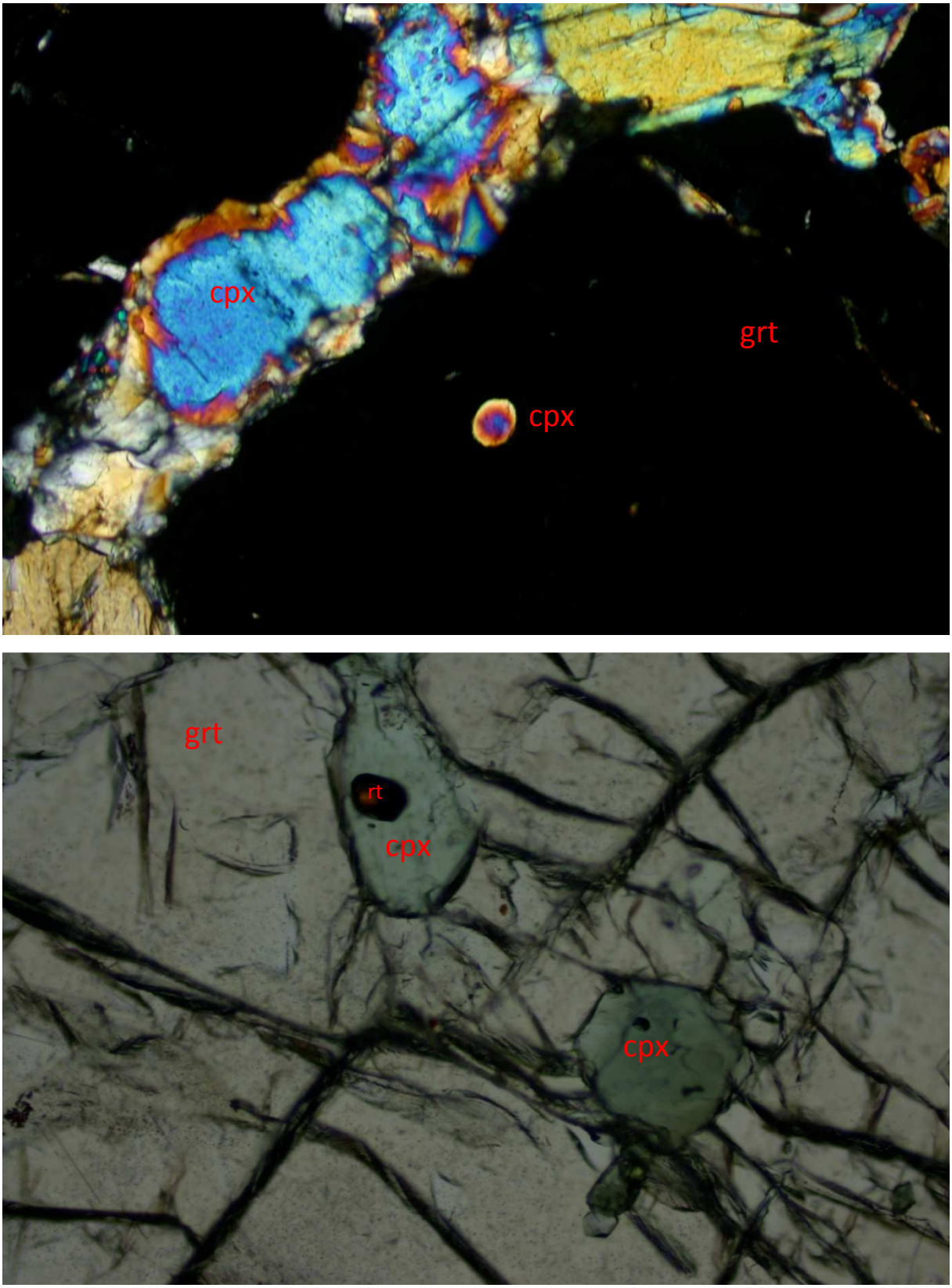

Fig. 13: Two different types of cpx inclusions in grt, rounded (upper picture, crossed polars) and euhedral (lower picture, plain polarized light). Base of both pictures 1mm. Sample BS1003A.

Fig. 12 shows an equi-granular cluster of omphacite and garnet which is embedded in a groundmass of xenoblastic plagioclase. In contrast to the garnet-omphacite assemblage in Fig. 10, both minerals are well mixed and garnet does not form a corona around omphacite nor does it show any inclusions of quartz. Similar to the porphyroblastic garnet in Fig. 11 exsolution of rutile follows the crystallographic axes of garnet.

Fig. 13 presents garnet and omphacite from an ultramafic layer within the omp-granulite (Fig. 9). Inclusions of clinopyroxene in garnet appear in two different shapes: Euhedral (see lower picture) and ovoid. The latter occur close to the boundary of garnet and omphacite. The boundary does not follow straight crystal faces but has embayments in garnet and omphacite.

3.2 Xenolith of layered garnetite-pyroxenite

3.1.2 Field observations

An ultramafic pod of layered garnetite-pyroxenite has been visited and described on a field trip in February 2009 by Watton (2009). It has been revisited and sampled for the purpose of this study in February 2010. The GPS reading gives a position of 2020300E/5499400S in the New Zealand coordinate grid. Fig. 14 gives an impression of the topographic setting and appearance of the outcrop.

The xenolith consists of alternate layers of garnetite and pyroxenite of a thickness of 2 to 30 cm. The layers run parallel and often merge into one another. Garnetite layers according to Watton (2009) and observations by this study consist of 80-85% garnet and 5-20% diopside. Pyroxenite layers consist of 95% diopside and 5% garnet. Instead of diopside the clinopyroxene can also appear as augite or as omphacite with a low jadeite component (see Fig.28). Grain sizes in both layers range between 1 and 5 mm, whereas garnets in garnetite layers tend to be bigger (up to 5 mm) than in the pyroxenite layers (1 mm). The layers show no foliation and in outcrop the pyroxenite usually shows a more prominent relief due to slightly higher resistance to weathering. A section of the layered sequence from a boulder (Fig. 15) which is regarded as representative for this lithology has been sampled (BS1010A-F) for further geochemical and microscopic investigation.

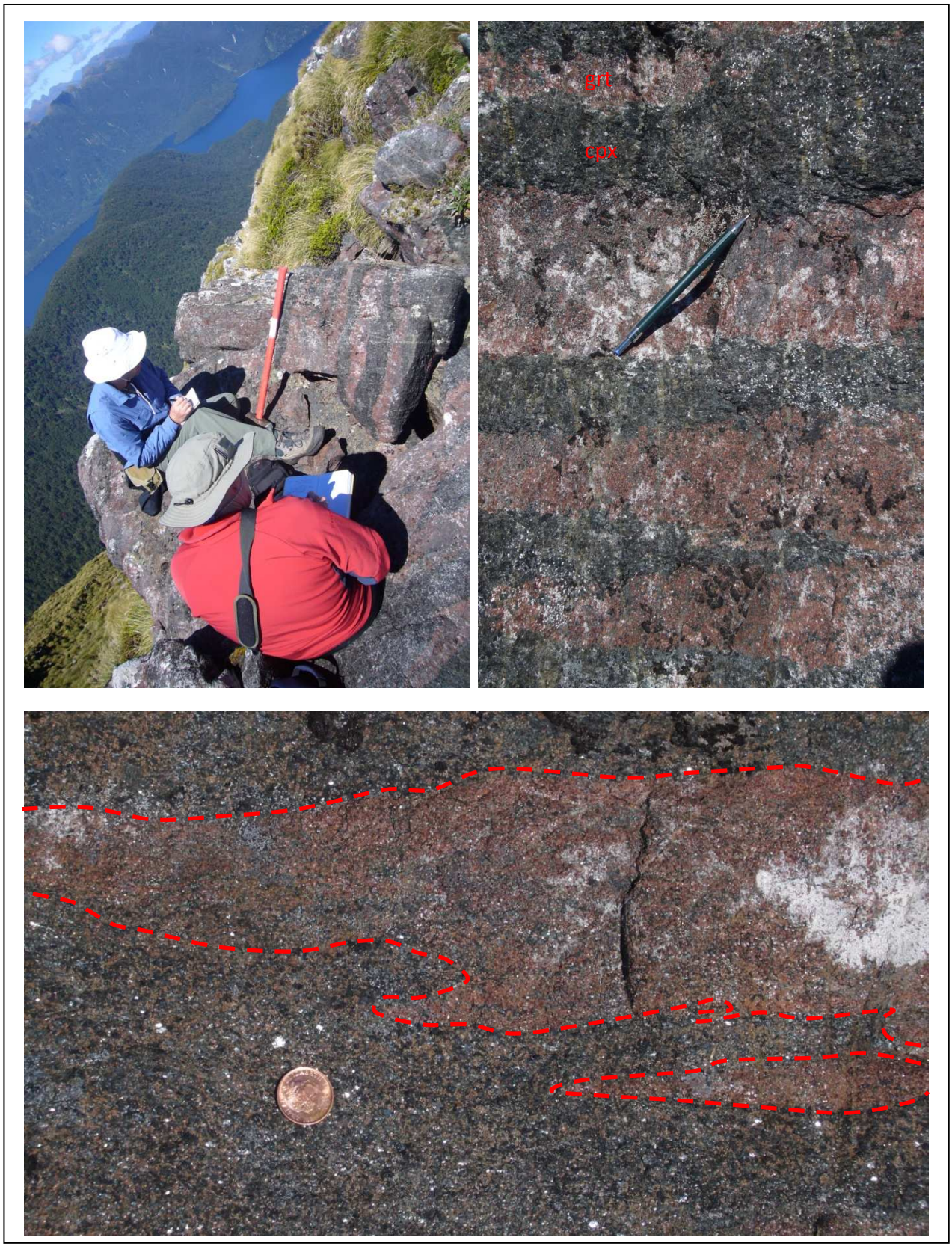

Fig. 14: Layered garnetite-pyroxenite (outcrop of samples BS1010A-F). Below: Section of layered garnetite-pyroxenite showing irregular structure of layers.

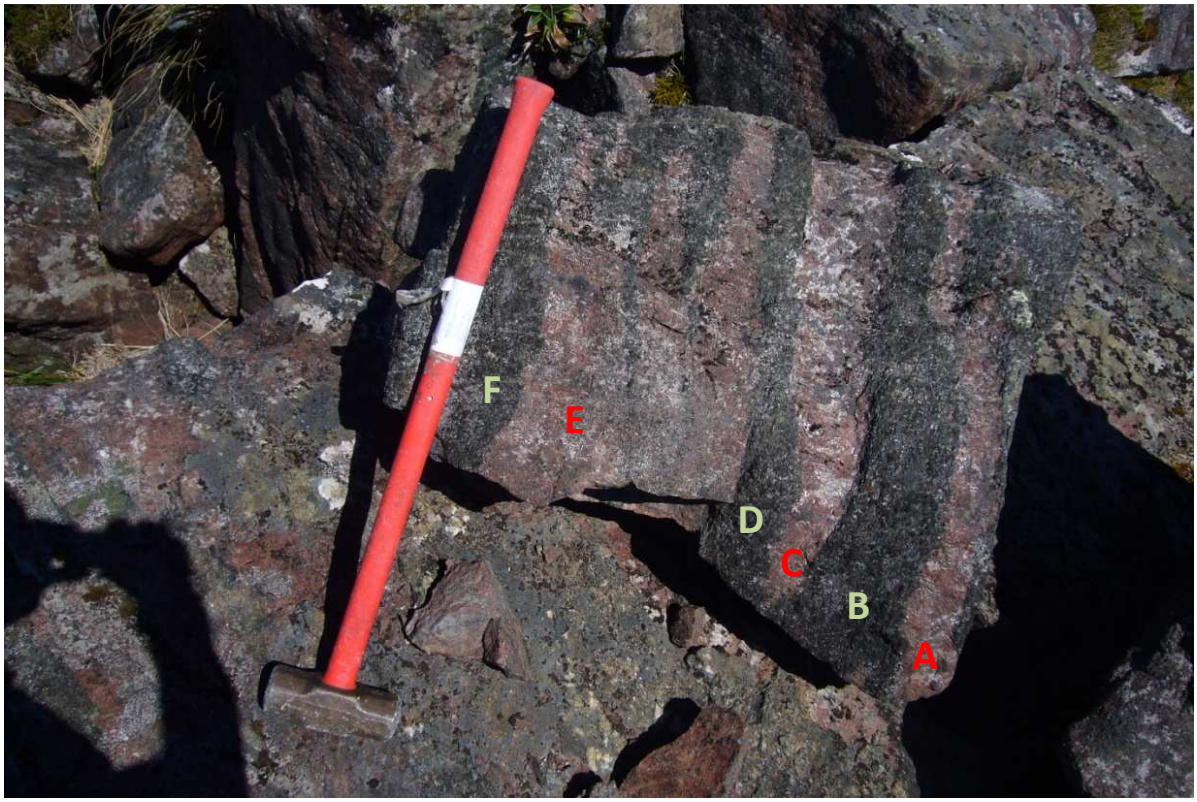

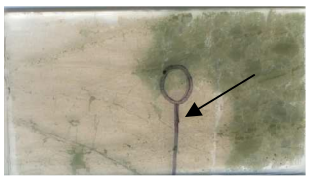

A (arrow indicates traverse, Fig. 31)

D

B

E

C

F

Fig. 15: The boulder of samples BS1010A-1010F. Letters indicate layers: garnetite (red), pyroxenite (green). Polished thin sections BS1010A-F have been analysed by EMP. Samples BS1010A and BS1010B display structures of interaction of garnetite and pyroxenite in encircled areas. These have been investigated by EMP and are shown in Figs. 16, 17 and 19. Results of the traverse (black arrow) are displayed in Fig. 31.

3.2.2 Garnetite-pyroxenite in thin section

The samples BS1010A-F stem from the layers labelled as A-F (Fig. 15). Of these samples, BS1010A (Fig. 16) allows the observation of the microstructure along the boundary between a pyroxenite layer and a garnetite layer. The relation between the two layers can be recognized by the nature of grain boundaries and inclusions and by the presence and the composition of garnet-veins.

In thin section (Fig. 16) the boundary between the two layers shows the relation of garnet and clinopyroxene (mostly diopside) by ovoid inclusions of clinopyroxene in garnet and by embayments in clinopyroxene grains along the contact with garnet.

Ovoid inclusions of clinopyroxene in garnet are also visible in single garnet grains which are within the pyroxenite layer close to the layer boundary (Fig. 17) and vice versa garnet inclusions occur in clinopyroxene (Fig. 18). It is noteworthy that in this case the garnet inclusion is euhedral opposed to the ovoid clinopyroxene inclusions in garnet. The boundaries between grains of clinopyroxene (seen in Figs. 16, 17, 19 and 20) are different from those between garnet and clinopyroxene in that only the latter show embayments and the first mostly run straight.

An additional property at the layer boundary is the presence of garnet films of significantly smaller grain size (~0.1mm) compared to the clinopyroxene grains of a size of 1-2mm. Garnet along these films also forms embayments into the surrounding clinopyroxene. Geochemical differences between garnet in films and in the layers are presented in Chapter 3.3.2 (Fig. 30).

In addition to the features described above the mentioned pictures show minerals formed during the retrogressive metamorphic history (S_2) which the xenolith shares with its host rock the omp-granulite. These are exsolutions of rutile and symplectites of amphibole and biotite.

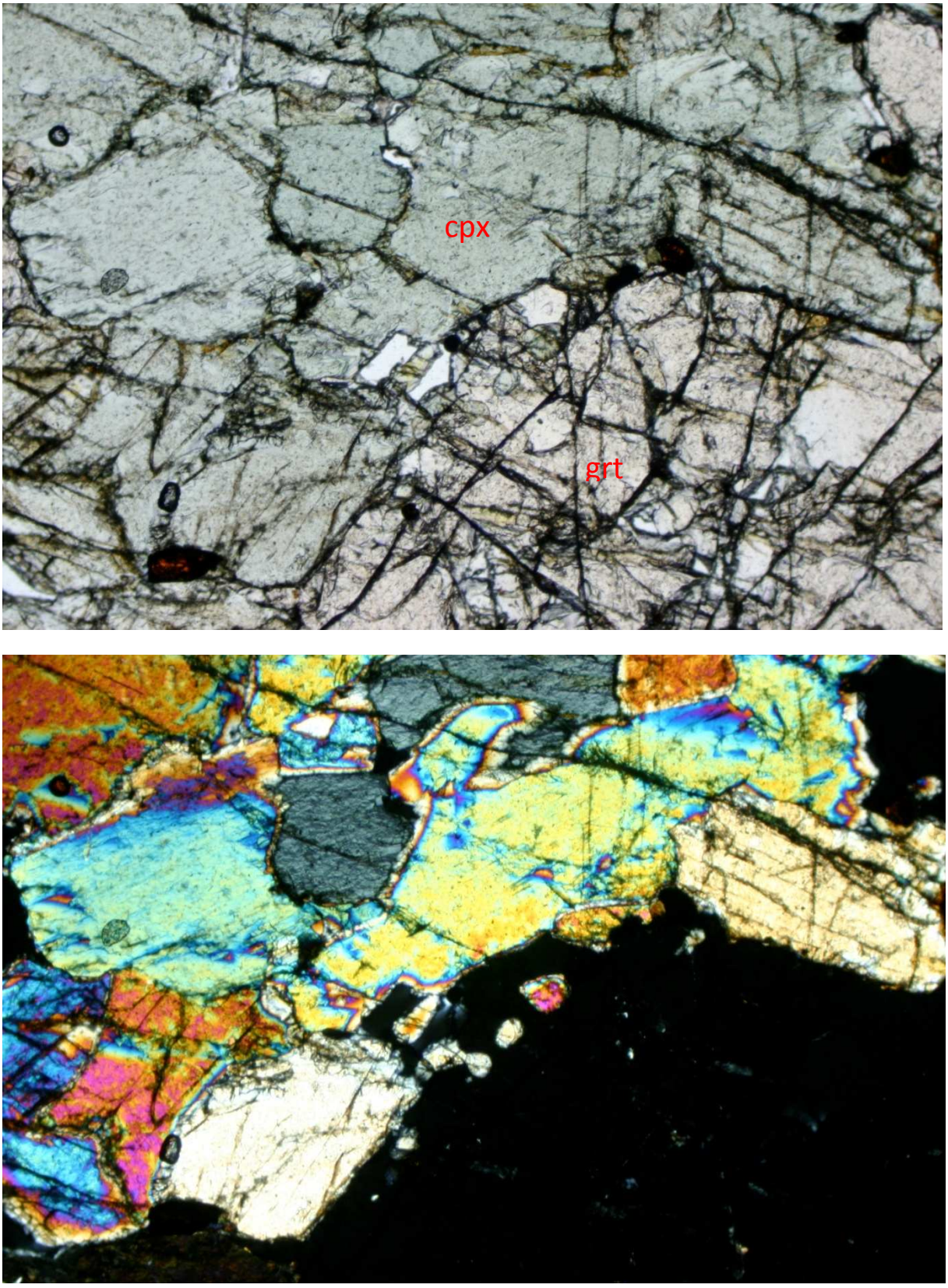

Fig. 16: Ovoid inclusions of clinopyroxene (cpx) in garnet (grt) along the boundary between a pyroxenite and a garnetite layer. Upper picture plane polarized light lower picture under crossed polars. Base of picture: 2.5mm. Sample BS1010A.

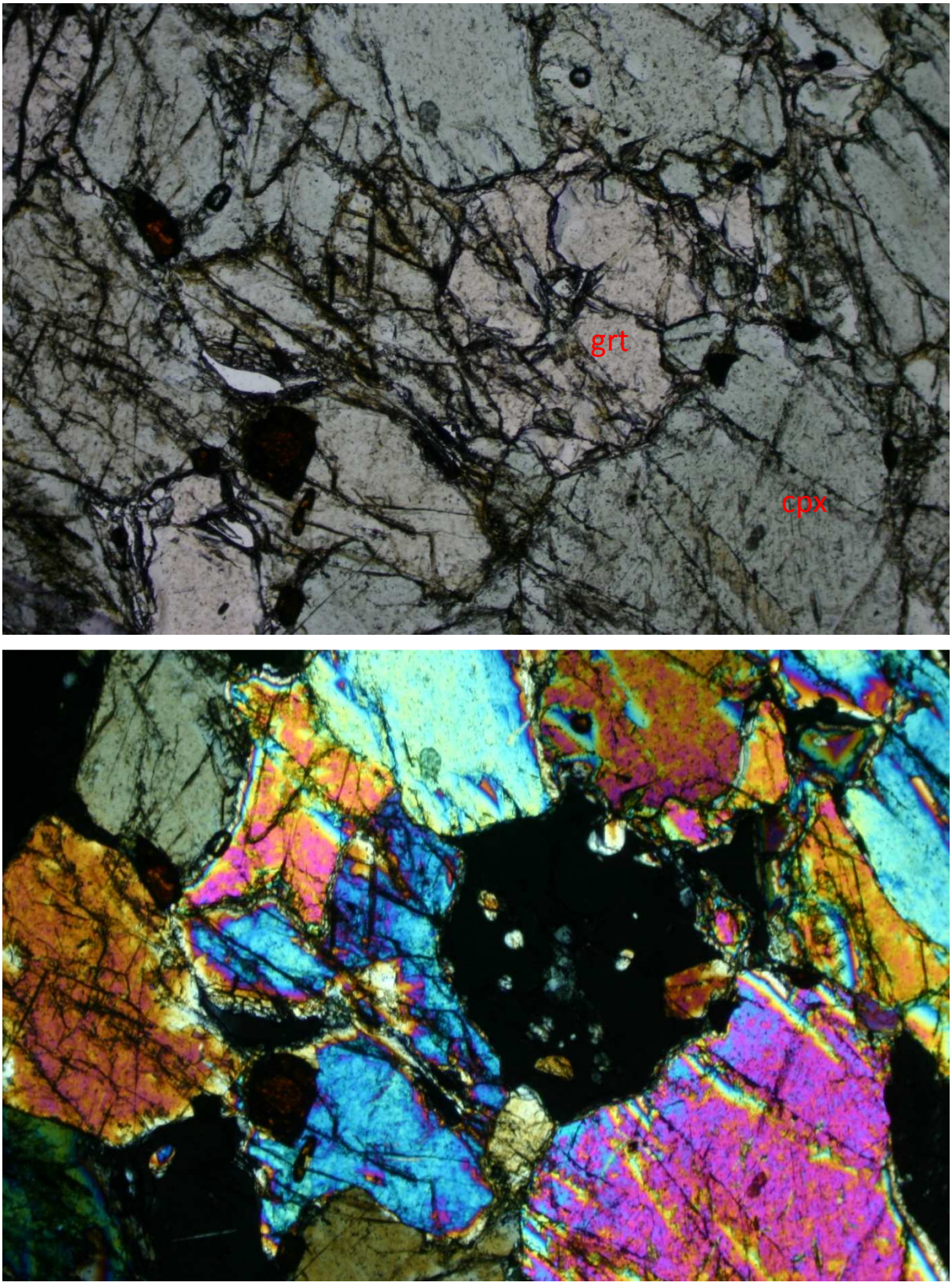

Fig. 17: Ovoid inclusions of clinopyroxene (cpx) in garnet (grt) close to the boundary between a pyroxenite and a garnetite layer. Upper picture plane polarized light lower picture under crossed polars. Base of picture: 2.5mm. Sample BS1010A.

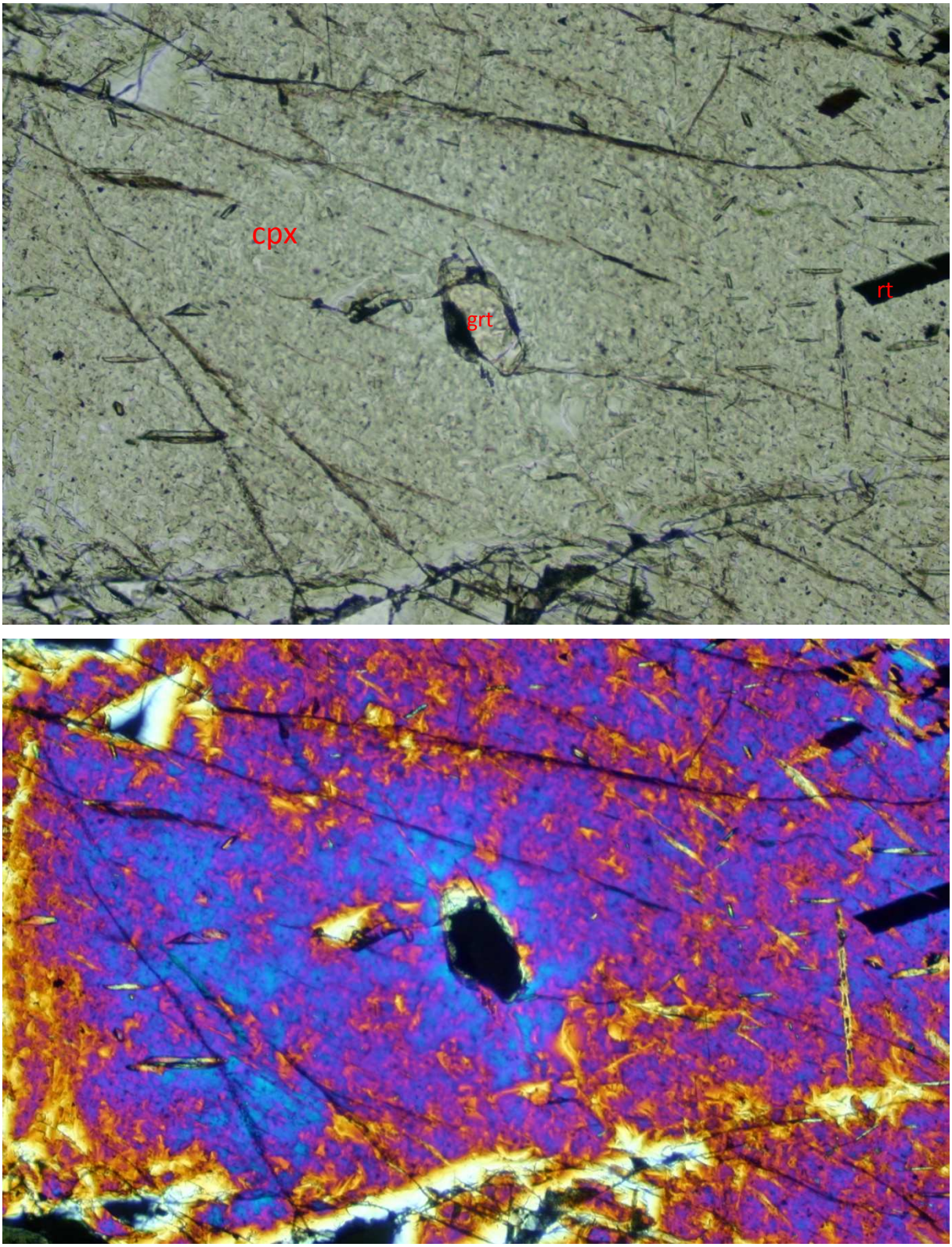

Fig. 18: A euhedral garnet (grt) inclusion in clinopyroxene (cpx) within the pyroxenite layer, close to the boundary between a pyroxenite and a garnetite layer, Sample BS1010A. Upper picture plane polarized light lower picture under crossed polars. Base of picture: 1mm.

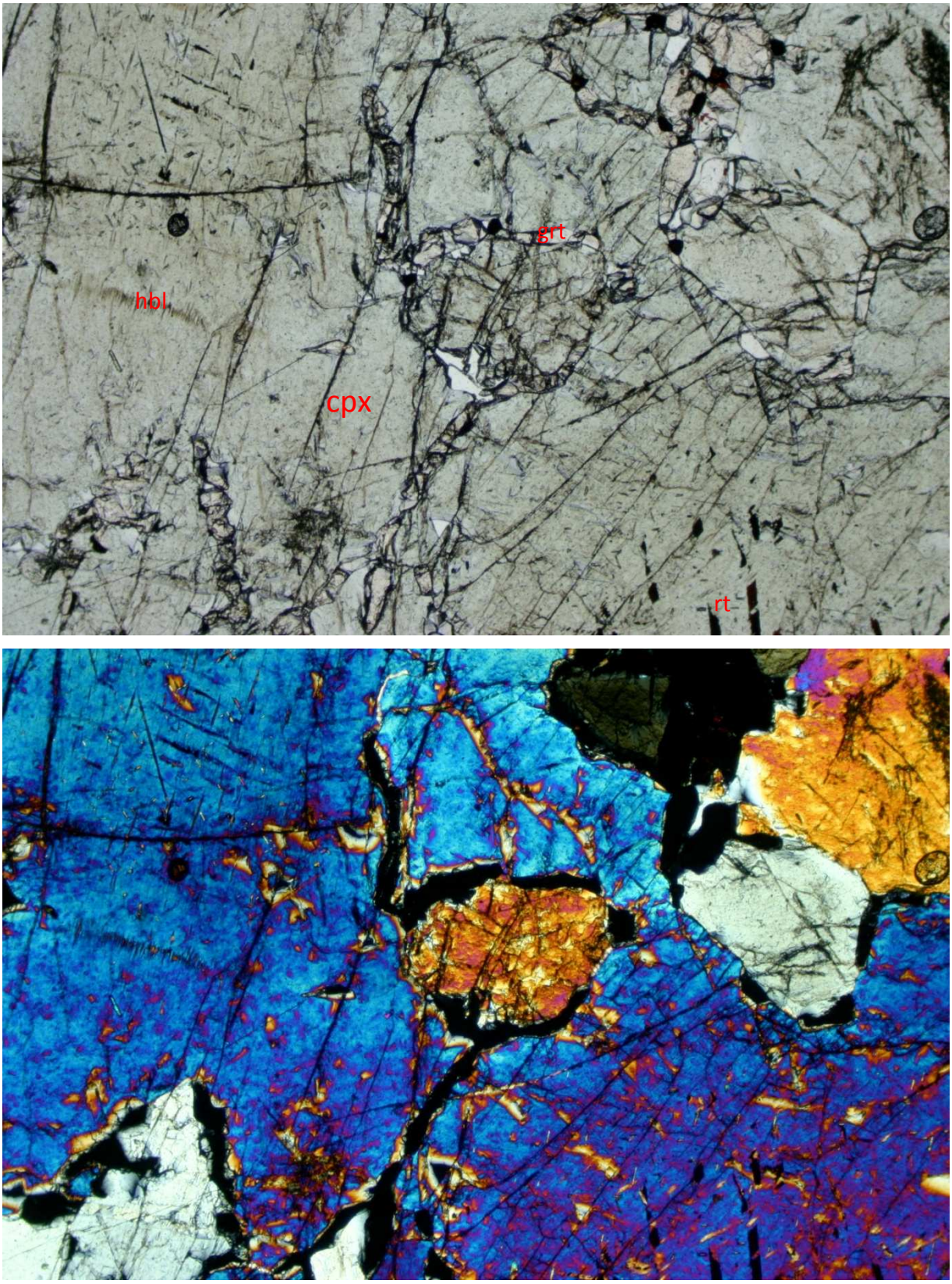

Fig. 19: Garnet (grt) films in the pyroxenite layer, Sample BS1010B. Upper picture plane polarized light, lower picture under crossed polars. Base of picture: 2.5mm.

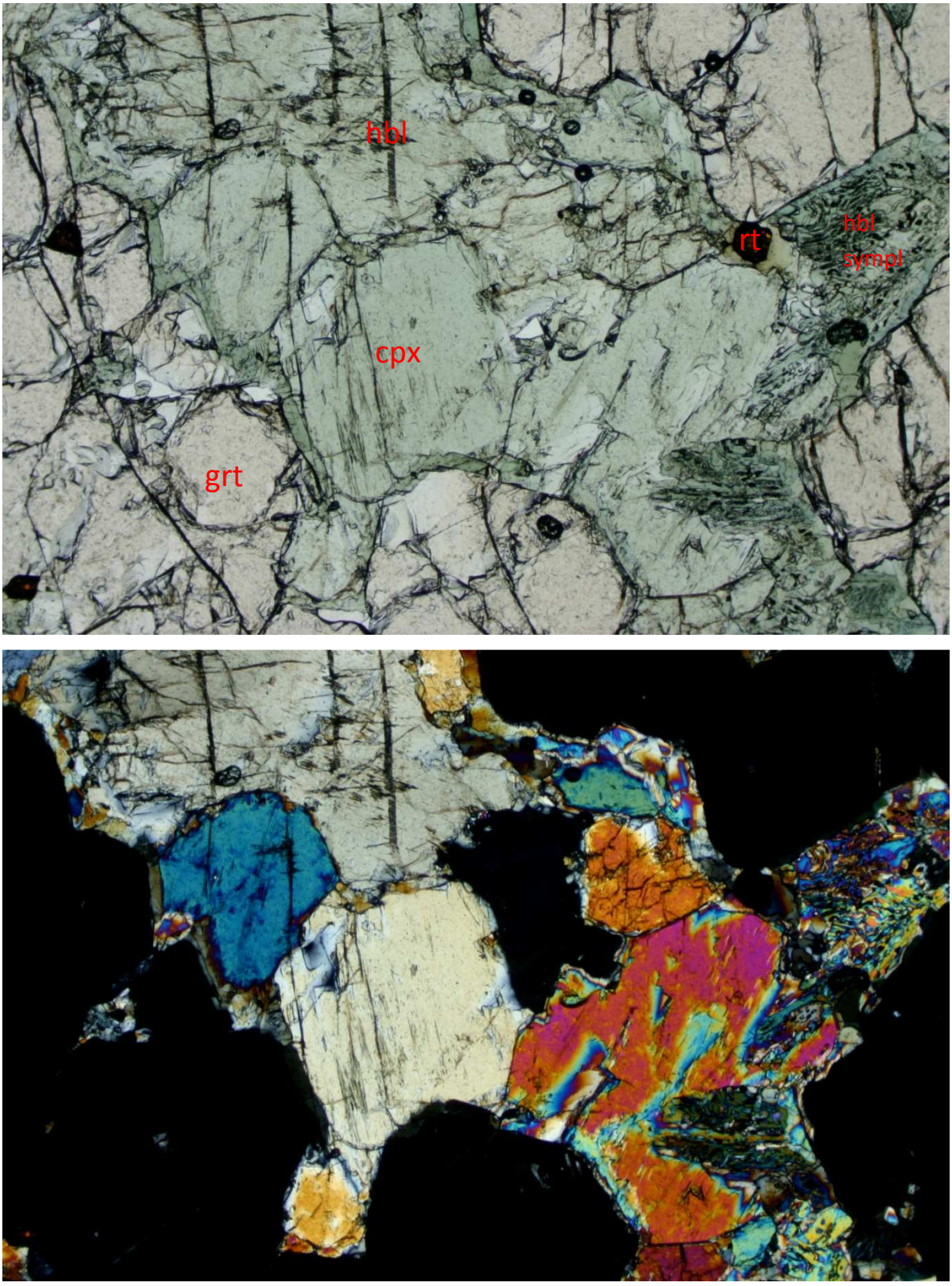

Fig. 20: A contact of garnetite and pyroxenite also containing rutile (rt) and retrogressive metamorphic hornblende-symplectites (hbl). Upper picture: plane polarized light. Lower: crossed polarized light. Base of photographs: 2.5 mm (sample BS1010F).

3.3 Geochemistry

3.3.1 Major element whole rock composition

In a TAS diagram (Fig. 21) the omp-granulite of the Breaksea Orthogneiss plots in a sequenze of increasing mafic component from meta-monzodiorite to meta-gabbro. The ultramafic xenoliths lie outside the range of a common Phanaerozoic magma.

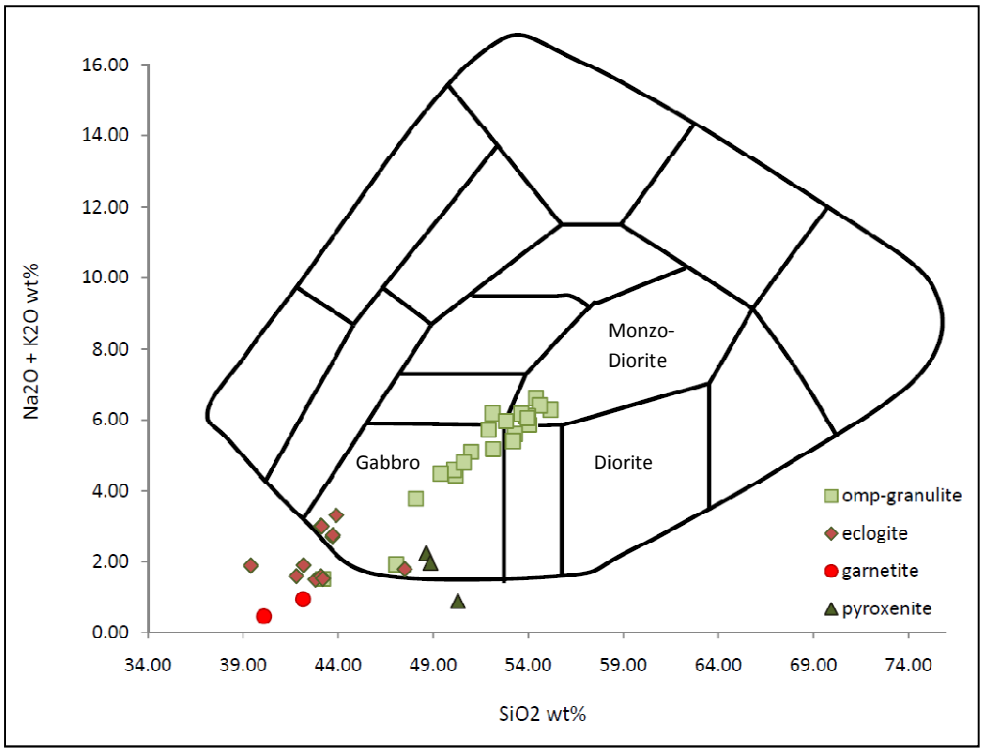

Fig 21: TAS diagram of BOG after Cox (1979). Produced by data from Watton (2009), De Paoli (2009) and Carroll (2005)

3.3.2 Major elements mineral composition

The classification of clinopyroxene, garnet and feldspar according to their major element composition and assigned to rock types is shown in Fig. 22.

Clinopyroxene dominantly occurs in two forms: as omphacite in granulite and eclogite and as the Quad-clinopyroxene diopside in garnetites and in pyroxenites. Additional minor amounts of augite can occur in pyroxenite and minor amounts of aegirine-augite and wolastonite in garnetite. Omphacite is also present in garnetite but only marginally contains enough of the

jadeite component to be classified as omphacite (composition: see attached data in Appendix 2).

End member proportions of feldspars calculated by X_{An}=Ca/(Ca+Na+K), X_{Ab}=Na/(Ca+Na+K), X_{Or}=K/(Ca+Na+K), in granulite mostly appear in the range of andesine with X_{An} (0.19-0.25) X_{Ab} (0.71-0.77) X_{Or} (0.01-0.03). K-Feldspar X_{An} (0.01) X_{Ab} (0.13) X_{Or} (0.86), have been analysed by Watton (2009) and according to the observations of De Paoli et al. (2009) are found in garnet inclusions in granulite and eclogite. Plagioclase with a higher component of anorthite can be found in symplectites indicating retrogressive metamorphism.

End member proportions in garnet are calculated as follows: X_{alm}=Fe/(Fe+Mg+Ca+Mn), X_{pyp}=Mg/(Fe+Mg+Ca+Mn), X_{grs}=Ca/(Fe+Mg+Ca+Mn), X_{sps}=Mn/(Fe+Mg+Ca+Mn). Garnet in all

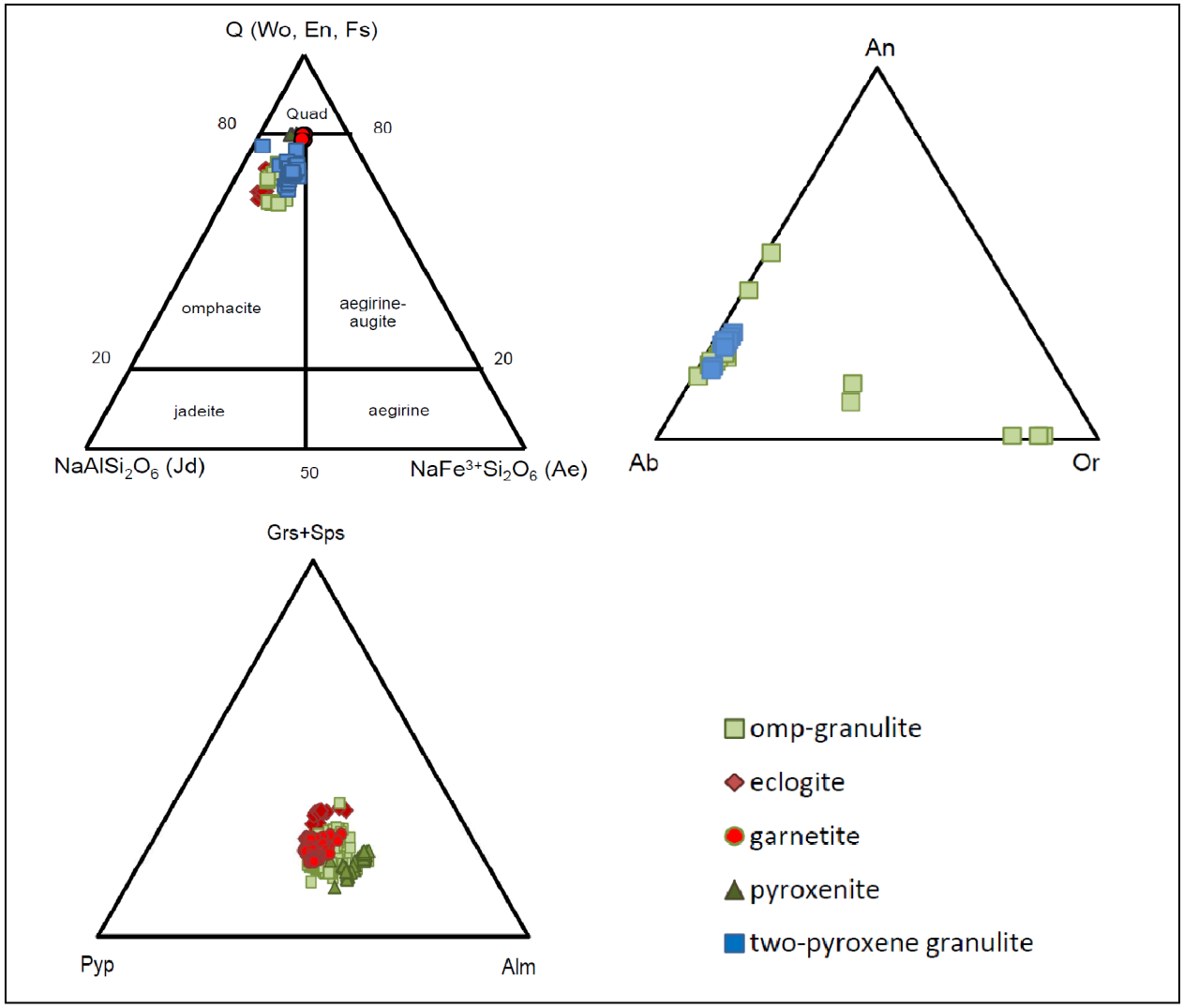

Fig. 22: Ternaries of clinopyroxene, garnet and feldspar in omphacite-granulite, two-pyroxene granulite, eclogite, garnetite and pyroxenite. (data by Watton (2009) and De Paoli et al. (2009) and from this study)

rock types shows a composition of approximately 40% alm, 40% pyp and 20% grs plus minor sps. The compositions per rock type range as follows: in garnetite alm (0.36-0.40), pyp (0-29-0.40), grs (19-26%), sps (0.01); in pyroxenite alm (0.37-0.45), pyp (0-29-0.38), grs (0.18-0.26), sps (0.01-0.02); in eclogite alm (0.38-0.44), pyp (0.27-0.40), grs (0.20-0.28), sps (0.01-0.20); in omp-granulite alm (0.41-0.47), pyp (0.29-0.40), grs (0.15-0.28), sps (0.01-0.02).

A compositional differentiation of garnet and clinopyroxene in different rock types can also be recognized in a diagram displaying Mg# (Mg/Mg+Fe) versus Ca-Cations in formula (Fig. 23). It shows a tendency of increasing Mg# in garnet from pyroxenite over omp-granulite to garnetite and eclogite. A clearer difference is observable in clinopyroxenes which divide into two groups. One with low Mg# and low Ca (omp-granulite and in eclogite) and one group characterised by high values in Mg# and Ca-Cations (pyroxenite and garnetite). A part of omphacite in eclogite plots in the group of garnetite and pyroxenite. It is the omphacite from the eclogite layer on Mt. Richards (Fig. 9).

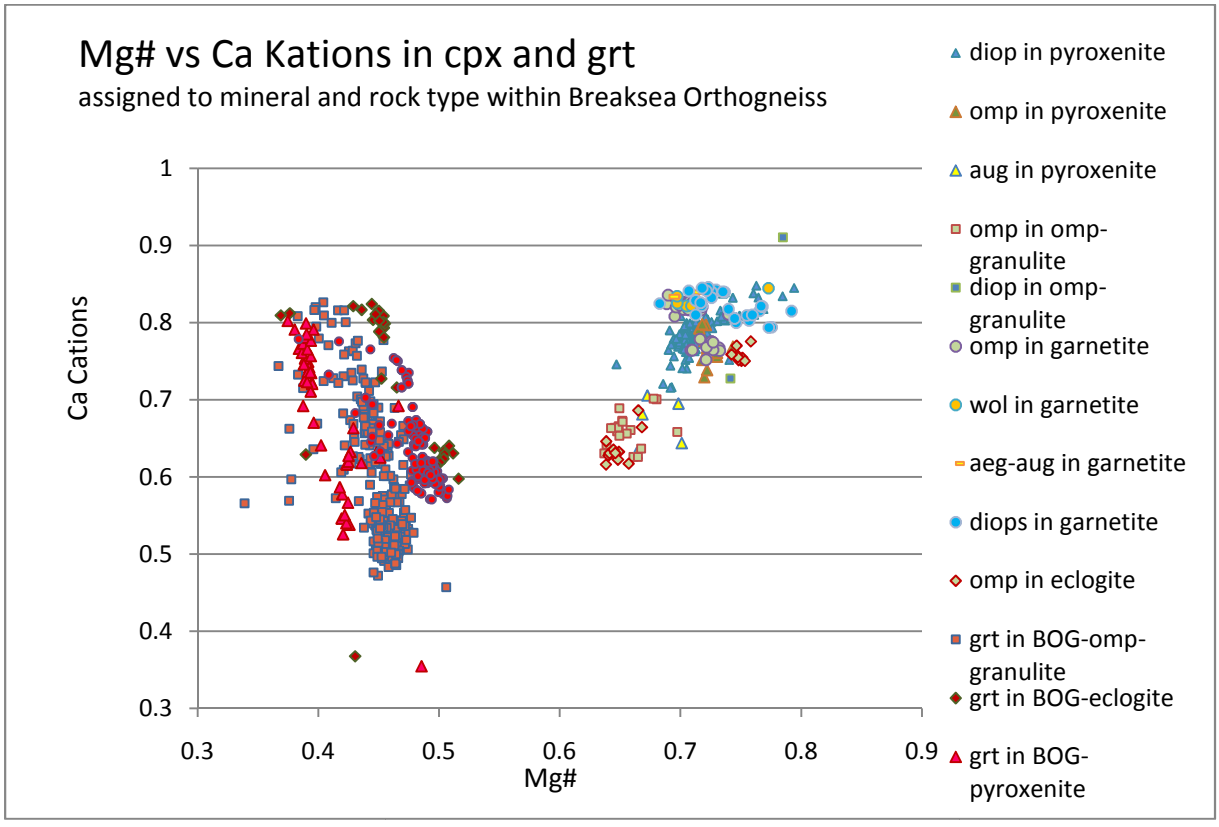

Fig. 24: Mg# vs Ca-Cations in clinopyroxene (O=6) and (O=12) garnet of different rock types of the BOG. Data from: Watton, (2009) and De Paoli et al. (2009) and measurements from this study.

Garnet in omp-granulite

The three different types of garnet in the host rock (Sample BS1008A and B) seem to form one single group on the ternary (Fig 25). But the comparison of their Mg# vs Ca-Cations (Fig. 26) reveals compositional differences. Garnet in equi-granular clusters with omphacite, are very close to the larger porphyroblastic garnet which lines up along veins. On the other hand garnet forming coronae around omphacite assemblages and containing quartz inclusions, displays a significantly higher amount of Ca-Cations in formula and a lower Mg#. For comparison, values of garnet in garnetite and in pyroxenite of the layered xenolith are also plotted in Fig. 26. It shows that garnet in omp-granulite lies between garnet in pyroxenite and garnet in garnetite, comparable to Fig. 24.

A traverse along one garnet grain within an equi-granular garnet-omphacite cluster (Fig. 27) displays a slight decline of pyp and an increase of grs and alm at the edges. This is in accordance to previous measurements carried out by Watton (2009) which were explained as very limited signs of retrograde metamorphism which lead to an exchange of Mg, Fe and Ca in narrow rims with adjacent clinopyroxene during uplift.

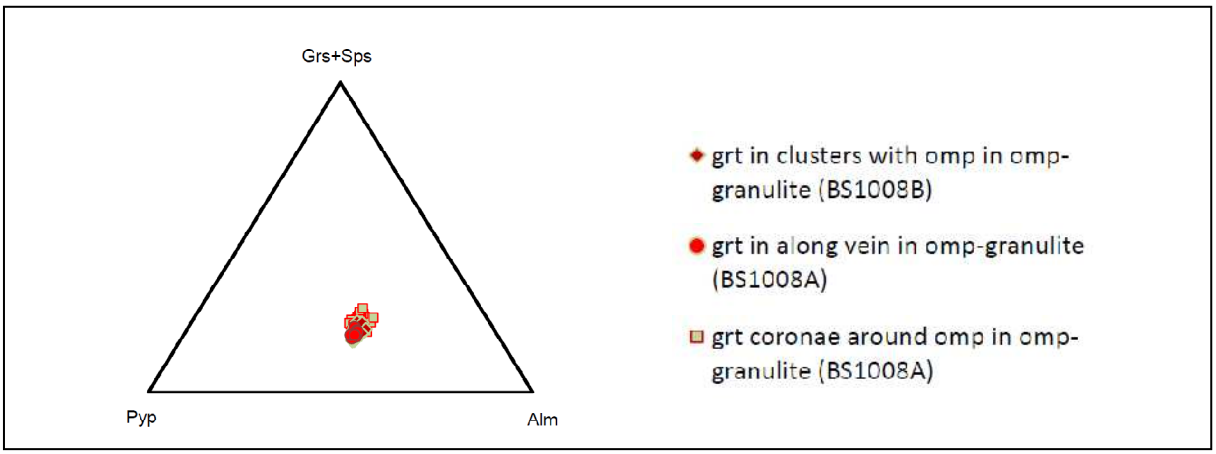

Fig. 25: Ternary of garnet in different textural settings within the omp-granulite. Samples BS1008A and BS1008B.

Garnet and pyroxene in garnetite-pyroxenite

Different structures in the layered garnetite-pyroxenite xenolith have been analysed by electron microprobe (EMP). These are: the nearly mono mineralic layers (Fig. 15), clinopyroxene and garnet inclusions within layers, and garnet films in pyroxenite layers.

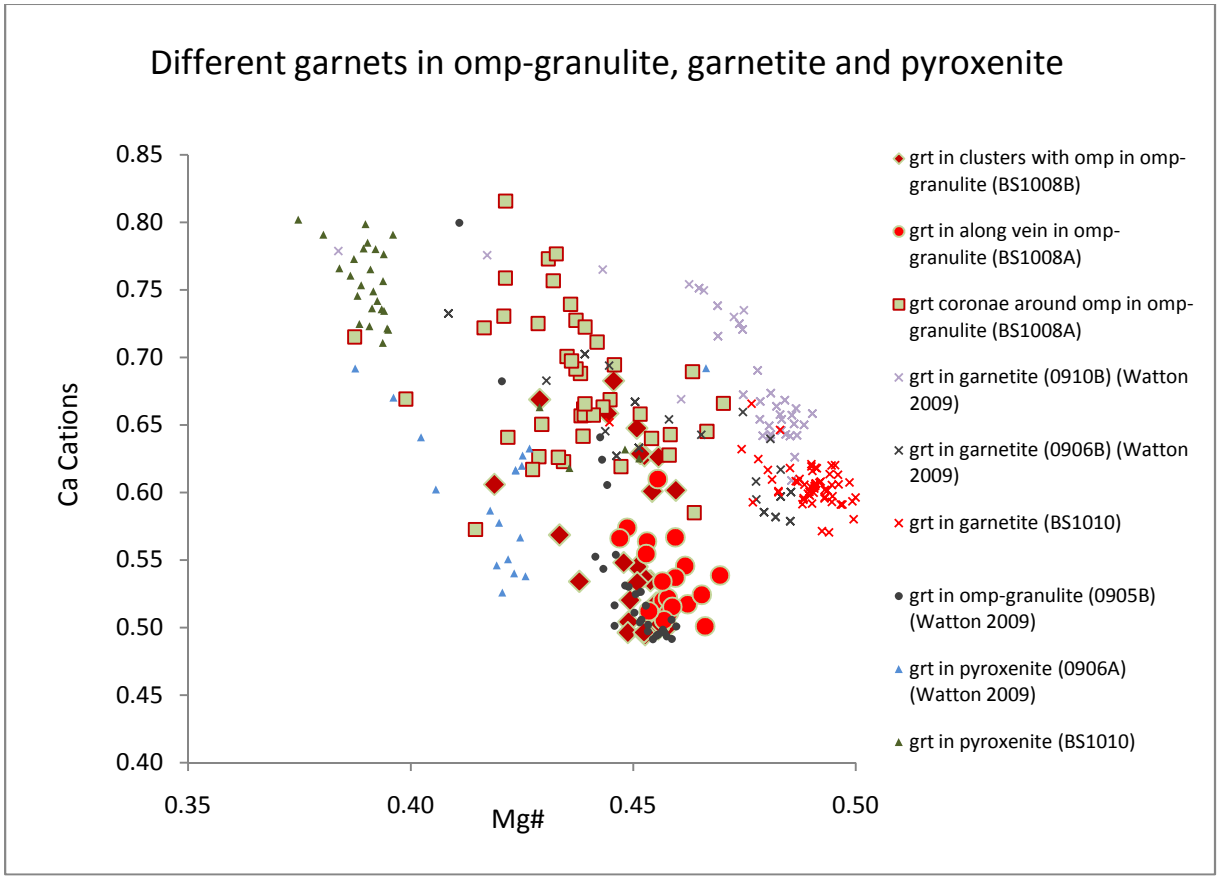

Fig. 26: Mg# vs Ca Cations (O=12) of garnet in different textural settings within omp-granulite, garnetite and pyroxenite.

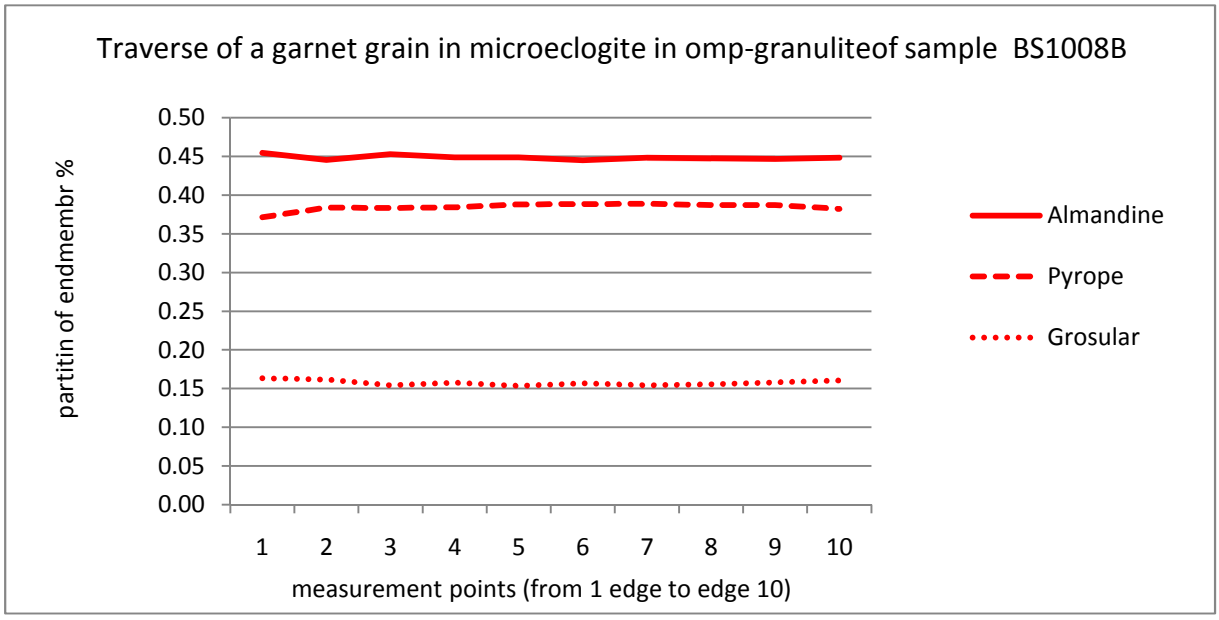

Fig. 27: Traverse of a garnet grain in an equi-granular garnet-clinopyroxene cluster in omp-granulite. Sample BS1008B.

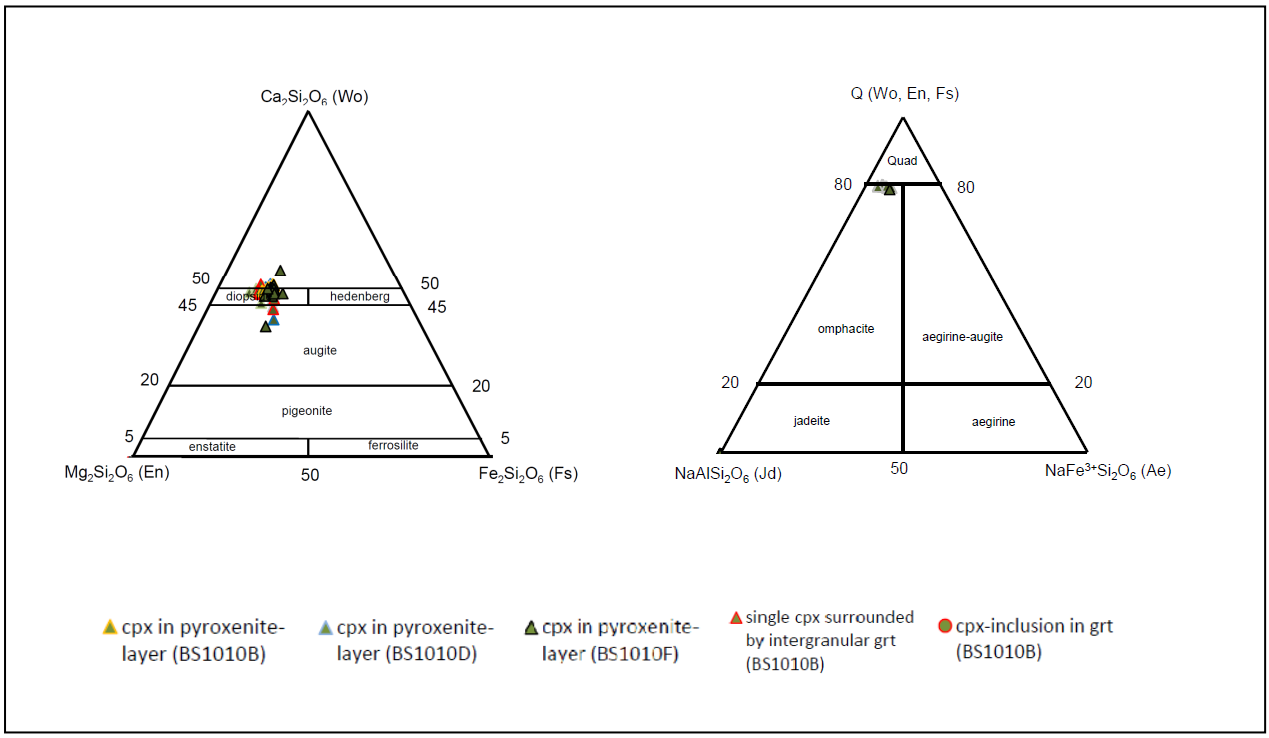

Fig. 28: Ternaries of pyroxene in different layers and textural settings within the layered garnetite-pyroxenite.

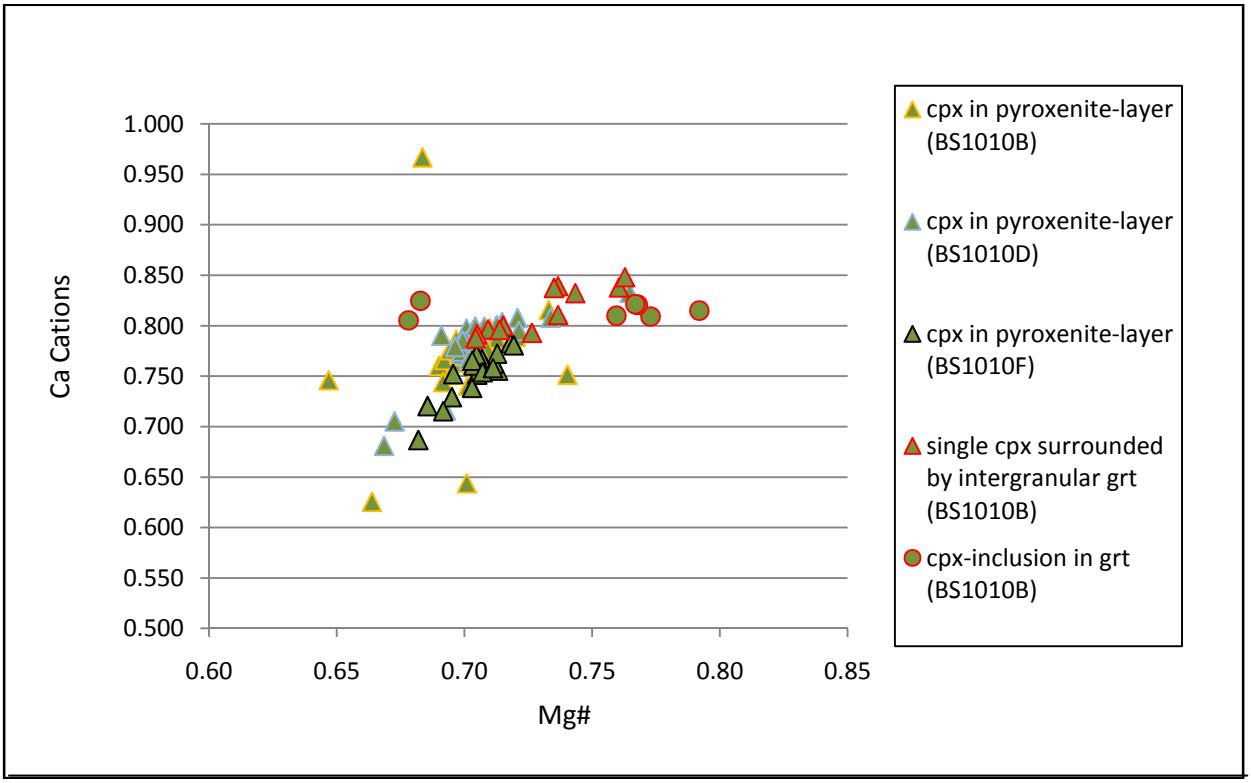

Fig. 29: Mg# vs Ca-Cations (O=6) of pyroxene in different textural settings within layered garnetite-pyroxenite.

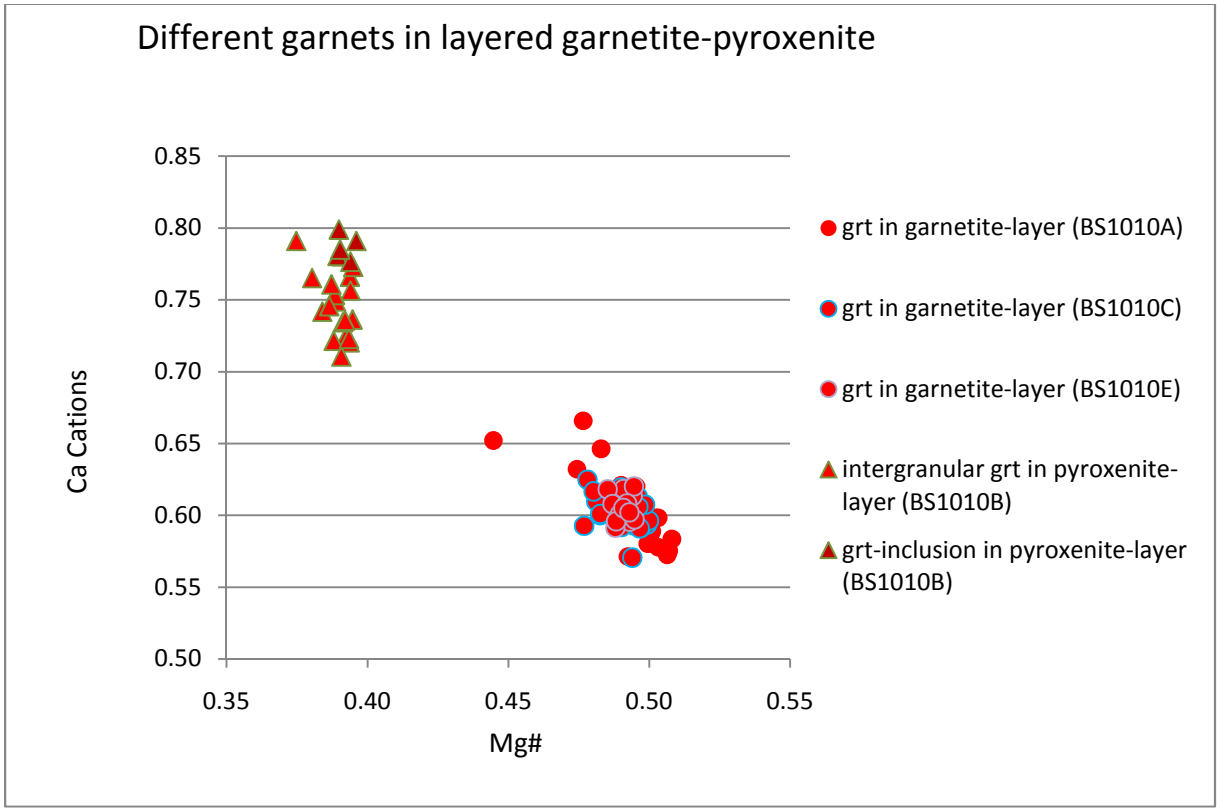

Fig. 30: Mg# vs Ca Cations (O=12) of garnets in different textural settings within the layered garnetite-pyroxenite.

A resulting a ternary (Fig. 28) shows clinopyroxene mostly as quad-pyroxenes, as diopside but also close to diopside as low Ca Mg-rich wollastonite or as Mg-rich augite or as omphacite with a low jadeite component.

No significant differences in clinopyroxene can be recognized with regard to Mg# vs Ca-Cations (Fig. 29). The values for clinopyroxene plot along a line which shows a positive trend of Mg# and Ca-Cations. Furthermore most data plot around Mg# of 0.72 and Ca 0.75 and 0.8 in formula. Thus the clinopyroxene in all layers seems to be of similar composition.

Like the pyroxenite layers the garnetite layers cannot be told apart by chemical composition (Fig. 30). But unlike the clinopyroxene, the garnet inclusions and the garnet films (Fig. 19) in the pyroxenite layer show significantly higher Ca in formula and a lower Mg#.

A Traverse (Fig. 31) from the pyroxenite layer over the boundary into the garnetite layer (track see Fig. 15, Sample BS1010A) has been taken along 11 measurement points in the pyroxenite layer and 9 measurement points in the garnetite layer. A minor decrease in CaO and Al_2O_3 and a minor increase in MgO can be observed in the pyroxenite layer when

approaching the boundary. In the garnetite layer a minor increase of CaO and Al_2O_3 and decrease of MgO can be recognised. However these observations are not very distinctive and the observed tendencies may be pure chance.

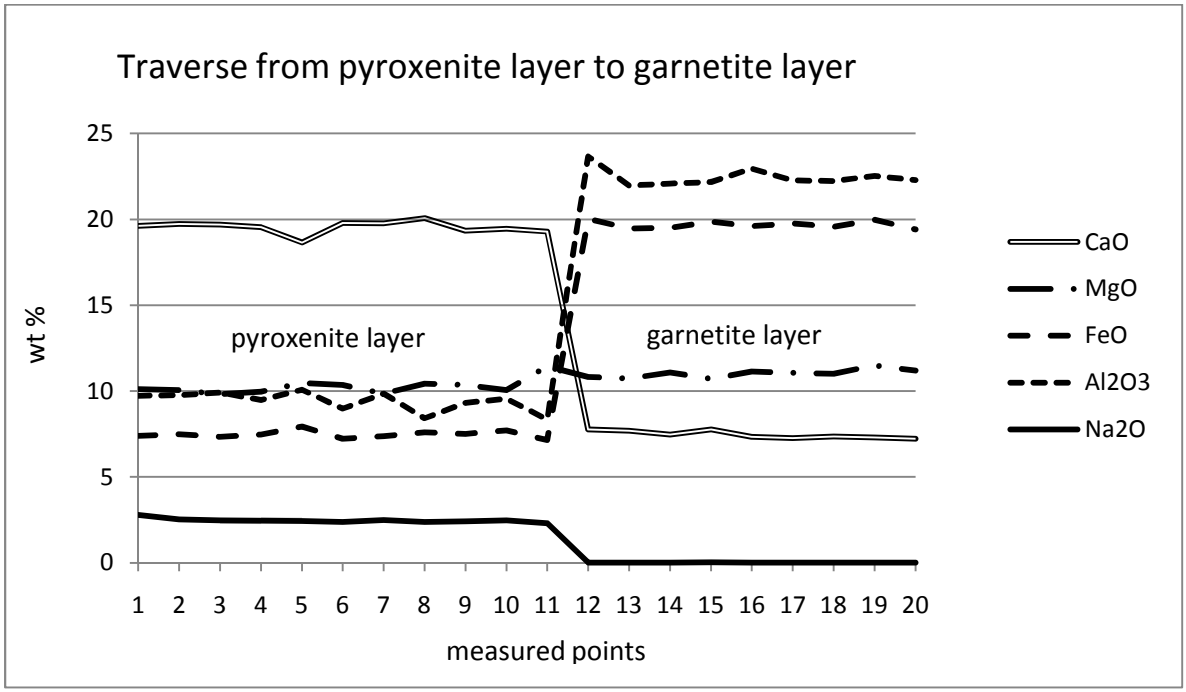

Fig. 31: Traverse over the boundary from the pyroxenite-layer to a garnetite layer. Sample 1010A. Run of traverse see Fig. 15.

3.3.3 Trace elements

Rare earth element (REE) data of clinopyroxene, garnet and plagioclase from samples collected and analysed by Watton (2009) have been C1-chondrite normalized according to Rollinson (1993). The data have been assigned to rock types for the purpose of this work. They are included in the attached electronic database.

Garnet

Most garnets in eclogite and omphacite-granulite show two similar properties (Fig. 32). These are: a positive Europium (Eu) anomaly and depletion in heavy rare earth elements (HREE) relative to medium rare earth elements (MREE).

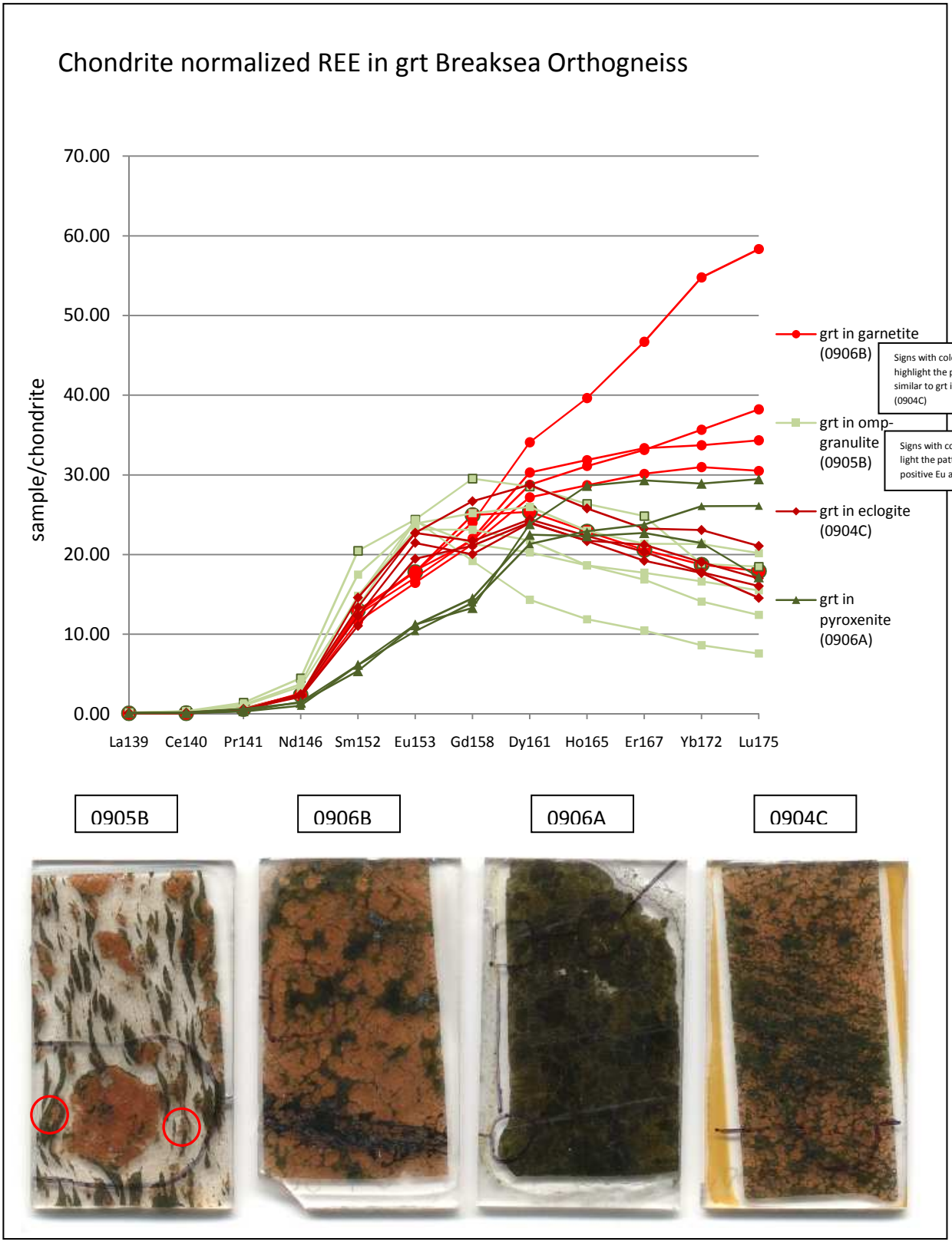

Fig. 32: Chondrite normalized (after Rollinson, 1993) REE-pattern of garnet in different rock types of BOG (after data from Watton, 2009). Below: Thick sections used for measurements by Watton (2009). The areas marked with a pen include measurement points of this Figure and of Figs. 33, 34 and 35. The two red circles in 0905B highlight areas which have been chosen by Watton (2009) for trace element analyses of garnet.

Garnet in pyroxenite and in garnetite does not display a Eu anomaly. Furthermore garnet in garnetite is enriched in HREE which is typical for garnet since this mineral has a preference for HREE. HREE enrichment is not distinctive in garnet in pyroxenite.

Three groups can be told apart: Garnet in garnetite, garnet in pyroxenite and garnet in omp-ganulite together with garnet in eclogite.

However, the delimitation of these groups is gradational since garnet in pyroxenite and in garnetite contains each one sample with HREE depletion. The one in garnetite is from a measurement taken from a garnet-core (Sample 0906B in Watton, 2009; see also attached electronic database), the one in pyroxenite has been taken from a garnet-rim (0906A in Watton, 2009; see also attached electronic database). The REE pattern of the one garnet in garnetite with a HREE-depletion is very similar to the REE pattern of one garnet in eclogite with a minor and one garnet in omp-granulite without a positive Eu anomaly.

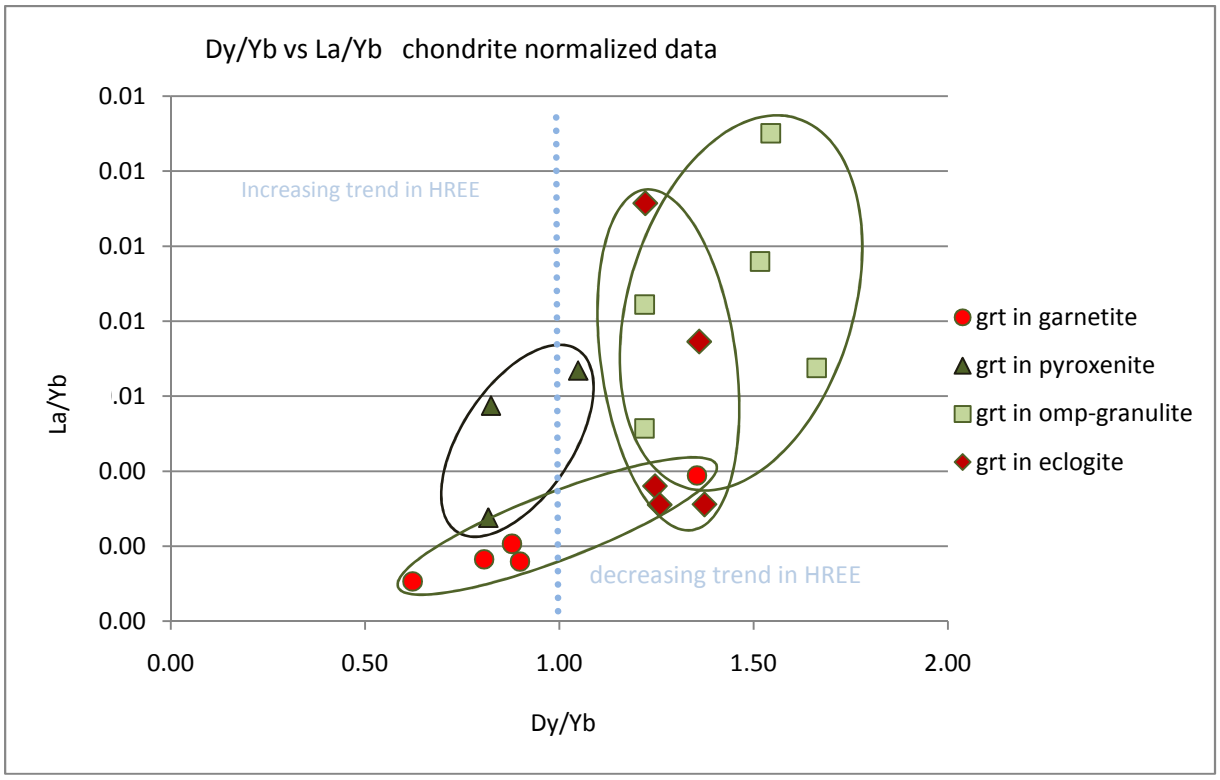

Fig.33: La/Yb versus Dy/Yb of garnet in different rock types of BOG (after data from Watton, 2009)

Differences in REE patterns can also be showed in a La/Yb versus Dy/Yb plot (Fig. 33) that highlights the different slopes of the REE graphs (Fig. 32). All samples have La/Yb <1 because

they show an overall increase in REE from La to Yb. The ratio Dy/Yb however gives values >1 for all garnets in omp-granulite and in eclogite. This emphasizes the decreasing trend of HREE in these samples. The increasing trend in pyroxenite and garnetite is expressed by Dy/Yb values <1. However the two samples with HREE depletion in garnetite and in pyroxenite do not fit in this trend. Therefore they plot on the right side of the separating blue line (Fig. 33)

Clinopyroxene

Clinopyroxene, which compared to garnet shows a very clear separation according to major element composition (Fig. 24) does not display significant differences in REE patterns (Fig. 34). The only observation is the difference in the total amounts of REE but this is of lower value for interpretation than the pattern. Regarding the concentrations of REE, there is an overlap of granulite and garnetite and a higher closeness of pyroxenite and eclogite. The highest amounts have been measured in inclusions in garnet.

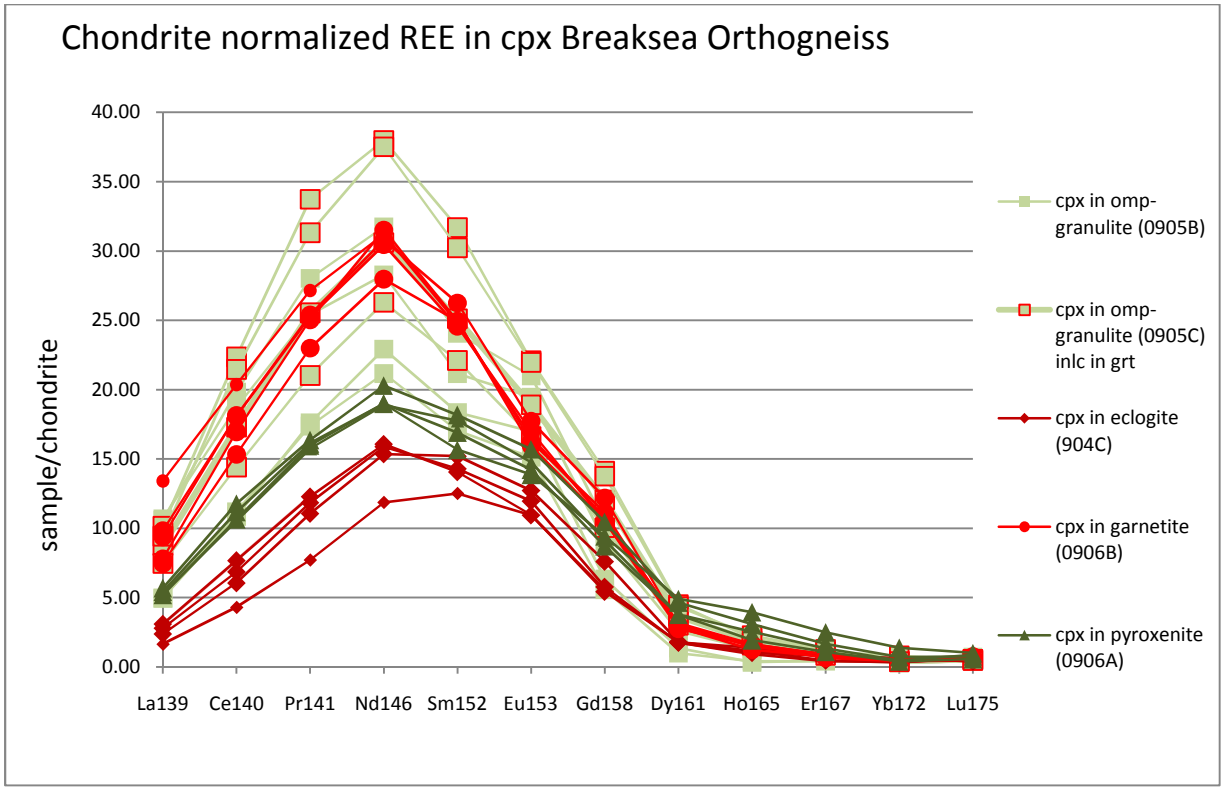

Fig. 34: Chondrite normalized (after Rollinson, 1993) REE in clinopyroxene in different rock types of BOG (after data from Watton, 2009)

Feldspar

The REE pattern of feldspar (Fig. 35) is typical for this mineral with a positive Eu anomaly and an overall falling tendency to include heavier REE. At most there is a slight preference for Er, Yb and Lu which is rather atypical for plagioclase, but in this case is not very distinctive.

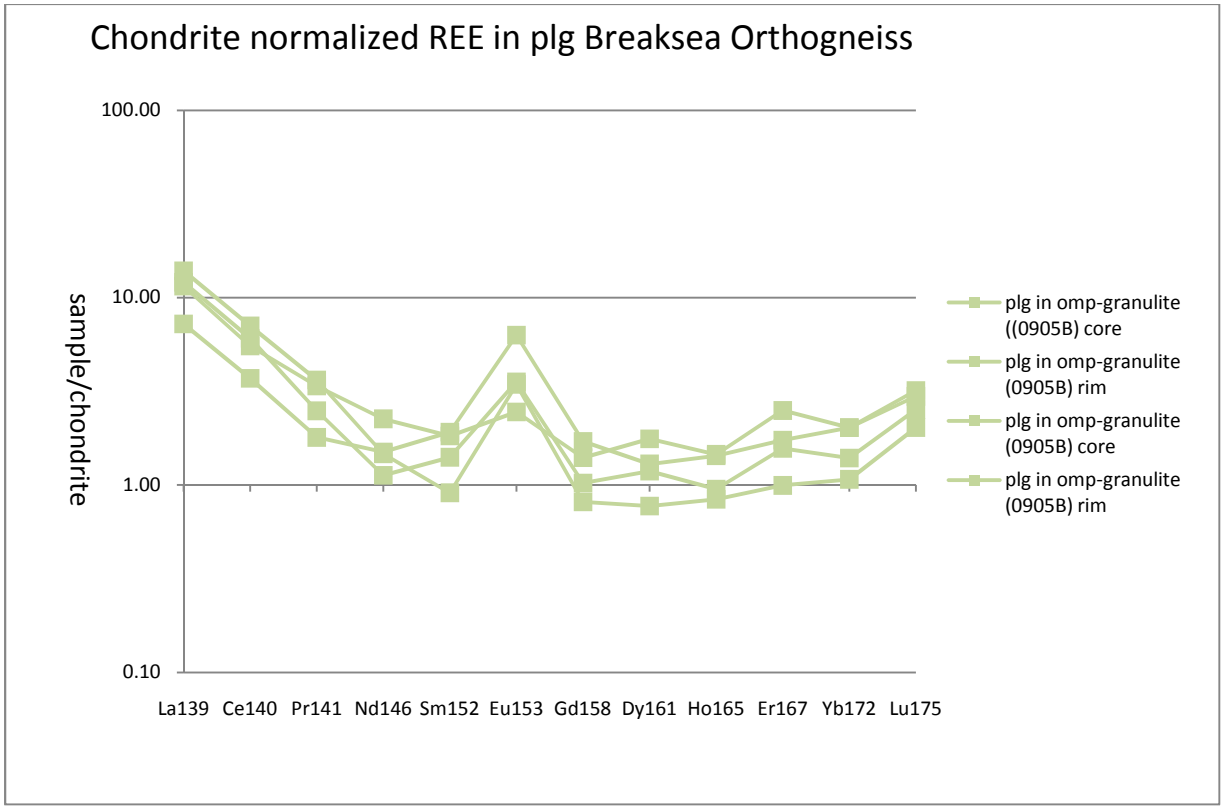

Fig. 35: Chondrite normalized (after Rollinson, 1993) REE in plagioclase in omp-granulite of BOG. (After data from Watton, 2009)

3.3.4 Liquids recalculated by partition coefficients

The liquids from which clinopyroxene and garnet crystallized have been recalculated assuming they are igneous grains. Using partition coefficients provided by Fujimaki et al. (1984) for basaltic andesite liquids (silica range 45-57 wt%) the following formula has been used:

$$D = C_m/C_L \quad \rightarrow \quad C_L = C_m/D$$

D (partition coefficient),
C_m (concentration of REE in mineral)
C_L (concentration of REE in liquid)

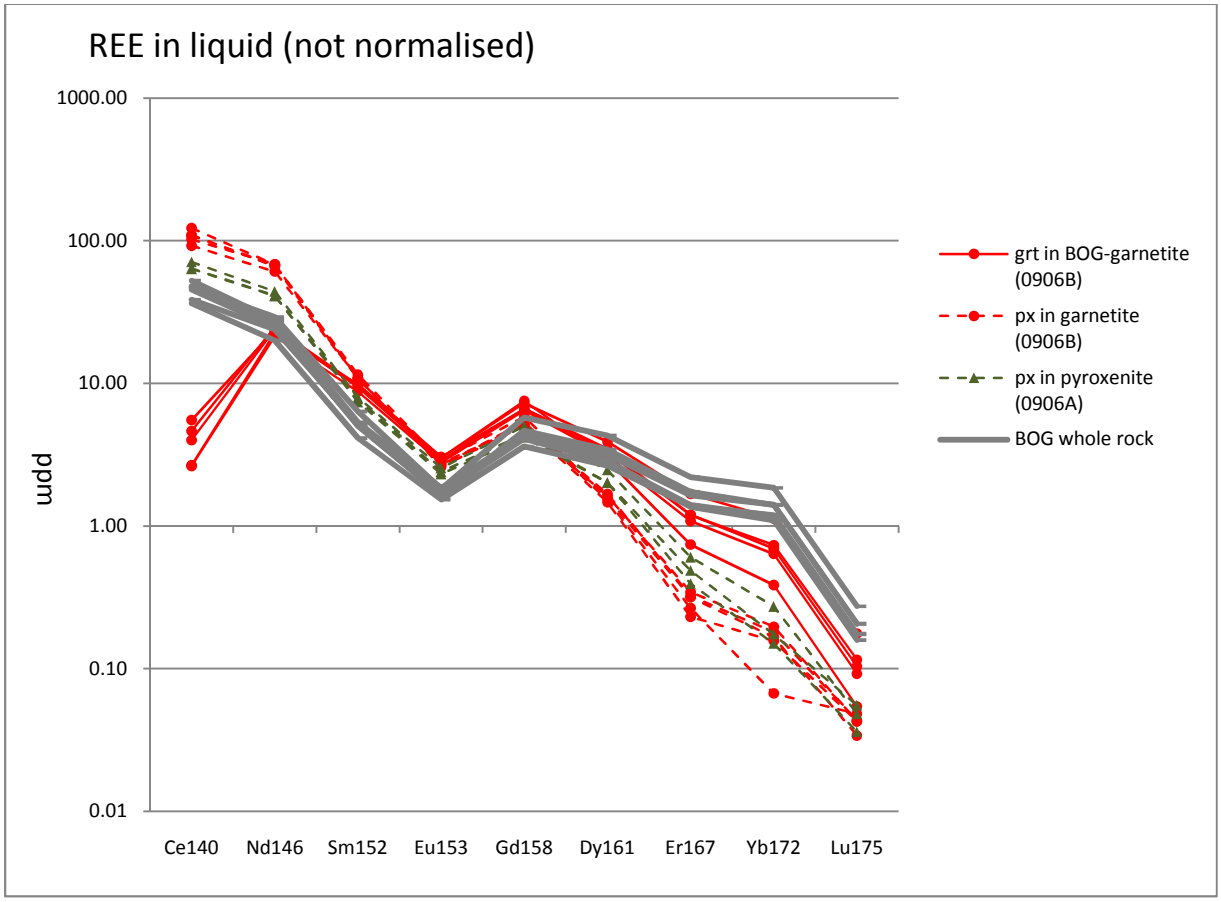

Fig. 36: Recalculated melts from partition coefficients. Data from: Carroll (2005), Watton (2009), De Paoli et al. (2009), Alibone et al. (2009)

The results are plotted in Fig. 36. For comparison it also displays the whole rock REE pattern of the BOG. The partition coefficients used for this calculation have not been determined for high pressure, comparable to the formation depth of the BOG. However, Green and Pearson (1983) showed that partition coefficients increase with increasing pressure and decrease with increasing temperature. Thus an equalizing effect of changing P-T conditions with increasing depth lowers the influence of increasing pressure. Therefore partition coefficients may still be valuable at least for a rough comparison of original liquids.

The whole rock REE-data of the BOG show congruencies with the calculated melt from which garnet and clinopyroxene crystallised. There is a certain congruence of the granulite whole rock pattern in MREE from Nd-146 to Gd-158 with the calculated liquids from which garnet and clinopyroxene crystallized. In the LREE section (Ce-140) and in the HREE-section (Dy-161 to Lu-175) the liquids are depleted compared to the whole rock.

4. Determining the age of the Breaksea Orthogneiss

4.1 Zircon separation

Zircon mineral grains have been separated from sample P78760 (0901C) which has been collected by Watton (2009) and is a typical omphacite-granulite. The work has been carried out by the following steps and techniques:

At first fragments of cobble size were crunched with an *Enerpac Hydraulic Crusher*. The resulting fine grained sand then was passed through a sieve of a mesh size of 200µm. This was panned in water in order to achieve a first rough separation of the minerals according to their density. The panning resulted in a wash out of most of the feldspar. Thus the leftover mainly contained garnet, pyroxene and rutile.

After drying in an oven, these grains were run through a *Frantz magnetic barrier laboratory separator (model LB-1)* at 15° forward slope and a 15° side tilt angle. Six runs were carried out beginning with a low magnetic field in order to separate minerals with a high magnetic susceptibility. The field strength was increased by each step starting at 0.2 amps and continuing to 0.4 amps, 0.6 amps, 0.8 amps, 1.2 amps and finally 1.5 amps. Zircon has an extract range of 0.1 to 1.75 amps. The range of best recovery lies between 1.7 and 1.75 amps. Runs at higher magnetic field strength then 1.2 amps were not done because of the small amount of leftover material and the instability of the magnetic field at higher voltages (this maybe due to air humidity). Despite that it was reasonable to expect a concentration of zircon in the leftover which had not yet responded to the highest magnetic field strength of the last run. Feldspar has a magnetic susceptibility range which is nearly identical to zircon. Therefore the left over was also enriched in feldspar that had not yet been washed out by the panning process. To separate zircon from feldspar, the leftover got immersed in sodium-poly-tungstate solution $Na_6(H_2W_{12}O_{40})\cdot H_{2O}$ with a density of ~3.0 g/cm^3, which is higher than the density of feldspar and lower than the density of zircon. The dregs of this last process then were ready for the last step, the manual picking of mineral grains under the binocular microscope in artificial daylight. This final step resulted in a harvest of 37 zircon grains (appendix-4).

4.2 U/Pb analyses

U-Pb analyses have been carried out by inductively coupled plasma mass spectrometry (ICP-MS). The measurement points on the zircon grains are marked by a black circle on the electron microscope cathode luminescence images in appendix-4. The instrument was a UP-266 built by New Wave which also processes the data by the computer program called Glitter. The resulting concordia age (116 +/-0.51 Ma) and the age distribution of selected single grains are displayed in Fig. 37.

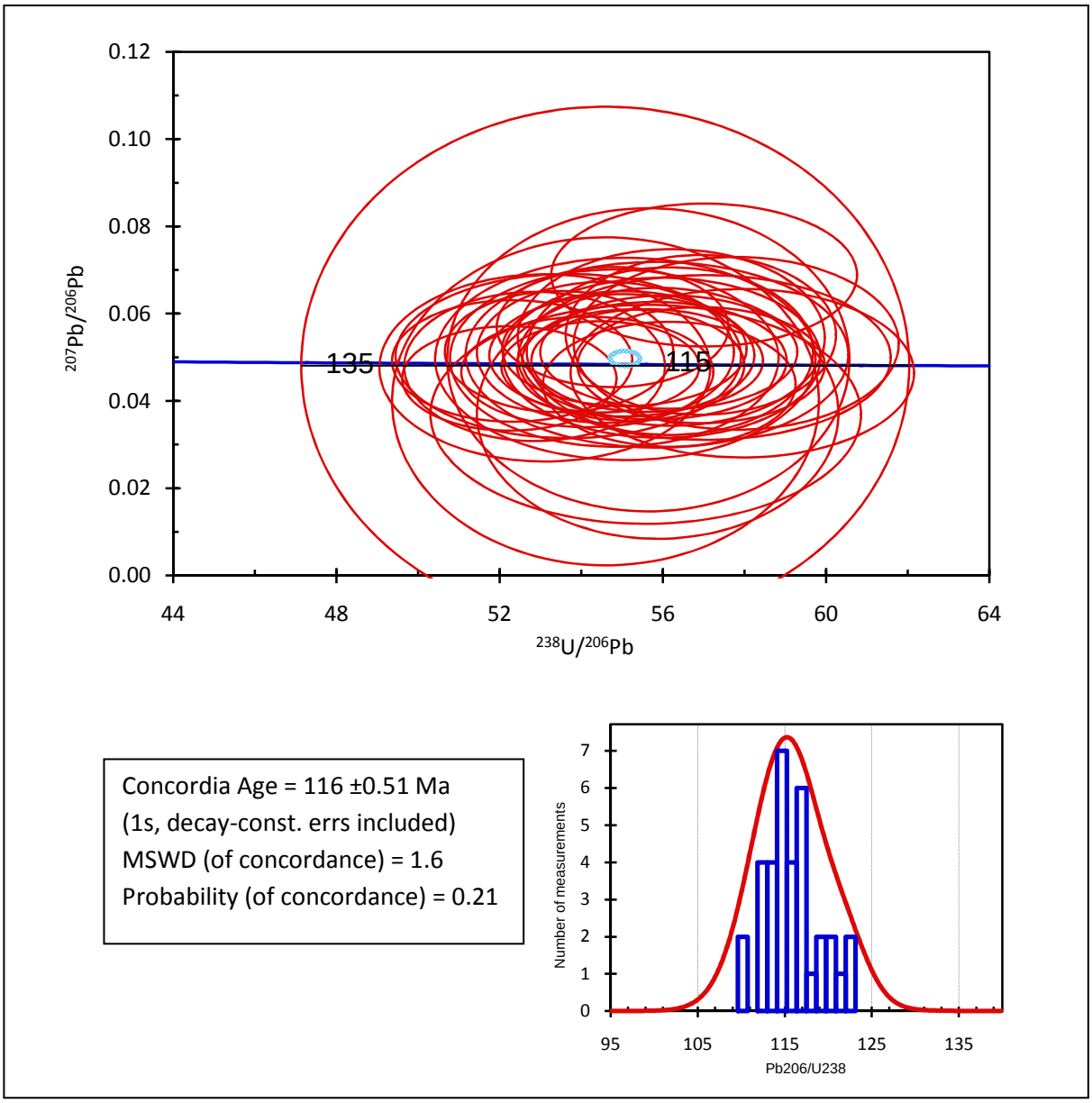

Fig. 37: Concordia age on an inverse Concordia and distribution of measured data.

4.3 Hf analyses

In addition to the U-Pb analyses, the content of Hf isotopes in 17 zircon grains has been measured by ICP-MS on a plasma multicollector built by Nu-Instruments. Fig. 38 shows the results by a plot Hf-176/Hf-177initial vs the Pb-206/U-238 age. The ages of the 17 analysed grains are distributed on a relatively wide band from 101 Ma to 121 Ma. Also the distribution of 176-Hf/177-Hf initial, ranging from 0.282761 to 0.282984 is relatively large. An interpretation of these results is given in Chapter 6.3.

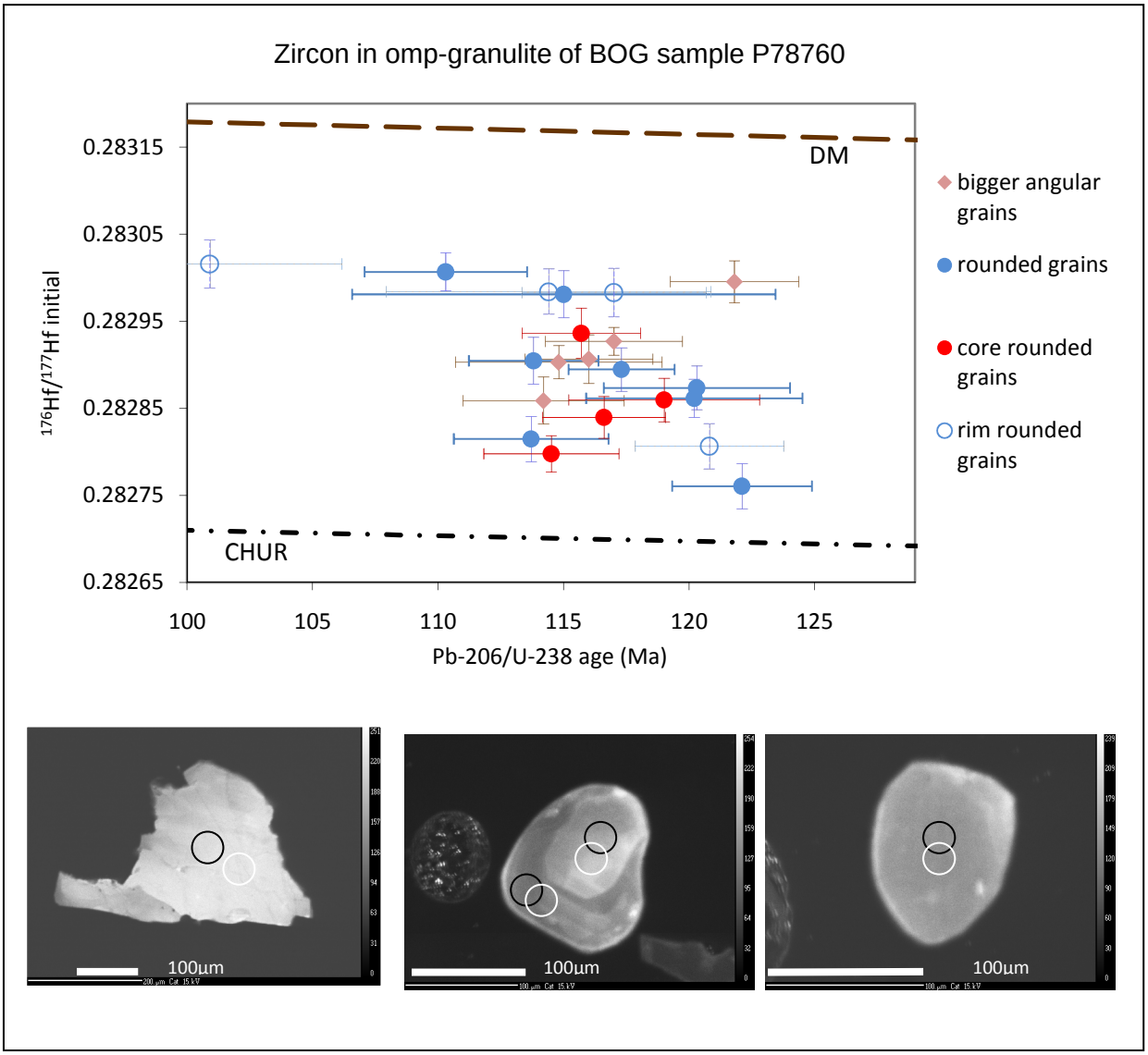

Fig. 38: Pb-206/U-238age vs 176-Hf/177-Hf initial of zircon grains in different appearances: Big and angular, small and rounded with or without distinctive zoning. Black circles indicate location of Pb-U measurement. White circles indicate location of Hf measurement.

Zircon grains of three different appearances were recognized and are displayed by different symbols: Big grains of approximately 300 µm and small rounded grains of approximately 100 µm in diameter.

Some of the smaller grains displayed distinctive zoning. In four of these, core and rim measurements have been taken. The pictures of all zircon grains found and used in this study with indication of Pb-U and Hf measure points are displayed in appendix-4.

5. Density measurements

In the course of this study, dry densities of BOG samples collected by Watton (2009) have been measured. The scale was a Mettler Toledo AG-204 Delta Range, equipped with density determination kit. Fig. 39 presents the results (values and sample numbers: Appendix 3) which are combined with density data obtained from the online PETLAB rock data base of GNS Science New Zealand. The figure also shows the density ranges of the minerals diopside, omphacite, garnet and plagioclase.

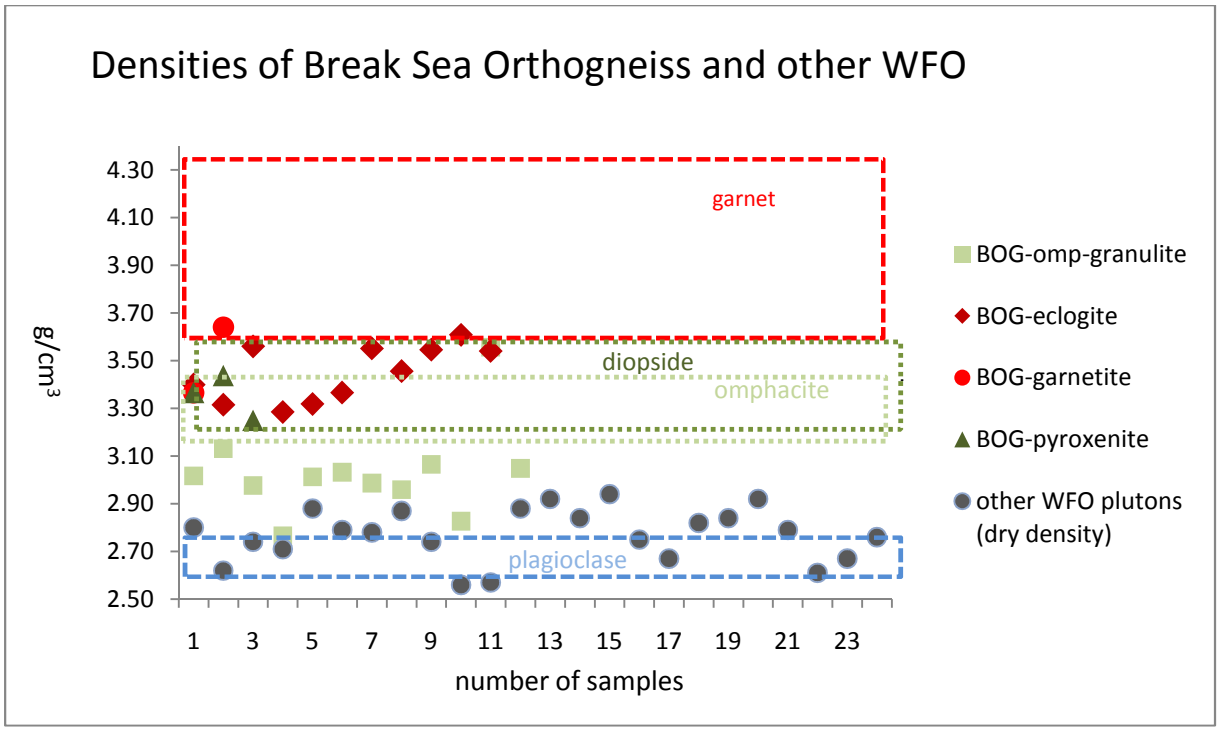

Fig. 39: Densities of different rock types of the BOG and other WFO plutons together with densities of the most common minerals discussed in this work (mineral data from Deer, Howie & Zussmann, 1992).

6. Discussion

6.1 Interpretation of field observations and thin sections

6.1.1 Garnet in omphacite-granulite

The structures seen in the field (sample BS1008A, Fig. 7) represent different phases of the igneous and metamorphic history of the omp-granulite:

The foliation S_1 most probably results from the primary deformation event which gave the rock a metamorphic overprint at granulite facies (Fig.4). The distinctive bigger garnet grains which are lined up along plagioclase rich lines may be interpreted as igneous minerals which formed along a vein during or after the deformation event D_1. The gradational boundaries with the surrounding omp-granulite suggest that these veins are a peritectic product of partial melting syntectonic with S_1. More evidence for that is given by the REE-pattern (Chap. 6.3.3) The compositional layering in the host rock seems to be a relict preserving motions in the magma before or coeval to crystallisation. But what has been taken as compositional layering by Watton (2009) could also be the reaction zone of the vein.

In thin section the recognition of garnet in coronae around omphacite (BS1008A, Fig. 10) is supported by the appearance of quartz inclusions in garnet. Since garnet contains only ~40wt% SiO_2 compared to ~50wt% in clinopyroxene, there is a surplus of SiO_2 which forms quartz inclusions when pyroxene is replaced by garnet. This garnet may therefore be taken as metamorphic garnet.

A similar arrangement or comparable inclusions are not present in the equi-granular garnet-omphacite clusters in sample BS1008B (Fig. 12). Garnet in these clusters characteristically has exsolution of rutile instead. The same kind of exsolution can be seen in the big garnets along veins (Fig. 11). Exsolution is absent in metamorphic coronae-garnet in sample BS1008A (Fig. 10). Rutile-exsolution together with symplectites involving biotite and pargasite (Fig. 10) document the retrogressive metamorphic history of the omp-granulite (S_2).

The mutual appearance of rutile exsolution in those two types of garnet suggests a closeness in respect of major element composition and origin which for the lack of replacement structures seems to be igneous or peritectic (see Chap 6.3.3).

The variations in mode of garnet and omphacite described in Chapter 3.1.1 (Fig. 8) might have the same reason as the eclogite bands on Mt. Richards (BS1003B, Fig. 9). Both could come from accumulation processes of the early crystallising and high density minerals garnet and omphacite. The bands (Fig. 9) could thus be regarded as igneous eclogite. Furthermore the equi-granular omphacite-garnet clusters in omp-granulite can be taken as igneous micro-eclogites, which occur in different modes due to different degrees of accumulation in different areas of the rock. Euhedral inclusions of clinopyroxene in garnet (Fig. 13) and vice versa indicate coeval growth of these two minerals. Ovoid inclusions of clinopyroxene and embayments in garnet (BS1003B, Fig. 13) suggest growth or overgrowth of garnet within an inter-cumulate liquid. These structures do not occur in the equi-granular garnet-omphacite clusters. Therefore the eclogite layers and the clusters presumably have assembled by different accumulation processes.

In summary the examination of outcrops and thin sections shows that garnet forming coronae around omphacite is metamorphic whereas garnet along veins and in equi-granular clusters with omphacite could either be igneous or peritectic or metamorphic.

6.1.2 Xenolith of layered garnetite and pyroxenite

Despite differences in mineralic composition and in some cases in scale, the layering appearance of the xenolith with its flame structures (Fig. 14) is similar to layered igneous rocks found in other places. Amongst these are the Bushfeld Complex of South Africa (Sharpe, 1985), the Stillwater Complex of Montana (McCallum et al., 1980) and the Skaegård Intrusion of Greenland (Irvine, 1980). Of course this similarity of the layered xenolith does not provide adequate evidence to explain it equally as an igneous cumulate.

A closer look at thin section reveals more. The ovoid inclusions of clinopyroxene in garnet and embayments in clinopyroxene at a layer boundary (Fig. 16 and 17) can be interpreted as metamorphic overprint or resorption features in an as igneous cumulate. These textures according to Winter (2009) result from re-fusion or dissolution of clinopyroxene into the melt from which the adjacent garnet crystallized. Euhedral inclusions of garnet (Fig. 18) in clinopyroxene and vice versa support the model of a coeval igneous origin. Since clinopyroxene tends to crystallize at higher temperatures than garnet (see Fig. 40a), it is

possible that in the cumulate of clinopyroxene and garnet, at least some garnet crystallized from an inter-cumulate liquid and also formed an ad-cumulate by resorption and overgrowth into the clinopyroxene (this is supported by geochemical data, see Chap. 6.2.2).
In the same way the garnet-films (Fig. 19) in the pyroxenite-layer seem to have formed after crystallisation of clinopyroxene and from the liquid between those grains, thus from the inter-cumulate liquid. These observations can support the model of an igneous origin of the layered garnetite-pyroxenite. But the liquid which accounts for the resorption structures does not necessarily need to be a magmatic inter-cumulate liquid. It could also have been peritectic. In this case the garnet forming films in the pyroxenite would have formed from overgrowth of metamorphic garnet into clinopyroxene.

6.2 Interpretation of geochemical data

6.2.1 Comparison with other ultramafic rocks

The TAS diagram (Fig. 21) depicts how mafic the layered garnetite-pyroxenite is, too mafic for Phanaerozoic plutonic rocks. Ultramafic rocks of comparable major element composition have been crystallized from very hot magmas during the Hadean to form komatites, but are not known from the Phanaerozoic when the crust had cooled down. Therefore it may be assumed that the ultramafic layered xenolith has not arisen from a melt of this composition but rather is a cumulate resulting from a fractionating process or is a residue from partial melting.
Despite their extraordinary composition, ultramafic xenoliths are not uncommon and exploring them has contributed to modelling the origin of continental crust. They have been described and investigated at sites such as the Kohistan sequence in Pakistan (Bard, 1983), the Sierra Nevada Batholith in California (Lee et al., 2006; Ducea and Salleby, 1996) the Tonsina sequence in Alaska (De Bari and Coleman, 1989) and in South African Kimberlites (Griffin et al. 1979), to name a few. In most of these sites ultramafic xenoliths or ultramafic sequences have been recognized as igneous products formed at the base of the continental crust close to the Mohorovicic discontinuity.

Experimental studies carried out by Wolf and Wyllie (1993), Alonso-Perez et al. (2009) and Müntener at al. (2001) have confirmed that ultramafic garnet-pyroxenites form and accumulate as first products from mantle melts at pressures of up to 1.2GPa and temperatures between 850 and 1000°C (see attached electronic data base). Melting experiments by Thompson (1972) showed that these minerals are the first to crystallize from a rock of basaltic composition, at P-T conditions around 1.8GPa and above 1200°C (Fig.40). When these ultramafic components are extracted and delaminated, the residual andesitic melt will be of the typical composition of the average continental crust. The amount of separated garnet-pyroxenite can be considerable. Müntener et al. (2001) give an estimate of 50% of the mantle-derived liquid from their experiments. Ducea and Saleeby (1998) allow up to 90% of the former mantle melt to be accumulated as garnet-pyroxenite

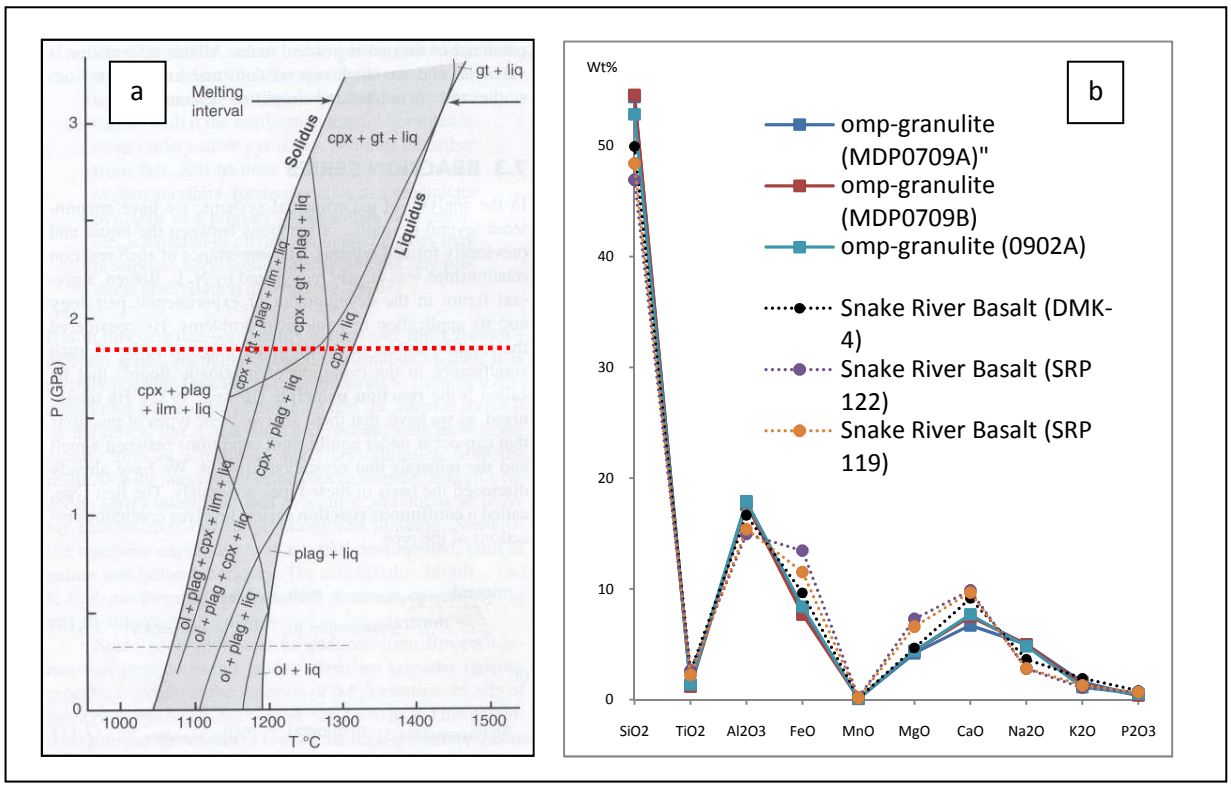

Fig. 40a: P-T phase diagram for the melting of Snake River (Idaho, USA) tholeiitic basalt under anhydrous conditions (after Thompson, 1972 in Winter, 2009). The area of formation of BOG is emphasized by a dotted red line. **b:** whole rock compositions of three representative samples of omp-granulite (Watton, 2009) and three samples of Snake River Basalt (Shervais & Vetter, 2009).

These models are deduced from field studies and geophysical considerations, which explain isostatic movements and the stability of the Sierra Nevada Batholith. Data of the mentioned authors are included in the electronic data base attached to this work.

Lee et al. (2006) distinguish two kinds of ultramafic xenoliths in the Sierra Nevada (see Figs. 41 and 42): High-MgO (> MgO 15wt%) and low MgO (< MgO 15wt%). High-MgO pyroxenites are derived from a primary mantle melt whereas low-MgO pyroxenites are formed by separation processes within the remaining andesitic continental crust. It is thought that high-MgO pyroxenite delaminates from the crust which explains the low density and the felsic andesitic composition of the average continental crust. Low-MgO pyroxenite represents deep parts of the crust which have a minor chance of being delaminated since they formed in shallower depth than the high MgO version. According to Müntener et al. (2001) high MgO garnet-pyroxenites at the base of arc sections are also characterised by relatively high Cr (Cr_2O_3 > 0.4wt%) and low Al_2O_3 (< 3wt%). Both properties do not apply to the garnetite-pyroxenite xenolith in the BOG (see electronic data base).

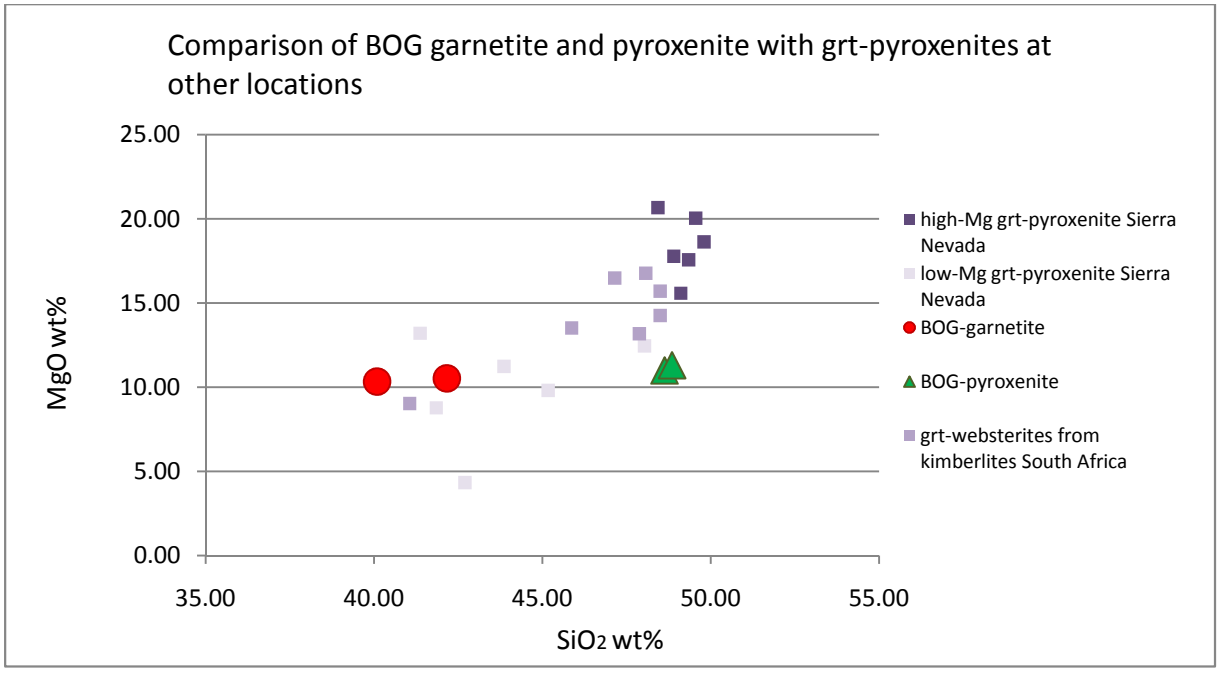

Fig. 41: Comparison of the layered garnetite-pyroxenite from BOG with ultramafics from other locations. Data from: Watton (2009), Lee et al. (2006), Griffin et al. (1979).

Fig. 41 depicts a compositional comparison of garnetites and pyroxenites from the layered xenolith of the BOG with the two types of pyroxenites in the Sierra Nevada and deep pyroxenites from South African Kimberlites (classified as websterites). With the exception of one sample (from De Paoli et al. 2009), the pyroxenites and garnetites in the BOG-xenolith are comparable to low MgO-pyroxenites.

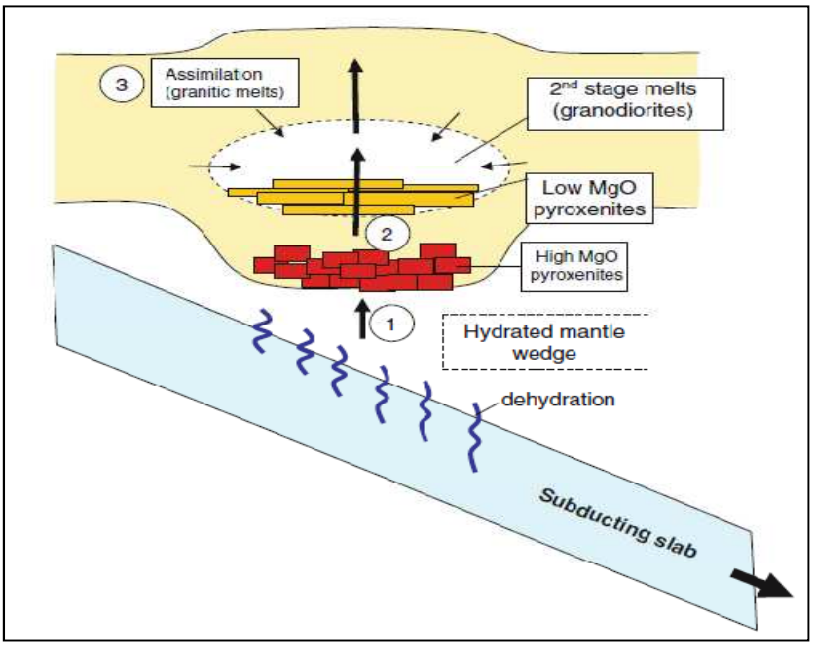

Fig. 42: Model for the formation of low- and high-MgO pyroxenites in a subduction setting. (Lee et al., 2006)

From their high Sr/Y ratio (Sr 800-1850ppm; Y <17ppm), Watton (2009) concludes that the plutons of the WFO are derived from a crustal source. This combined with the low MgOwt% (< 11wt%), high Al_2O_3 (8-9 wt%) and low Cr_2O_3 (269-411ppm) in pyroxenite suggests an origin of the xenolith not from a primary mantle melt but from the crust. Thus the garnetite-pyroxenite xenoliths may represent a lower part of a pluton. Major element analysis is not capable of attributing it to a specific pluton.

6.2.2 Mineral major element composition

Garnet in omphacite-granulite

The three textural types of garnet show compositional differences. The Mg# and Ca-Cations (Fig. 30) of garnet in equi-granular clusters with omphacite are similar to larger garnet grains lined up along veins.

Garnet forming coronae around omphacite and containing quartz inclusions (BS1008A, Fig. 10), has a significantly higher amount of Ca-Cations and a lower Mg# (Fig. 30). Taking into account the textural context of the garnet coronae, the higher amount of Ca-Cations presumably is an inheritance from clinopyroxene and plagioclase which compared to garnet are relatively rich in Ca.

The traverse along one garnet grain within an omphacite-garnet cluster (Fig. 31) displays a slight decline in pyp and an increase in grs and alm at the edges. This is in accordance to previous analyses made by Watton (2009) who interpreted this pattern as a retrogressive metamorphic feature resulting from exchange of Mg, Fe and Ca with the adjacent clinopyroxenes.

Xenolith of layered garnetite and pyroxenite

The pyroxene in different pyroxenite layers cannot be told apart by the major element composition (Fig. 29); the same applies for the garnetite layers (Fig. 30).

But garnet inclusions and films in the pyroxenite layer show significantly higher Ca-Cation amounts and a lower Mg# than garnet in the garnetite layers. This corresponds to the structures described in Chapter 3.2.2. It also suggests that the inter-granular garnet in the pyroxenite layer has been crystallised from an inter-cumulate liquid or from a peritectic liquid. The Ca-Cation rich composition could origin from re-fusion of parts of the pyroxenite layer into the liquid which then formed the garnet film.

The plot of Mg# vs Ca-Cations in Fig. 24 shows a separation of clinopyroxene into two groups. Clinopyroxene in garnetite and pyroxenite has a high Mg# and high amount of Ca-Cations opposed to clinopyroxene in omp-granulite and in eclogite with a lower Mg# and less Ca-Cations. The boundary between the two groups is slightly blurred by clinopyroxene from the eclogite layer at Mt. Richard (Fig. 9, sample BS1003B) which has a Mg# and Ca-Cation amount similar to the garnetite-pyroxenite. A high Mg# might result from early crystallisation at high temperatures in a compositionally different environment than clinopyroxene with a lower Mg#. This supports the model of the igneous cumulate character of the layered xenolith.

On the other hand metamorphic processes are conceivable in which an exchange of Ca, Mg and Fe involving olivine leads to a similar major element composition. However, no textural evidence points into that direction.

6.3.3 Rare earth elements in garnet

There are two possibilities to explain the REE pattern in garnet. One is to regard garnet in different rock types of BOG as a sequence from one continuous fractionation process. The other way is to take variable patterns as evidence for different origins, metamorphic and igneous.

A fan-like stretched out sequence of HREE-patterns comparable to Fig. 32, which includes all four rock types, has been examined within zones of single metamorphic garnet grains from experiments with Norwegian ultrahigh pressure rocks (Konrad-Schmolke et al., 2008). The change from high HREE concentrations in garnet-cores to HREE depletion in garnet-rims was explained with increasing HREE depletion of the environment from which garnet crystallized.

It is conceivable that a similar pattern of increasing HREE depletion in igneous garnet can form from fractional crystallisation in an evolving magma. Late grown garnets are depleted in HREE because the magma progressively becomes depleted in HREE during the process of garnet crystallisation. If this model is applied to the REE-patterns presented in this study (Fig. 32), then garnet in the garnetite represents a stage of early growth whereas garnet in the granulite crystallized later. Garnet in eclogite and pyroxenite would then represent the intermediate stage. In this case all garnet could have crystallized from the same melt.

This interpretation fits well for the HREE pattern of garnet in garnetite but is in conflict with the metamorphic structure of garnet forming coronae around omphacite in the omp-granulite (Fig. 10). Furthermore it does not account for the positive Eu anomaly of garnet in omp-granulite and in eclogite. The latter indicates either an origin from a magma which was created by batch melting of a plagioclase source or it could be inherited from plagioclase by metamorphic breakdown. In any case it suggests a different origin of garnet in eclogite and omp-granulite opposed to garnet in garnetite and pyroxenite.

Watton (2009) only analysed two garnet grains in omp-granulite very close to a large garnet from a plagioclase vein (Fig. 32). These analyses probably just give the trace element

composition of garnet within the reaction zone of a vein and do not represent the garnet composition in equi-granular clusters with omphacite nor in metamorphic garnet forming the coronae. More analyses of the various textural types of garnet identified in this study are needed to address the question about their origin in a more accurate way.

6.2.4 Recalculated liquid

We may assume that the protolith of the BOG was formed after fractional crystallisation, accumulation and delamination of high amounts of garnet and clinopyroxene, comparable to what has been suggested for the Sierra Nevada (Fig. 42). In this scenario early crystallized high density minerals like garnet and clinopyroxene descend to the bottom of the magma chamber. The remaining liquid eventually solidifies to a rock of andesitic composition, comparable to the BOG. The REE pattern of the melt calculated to be in equilibrium with the cumulate phases should be congruent with the whole rock REE pattern of the BOG.

There is in fact congruence from Nd to Dy (Fig. 36) but in two sections the whole rock values of BOG are higher in REE than the melts calculated from garnetite and pyroxenite. This can be interpreted as an indicator for the BOG containing a component of cumulate of garnet and clinopyroxene.

As stated before, such interpretations must be made with caution since the model of an igneous origin from a single magma may be too simple. This becomes obvious by comparing the calculated melts of garnet and pyroxene in ultramafic xenoliths (eclogite and garnetite-pyroxenite). If garnet and clinopyroxene had mutually crystallized from the same liquid then the recalculated liquid should be the same. But this is not the case. Thus these minerals could be of different origin and just have assembled in a cumulate. But incongruence could also result from use of inadequate partition coefficients. The layered garnetite-pyroxenite could even be the metamorphic product from an olivine bearing rock. In that case the whole approach would be wrong. On the other hand there is no structural evidence in the layered garnetite-pyroxenite for any replacement of olivine or any other mineral. Therefore a metamorphic origin of the layered xenolith seems unlikely.

6.3 Interpretation of Pb/U and Hf data

Ages of other WFO plutons are: Worsely Pluton of 124 ±1 Ma (Tulloch & Kimborough, 2003), 122 ±2 and 124 ±3 Ma (Hollis et al., 2004), 123 ±1Ma(Bolhar et al., 2008) and 126 ±2 Ma (Muir et al., 1998). Alibone et al. (2009) describe the following field observations which refer to the relative age of the BOG:

"Both the Resolution Orthogneiss and the Malaspina Pluton are inferred to intrude the Breaksea Orthogneiss. Xenoliths of Breaksea Orthogneiss meta-diorite with omphacite granulite assemblages and meta-gabbro-norite with eclogite assemblages up to several hundred metres across occur within the Resolution Orthogneiss. Rare dikes of garnet, two-pyroxene diorite similar to the Malaspina Pluton, cut layering in the Breaksea Orthogneiss. Retrograde amphibolite facies ductile shear zones that locally cut Breaksea Orthogneiss are texturally and mineralogically similar to the foliated dikes of Resolution Orthogneiss which also cut Breaksea Orthogneiss."

Therefore an age older than the Malaspina Pluton and the Resolution Orthogneiss is expected. The Resolution Orthogneiss has not yet been dated but an age of 116 +/-1 Ma (Tulloch & Kimborough, 2003) and 115 +/-2 Ma (Hollis et al., 2004) has been determined for the Malaspina Pluton.

The age of 116 +/-0.51Ma determined for the BOG in this study is slightly higher than that of the Malaspina pluton. This is in agreement with field observations. But the data smear from 121Ma to 101Ma, which suggests that the Zircon grains in fact are older than 116 Ma. Two reasons for that may be found in the shapes of zircon grains: The bigger angular grains probably are igneous zircons which suffered from Pb-loss while the rounded shape of the small zircon grains is a typical metamorphic shape in granulite. These grains are probably neo-crystallized and their age indicates the time of the S_1 metamorphism. More evidence for the metamorphic nature of the rounded grains can be found in the amounts of Y in garnet (39-51ppm) compared to clinopyroxene (0.8-2.7) and in plagioclase (<0.2ppm) of the same rock (sample 0905B electronic data base). This combined with a median of 0.0243wt% YO_2 in rounded grains and of 0.0389wt% in angular grains, indicates a loss of Y in zircon and an intake by garnet during metamorphism (S_1). At the same time this can be taken as an additional support for the garnet from sample 0905B as being metamorphic. Values of (176-Hf/177-Hf initial) ranging from 0.282761 to 0.282984 indicate that the source is partly from the mantle and not only from the crust as indicated by Sr/Y ratio (see Chapter 6.2.1).

6.4 Hypothesis on the origin of different garnets in the BOG and of the layered garnetite-pyroxenite xenolith

The observations and analyses presented in this study can be summarized in a hypothesis on the origin of the layered pyroxenite-garnetite and of the three garnet populations in the BOG. A prerequisite to accomplish this task is to decide if the garnets in omp-granulite and in the layered garnetite-pyroxenite are igneous or metamorphic.

In general garnet is a metamorphic mineral characteristic for granulite and eclogite facies. But at high P-T conditions it can also crystallize from a magma and form igneous rocks. A P-T phase diagram for a basalt from NW North America (Fig. 40a) shows that at 1.8 GPa clinopyroxene crystallizes at first and is followed by garnet and plagioclase. A comparison of whole rock compositions of this Snake River Basalt (Shervais & Vetter, 2009) and the omp-granulite (BOG) is presented in Fig. 40b. In addition to that a CIPW-norm calculation has been carried out for both rock types (see appendix 8). CIPW-norm values and a comparison of major element compositions (Fig 40b) show that the Snake River basalt is more mafic than the average omp-granulite which tends to be of a dioritic to gabbroic composition. But taking into account an early crystallisation of mafic minerals like clinopyroxene and garnet and their accumulation at the base of the magma chamber, it is reasonable to assume that the liquid from which they crystallized and accumulated was more mafic than the remaining omp-granulite.

Melting experiments with websterites undertaken by Müntener et al. (2001) (composition see attached electronic data base) show that andesitic rocks can form from more mafic liquids after crystallisation and extraction of pyroxene and garnet by accumulation. These experiments and experiments of other workers which have delivered comparable results were carried out lower pressure of 1.2 GPa though (see Chap. 3.3.2).

However, garnet can also be formed by metamorphic reaction involving minerals like plagioclase, amphibole, pyroxene and olivine. Therefore only textural and geochemical analyses are able to give evidence if a garnet is igneous or metamorphic. An overview of evidence which not in every case is unambiguous is given in Tab. 2.

6.4.1 Garnet in omphacite-granulite

The trend in the TAS diagram (Fig. 21) and the varying modes of garnet and clinopyroxene observed in the field can be taken as evidence for the BOG involving cumulate processes. High modes of mafic minerals represent higher degrees of accumulation whereas more felsic areas represent lower degrees of accumulation. Layers of eclogite (Fig. 9) within omp-granulite are areas with high degrees of accumulation.

Equi-granular garnet-clinopyroxene clusters

Taking into account the results of melting experiments mentioned above, it is possible that garnet and omphacite crystallized more or less simultaneously as igneous minerals. Due to their high density they subsided in the melt before crystallisation of plagioclase and finally came to a stop when plagioclase crystallized and the liquid reached solidus.

Fig. 43 shows that from a rough quantitative approach based on data from Watton (2009), it is also possible to form metamorphic equi-granular garnet-omphacite clusters from pargasite, clinopyroxene and orthopyroxene. However there is still a surplus of 15wt% SiO_2 and 5wt% MgO. Furthermore approximately 5wt% of H_2O which would get released by this reaction should have an impact on the mineralogy and texture. H_2O increases the pressure and consequently can lead to a breakdown of plagioclase. Because of the absence of any replacement structures or signs of plagioclase breakdown in and around these assemblages it is rather likely that they are of igneous origin.

Garnet in coronae around omphacite

The textural setting in coronae around omphacite, combined with the presence of quartz inclusions, the lower amount of Ca-Cations and lower Mg# give strong evidence to call this garnet (Fig. 10) a metamorphic mineral.

Garnet along veins

Regarding the REE-pattern with a positive Eu-anomaly those garnet grains might have crystallized as igneous minerals from a plagioclase source. But the gradational boundaries of the veins (Fig. 7) suggest an origin syntectonic with S_1 and it is likely that they crystallized

from a peritectic liquid formed by the metamorphic breakdown of plagioclase. The break down of plagioclase is expected to occur close to the boundary of eclogite facies.

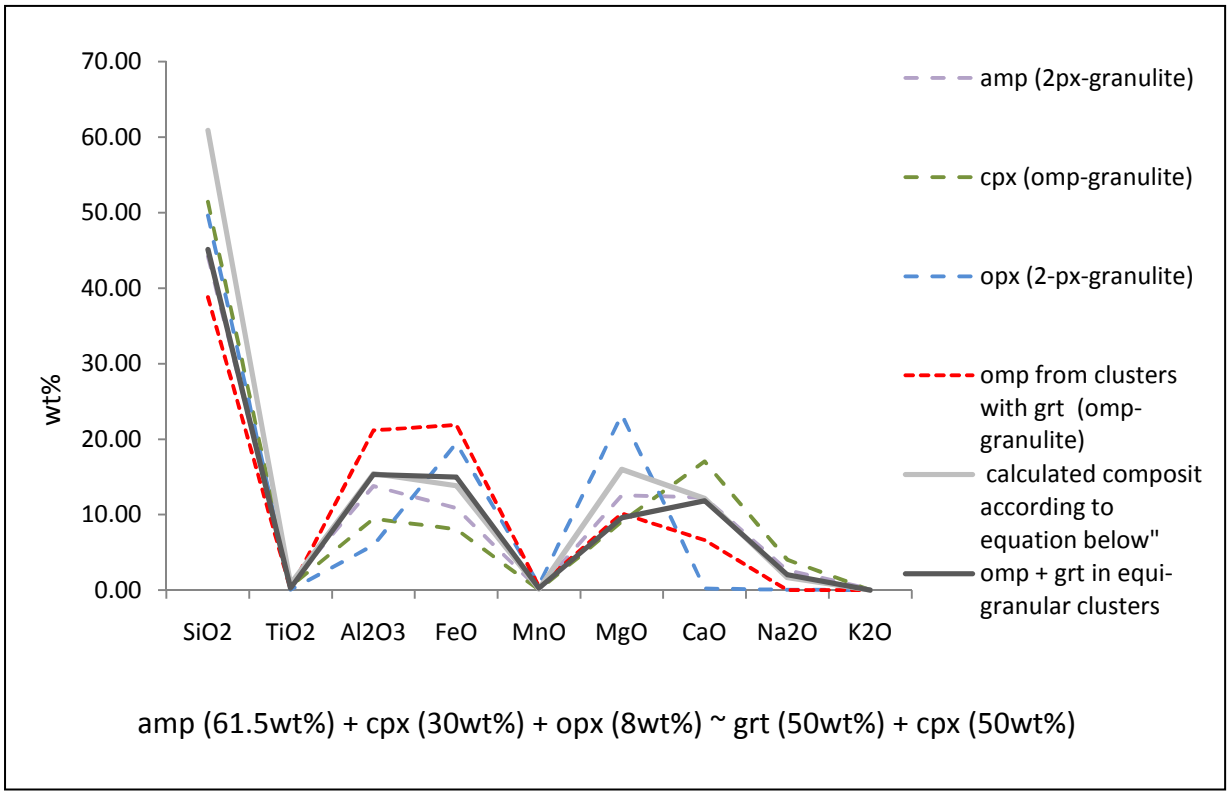

Fig. 43: Model for the metamorphic origin of equi-ganular grt-cpx clusters. Major element composition of amphibole, garnet pyroxene in BOG. The calculation below shows that quantitatively it is possible to form garnet-clinopyroxene assemblages from amphibole, clinopyroxene and orthopyroxene.

6.4.2 Layered pyroxenite-garnetite

As discussed before, the first minerals which crystallize from a basaltic magma at P-T conditions at 60 km depth (1.8 GPa) are clinopyroxene and garnet (Fig. 40a). The densities allow a mutual sinking of these minerals and the formation of an ultramafic cumulate at deep parts of a magma chamber. The coexistence of garnetite and pyroxenite is in accordance with the origin of these minerals under similar P-T conditions. The ultramafic and nearly mono-mineralic composition of the layers suggests an origin as early cumulates. Euhedral inclusions of garnet in clinopyroxene and vice versa support the model of simultaneous crystallization from the same liquid.

The layers can be explained by the double diffusion model (Fig. 44) described in Winter (2009). It says that the alternation of mono-mineralic layers is controlled by changes of buoyancy resulting from differences in density due to varying temperatures. The antagonistic behaviour of descend due to gravity and ascend due to lower density because of high temperature, leads to multiple convection cells. These are preserved in the layers. The flame-like shape of boundaries between layers supports the explanation of an origin from a liquid in motion.

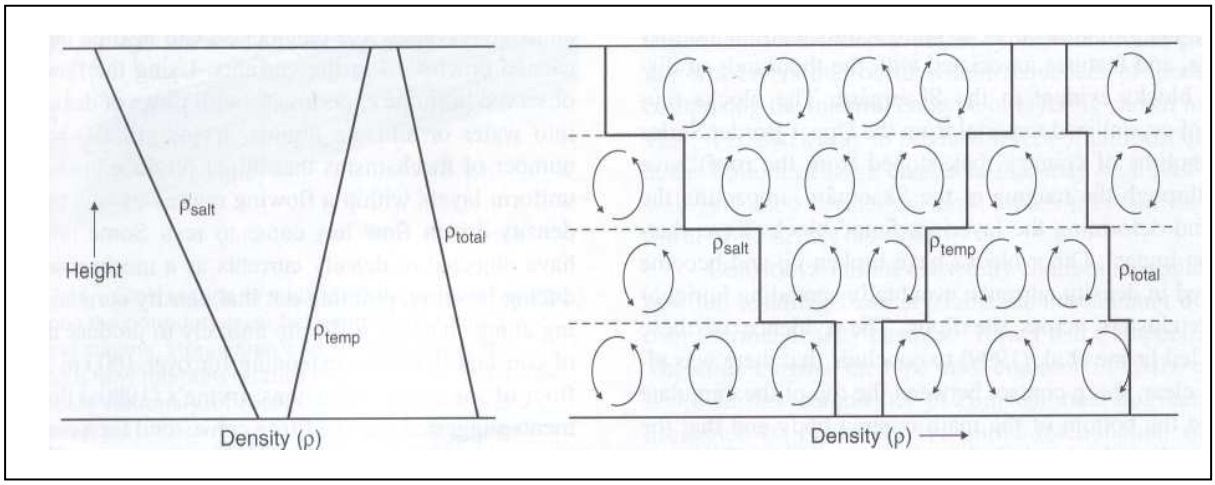

Fig. 44: Double diffusion model for the formation of layers in mafic layered intrusions (Winter, 2009).

Resorption structures in clinopyroxene are in accordance to experimental results of Müntener et al. (2001), Alonso et al. (2009), Wolf & Wyllie (1993), DeBari & Coleman (1989) Lee et al. (2006) and Thompson (1972) which all say that clinopyroxene crystallizes slightly earlier than garnet at pressures above 1GPa (and at 1.8 GPa) and temperatures above 850°C. Therefore it is possible that pyroxene crystallized at first and was followed by garnet. Both sank and mingled in a cumulate which became layered by double diffusion convection. Since garnet still crystallizes when clinopyroxene also has already precipitated, a part of the garnet in the garnetite layer may have formed from the inter-cumulate liquid. This is most probably true for the garnet forming films within the pyroxenite layer. Due to the closeness of clinopyroxene and garnet crystallization temperatures small amounts of clinopyroxene became resorbed in the inter-cumulate liquid. Higher Ca-Cations in garnet films and in

garnet inclusions in pyroxenite together with the presence of resorption structures in clinopyroxene at the contact of layers supports this.

The igneous character of the garnetite-pyroxenite is also indicated by the REE pattern of garnet (Fig. 32) with HREE enrichment in garnetite and a fractional trend towards HREE depletion in garnet in pyroxenite, comparable to Fig. 43.

However it is once again conceivable that the layered xenolith is a metamorphic rock. The layered structure and the cumulate nature could still be inherited properties from a protolith. But no textural evidence can be seen to support this hypothesis. Therefore it seems not very probable.

It is possible that the xenolith is cognate and formed from the same magma as the host rock. Cumulate properties of the omp-granulite like the presence of igneous garnet which occurs in varying modes and in cumulate layers would support this hypothesis. In this case the REE patterns of garnet in garnetite and in omp-granulite could be interpreted as part of one sequence with early garnet containing high HREE in the garnetite and late garnet with HREE depletion in the omp-granulite. This is a possibility but no evidence for this relation has been found to support it nor is there any evidence which would help to rule it out.

Rock Mineral	Igneous character	Igneous cumulate character	Metamorphic character
Omp-granulite Colours indicate evidence specifically attributed to one of the following structural grt types: Vein-grt Coronae-grt Cluster-grt	**Field observations** • Compositional layering. • Grt bearing plg-veins. **Thin section** • Lack of replacement textures in omp-grt clusters. **Geochemistry** • positive Eu anomaly in grt suggests origin from plg source. • HREE depletion in grt relative to grt in garnetite and pyroxenite, suggests later formation from same melt.	**Field observations** • Varying modes of mafic minerals (grt, omp) • Eclogite layers on Mt. Richards **Thin section** • Resorption textures in eclogite layers (ovoid cpx inclusions and embayments of grt in cpx). **Geochemistry** • Trend of TAS running from monzo-diorite over gabbro into ultramafic composition. • HREE depletion in grt relative to grt in garnetite and pyroxenite, suggests formation as later grt generation in melt. • Similar REE-pattern in all cpx.	**Field observations** • Foliation • syntectonic structure of grt bearing veins (gradational boundaries). • grt-coronae around omp mineral grains. **Thin section** • qtz inclusions in grt forming coronae around omp. **Geochemistry** • high Ca in grt forming coronae around omp. • positive Eu anomaly in grt suggests formation from plg. • HREE depletion suggests inheritance from other minerals (cpx, hbl) • Similar major element composition of vein grt and cluster grt. • Y loss in zircon and high Y values in grt compared to cpx and plg.
Xenolith of layered garnetite-pyroxenite	**Field observations** • Layered structure interpreted as result from double diffusion convection. **Thin section** • Lack of replacement textures. **Geochemistry** • HREE enriched REE pattern, characteristic for igneous grt.	**Field observations** • Mono-mineralic composition of layers. • flow pattern of layers. **Thin section** • Resorption structures close to layer boundary suggesting later formation of grt and partly formation from inter-cumulate liquid. **Geochemistry** • Ultramafic composition of xenolith. • High Ca in grt veins in pyroxenite suggesting origin from inter-cumulate liquid. • Similar REE-pattern in all cpx.	**Field observations** • Layered structure interpreted as relict of layering in protolith is conceivable but no evidence found.

Tab. 2: Overview of evidence for either an igneous, cumulate igneous or metamorphic character of the omp-granulite and the layered garnetite-pyroxenite. Evidence which may be interpreted in opposing ways is coloured.

3. Conclusion

There is adequate evidence that two of the three textural types of garnet in the omp-granulite are metamorphic. These are the textural setting and the REE pattern of larger garnet grains along plagioclase veins and the major element composition of garnet forming coronae around omphacite grains.

The origin of garnet in equi-granular clusters with omphacite cannot clearly be defined. However, experimental results from other workers indicate that garnet and clinopyroxene crystallize at first from melts under P-T conditions similar to those defined for the BOG. Because of their high density these two minerals may descend towards the base of the magma chamber. Consequently their mode will be higher in deeper parts and lower in upper parts of the magma chamber. This is in accordance to the varying amounts of garnet-omphacite clusters in the omp-granulite. It is conceivable that these clusters are the metamorphic product of another high density mineral which accumulated in the magma chamber. But no observation made in this study gives evidence which points toward this direction. Thus from the perspective of this study it seems reasonable to assume that the equi-granular garnet-omphacite clusters are igneous.

The ultramafic character and the mono-mineralic composition combined with the REE-pattern and texture suggest that the layered xenolith is of igneous origin and represents a cumulate from the base of a magma chamber. The REE-pattern of clinopyroxene is the same in omp-granulite and in the xenolith. But there is no further evidence which allows deciding if it formed from the same magma as the omp-granulite.

Only a limited selection of trace element data from garnet in omp-granulite was available for this study. The grains analysed by Watton (2009) come from very close or even within a plagioclase vein.

More evidence about the relation between the xenolith and BOG, and at the same time of the origin of garnet in equi-granular clusters could be produced by trace element analyses in all three structural types of garnet. In addition to that an age determination of the xenolith would allow a correlation with the host rock. Maybe future workers will find less complex zircon mineral grains in the BOG which reveal an unambiguous age.

References

Allibone, A.H. Jorgens, R. Turnbull, I.M. Milan, L. A. Dazcko, N.R. De Paoli, M.C. and Tulloch, A.J. 2009. Plutonic rocks of western Fjordland, New Zealand: field relations, geochemistry, correlation and nomenclature. New Zealand Journal of Geology and Geophysics, volume 52, 101-148.

Alonso-Perez, R. and Müntener, O. and Ulmer, P., 2009. Igneous garnet and amphibole fractionation in the roots of island arcs: experimental constraints on andesitic liquids. Contributions to Mineral Petrology 157, 541-558.

Bolhar, R. Weaver, S.D. Palin, J.M. Cole, J.W and Paterson, L.A. Systematics of Zircon crystallisation in Cretaceous Separation Point Suite, Fiordland, New Zealand, using U/Pb isotopes, REE and Ti geothermometry. 2008. Contributions to Mineral Petrology 156, 133-160.

Carroll, S. 2005. Plutonism and metamorphism at the root of a Cretaceous magmatic arc, Fiordland New Zealand. Honours, BSc. Presented to the Department of Earth and Planetary Science, Macquarie University. Unpublished.

Clarke, G.L., 2002. The Geology of Australia. Encyclopedia of Life Support Systems. Online: www.eolss.net

Cox K.G., Bell, J.D. and Pankhurst, R.J. 1979, The interpretation of igneous rocks. George, Allen and Unwin, London.

DeBari, S.M. and Coleman, R.G., 1989. Examination of the deep levels of an island arc: evidence from the Tonsina ultra-mafic assemblage, Tonsina, Alaska. Journal of Geophysical Research 94, 4373-4391.

Deer, W.A. Howie, R.A. and Zussmann, J. 1992. Introduction to the rock forming minerals. Harlow, Essex, England : Longman Scientific & Technical ; New York, NY : Wiley. (2nd edition)

De Paoli, M.C. Clarke, G.L. Klepeis, K.A. Allibone, A.H. and Turnbull, I.M. 2009. The Eclogite-Granulite Transition: Mafic and Intermediate Assemblages at Break Sea Sound, New Zealand. Journal of Petrology, volume 50, 2307-2343.

Ducea, M.N. and Saleeby, J.B., 1996. Buoyancy sources for a large, unrooted mountain range, the Sierra Nevada, California: Evidence from xenoliths thermobarometry. Journal of Geophysical Research 101, 8229-8244.

Fujimaki, H. Tatsumoto, M. and Aoki, K. 1984. Partition coefficients of Hf, Zr and REE between phenocrysts and groundmasses. Proceedings of the fourtheenth lunar and planetary science conference, Part 2. Journal of Geophysical Research, 89, Suppl. B662-672.

Graham, I.J (chief editor). 2008. A Continent on the Move, New Zealand Geoscience into the 21th century. Published by the Geological Society of New Zealand in association with GNS Science.

Green, T.H. and Pearson, N.J. 1983. Effect of pressure on rare earth element partition coefficients in common magmas. Letters to nature, Natur vol. 305, 414-416.

Griffin, W.L. and Carswell, D.A. and Nixon, P.H., 1979. Lower-Crustal Granulites and Eclogites from Lesotho, Southern Africa.

Hollis, J.A. Clarke G.L. Klepeis K. A. Daczko, N. R. and Ireland T. R. 2004. The regional significance of Cretaceous magmatism and metamorphism in Fiordland, New Zealand, from U–Pb zircon geochronology. Journal of Metamorphic Geology, Volume 22 Issue 7, 607 – 627.

Irvine, T.L. 1980. Magmatic density currents and cumulus processes. American Journal of Science 280A, 1-58.

Konrad-Schmolke, M. Zack, T. O'Brian, P.J., Jacob, D.E. 2008. Combined thermodynamic and rare earth element modeling of garnet growth during subduction: Examples from ultrahigh-pressure eclogite of Western Gneiss Region, Norway. Earth and Planetary Science Letters 272, 488-498.

Lee, C.T.A. and Cheng, X. and Horodyskyj, U., 2006. The development and refinement of continental arcs by basaltic magmatism, garnet pyroxenite accumulation, basaltic recherché and delamination: insights from the Sierra Nevada, California. Contributions to Mineral Petrology 151, 222-242.

McCallum, I.S. Raedeke and D. Mdezh, A.E. 1980. Investigations of the Stillwater Complex: Part I. Stratigraphy and structure of the Banded Zone. American Journal of Science 280A, 59-87.

McDonough, W.F., Sun, S. Ringwood, A.E. Jagouth, E. and Hofmann, A.W. 1991. K, Rb and Cs in the earth and moon and the evolution of the earth's mantle. Geochim. Cosmochim Acta, Ross Taylor Symposium Volume.

Muir, RJ; Ireland, TR; Weaver, SD; Bradshaw, JD; Evans, JA; Eby, GN; Shelley, D. 1998. Geochronology and geochemistry of a Mesozoic magmatic arc system, Fiordland, New Zealand. Journal of the geological society, 155: 1037-1052

Müntener, O. and Kelemen, P.B. and Grove, T.L., 2001. The role of H_2O during crystallization of primitive arc magmas under uppermost mantle conditions and genesis of igneous pyroxenites: an experimental study. Contributions to Mineral Petrology 141, 643-658.

Rey, P.F. and Müller, R.D. 2010. Fragmentation of active continental plate margins owing to the buoyancy of the mantle wedge. Nature Geoscience, vol. 3, 257-261.

Rollinson, H.R. 1993. Using Geochemical Data. Evaluation, presentation, interpretation. Longman scientific & technical, New York.

Sharpe, M.R. 1985. Strontium isotope evidence for preserved density stratification in the main zone of the Bushveld Complex, South Africa. Nature vol. 316, 119-126.

Shervais, W.J. and Vetter, S.K. 2009. High-K alkali basalt of the western Snake River Plain (Idaho): Abrupt transition from tholeiithic to mildly alkaline plume derived basalts. Journal of Volcanology and Thermal Research. 188, 141-152.

Thompson, R.N. 1972. Melting behaviour of two Snake River lavas at pressures up to 35 kb. Carnegie Institution Washington, Year Book, 71, 406-410.

Tulloch, A.J.; Kimbrough, D.L. 2003. Paired plutonic belts in convergent margins and the development of high Sr/Y magmatism : Peninsular Ranges batholith of Baja-California and Median batholith of New Zealand. p. 275-295 IN: Johnson, S.E.; Paterson, S.R.; Fletcher, J.M.; Girty, G.H.; Kimbrough, D.L.; Martin-Barajas, A. (eds) *Tectonic evolution of northwestern Mexico and the southwestern USA.* Boulder, Colo., USA: Geological Society of America. *Special papers / Geological Society of America 374.*

Watton, J. 2009. Petrographic and geochemical characterisation of the Break Sea Orthogneiss, Fjordland, New Zealand. Honours, BSc. Presented to the Department of Earth and Planetary Science, Macquarie University. Unpublished.

Winter, J. D. 2009. Principles of igneous and metamorphic petrology, second edition, Prentice Hall, New Jersey.

Wolf, M.B. Wyllie, P.J. 1993. Garnet Growth during Amphibolite Anatexis: Implications of a Garnetiferous Restite. The Journal of Geology, 1993, volume 101, p. 357–373.

Appendix 1 – EMP garnet

Rocktype	omp-granulite									
Sample	BS1008A grt corona 1 around cpx	BS1008A grt corona 1 around cpx	BS1008A grt corona 1 around cpx	BS1008A grt corona 1 around cpx	BS1008A grt corona 1 around cpx	BS1008A grt corona 1 around cpx	BS1008A grt corona 1 around cpx	BS1008A grt corona 1 around cpx	BS1008A grt corona 1 around cpx	BS1008A grt corona 1 around cpx
SiO2	39.68	39.82	39.55	39.64	39.51	39.32	39.43	39.41	39.50	39.07
TiO2	0.05	0.07	0.07	0.05	0.05	0.08	0.11	0.06	0.04	0.09
Al2O3	21.50	21.67	21.65	21.57	21.51	21.49	21.19	21.35	21.26	21.59
Cr2O3	0.00	0.00	0.00	0.00	0.01	0.01	0.06	0.00	0.00	0.00
FeO	20.75	21.08	20.45	21.23	21.13	21.90	22.61	21.31	21.41	21.91
MnO	0.45	0.48	0.48	0.49	0.44	0.49	0.43	0.45	0.47	0.46
MgO	9.36	10.00	9.08	9.31	9.24	9.44	8.42	8.69	9.37	9.40
CaO	8.55	7.79	8.74	8.15	8.46	7.64	8.18	8.94	8.05	7.66
Na2O	0.04	0.13	0.02	0.03	0.02	0.04	0.02	0.02	0.03	0.03
K2O	0.01	0.00	0.00	0.01	0.01	0.01	0.00	0.00	0.01	0.01
Total	**100.39**	**101.03**	**100.04**	**100.49**	**100.39**	**100.42**	**100.44**	**100.24**	**100.15**	**100.21**
Num ox	12.00	12.00	12.00	12.00	12.00	12.00	12.00	12.00	12.00	12.00
Si	3.01	3.00	3.01	3.00	3.00	2.99	3.01	3.00	3.01	2.98
Ti	0.00	0.00	0.00	0.00	0.00	0.00	0.01	0.00	0.00	0.00
Al	1.92	1.92	1.94	1.93	1.93	1.93	1.91	1.92	1.91	1.94
Cr	0.00	0.00	0.00	0.00	0.00	0.00	0.00	0.00	0.00	0.00
Fe3+	0.00	0.00	0.00	0.00	0.00	0.00	0.00	0.00	0.00	0.00
Fe2+	1.31	1.33	1.30	1.35	1.34	1.39	1.44	1.36	1.36	1.40
Mn	0.03	0.03	0.03	0.03	0.03	0.03	0.03	0.03	0.03	0.03
Mg	1.06	1.12	1.03	1.05	1.05	1.07	0.96	0.99	1.06	1.07
Ca	0.69	0.63	0.71	0.66	0.69	0.62	0.67	0.73	0.66	0.63
Na	0.01	0.02	0.00	0.00	0.00	0.01	0.00	0.00	0.00	0.00
K	0.00	0.00	0.00	0.00	0.00	0.00	0.00	0.00	0.00	0.00
Ni	0.00	0.00	0.00	0.00	0.00	0.00	0.00	0.00	0.00	0.00
Total	**8.03**	**8.05**	**8.02**	**8.03**	**8.04**	**8.05**	**8.03**	**8.03**	**8.04**	**8.05**
XAlm	0.42	0.43	0.42	0.44	0.43	0.45	0.47	0.44	0.44	0.45
XPyp	0.34	0.36	0.34	0.34	0.34	0.34	0.31	0.32	0.34	0.34
XGrs	0.22	0.20	0.23	0.21	0.22	0.20	0.22	0.24	0.21	0.20
XSps	0.01	0.01	0.01	0.01	0.01	0.01	0.01	0.01	0.01	0.01

Rocktype	omp-granulite									
Sample	BS1008A grt corona 1 around cpx	BS1008A grt corona 1 around cpx	BS1008A grt corona 1 around cpx	BS1008A grt corona 1 around cpx	BS1008A grt corona 1 around cpx	BS1008A grt corona 1 around cpx	BS1008A grt corona 1 around cpx	BS1008A grt corona 1 around cpx	BS1008A grt corona 1 around cpx	BS1008A grt corona 1 around cpx
SiO2	39.27	39.10	39.24	39.50	39.40	39.31	39.44	39.61	39.47	39.47
TiO2	0.08	0.05	0.06	0.08	0.03	0.06	0.06	0.06	0.09	0.08
Al2O3	21.51	21.48	21.68	21.44	21.56	21.45	21.46	21.43	21.55	21.46
Cr2O3	0.03	0.00	0.00	0.00	0.00	0.00	0.00	0.02	0.00	0.04
FeO	21.73	21.56	20.76	21.21	21.00	20.70	20.70	21.25	21.25	21.24
MnO	0.47	0.41	0.46	0.50	0.45	0.47	0.47	0.49	0.49	0.53
MgO	9.18	8.63	9.05	9.32	9.44	9.09	8.98	9.49	9.41	9.33
CaO	7.97	8.81	8.93	8.07	8.21	8.84	9.07	8.17	8.08	8.18
Na2O	0.02	0.02	0.03	0.03	0.02	0.02	0.01	0.02	0.02	0.01
K2O	0.00	0.00	0.01	0.02	0.01	0.00	0.01	0.00	0.00	0.00
Total	**100.26**	**100.05**	**100.23**	**100.16**	**100.12**	**99.95**	**100.19**	**100.55**	**100.37**	**100.34**
Num ox	12.00	12.00	12.00	12.00	12.00	12.00	12.00	12.00	12.00	12.00
Si	2.99	2.99	2.98	3.00	3.00	3.00	3.00	3.00	3.00	3.00
Ti	0.00	0.00	0.00	0.00	0.00	0.00	0.00	0.00	0.01	0.00
Al	1.93	1.94	1.94	1.92	1.93	1.93	1.92	1.91	1.93	1.92
Cr	0.00	0.00	0.00	0.00	0.00	0.00	0.00	0.00	0.00	0.00
Fe3+	0.00	0.00	0.00	0.00	0.00	0.00	0.00	0.00	0.00	0.00
Fe2+	1.38	1.38	1.32	1.35	1.34	1.32	1.32	1.35	1.35	1.35
Mn	0.03	0.03	0.03	0.03	0.03	0.03	0.03	0.03	0.03	0.03
Mg	1.04	0.98	1.03	1.06	1.07	1.03	1.02	1.07	1.06	1.06
Ca	0.65	0.72	0.73	0.66	0.67	0.72	0.74	0.66	0.66	0.67
Na	0.00	0.00	0.00	0.00	0.00	0.00	0.00	0.00	0.00	0.00
K	0.00	0.00	0.00	0.00	0.00	0.00	0.00	0.00	0.00	0.00
Ni	0.00	0.00	0.00	0.00	0.00	0.00	0.00	0.00	0.00	0.00
Total	**8.04**	**8.04**	**8.04**	**8.03**	**8.04**	**8.04**	**8.03**	**8.04**	**8.04**	**8.04**
XAlm	0.45	0.44	0.43	0.44	0.43	0.42	0.42	0.43	0.43	0.43
XPyp	0.34	0.32	0.33	0.34	0.34	0.33	0.33	0.34	0.34	0.34
XGrs	0.21	0.23	0.23	0.21	0.22	0.23	0.24	0.21	0.21	0.21
XSps	0.01	0.01	0.01	0.01	0.01	0.01	0.01	0.01	0.01	0.01

Rocktype	omp-granulite									
Sample	BS1008A grt corona 1 around cpx	BS1008A grt corona 1 around cpx	BS1008A grt corona 1 around cpx	BS1008A grt corona 1 around cpx	BS1008A grt corona 1 around cpx	BS1008A grt corona 1 around cpx	BS1008A grt corona 1 around cpx	BS1008A grt corona 1 around cpx	BS1008A grt corona 1 around cpx	BS1008A grt corona 1 around cpx
SiO2	38.83	39.22	39.19	39.50	39.08	39.01	39.32	39.55	39.50	39.70
TiO2	0.08	0.05	0.03	0.05	0.06	0.06	0.04	0.05	0.07	0.06
Al2O3	21.30	21.29	21.51	21.24	21.11	21.44	21.45	21.67	21.53	21.41
Cr2O3	0.00	0.00	0.03	0.05	0.01	0.01	0.00	0.00	0.01	0.01
FeO	22.07	22.03	20.75	21.14	22.62	21.09	21.20	20.61	20.63	20.65
MnO	0.42	0.44	0.40	0.35	0.44	0.41	0.41	0.37	0.43	0.36
MgO	9.04	9.28	8.86	9.14	8.03	8.62	8.93	8.76	8.83	8.44
CaO	7.78	7.65	9.26	8.58	8.69	9.25	8.88	9.52	9.56	10.04
Na2O	0.03	0.04	0.03	0.03	0.02	0.01	0.00	0.02	0.02	0.02
K2O	0.01	0.01	0.01	0.01	0.01	0.00	0.01	0.01	0.01	0.01
Total	99.56	100.02	100.07	100.09	100.06	99.92	100.24	100.56	100.58	100.68
Num ox	12.00	12.00	12.00	12.00	12.00	12.00	12.00	12.00	12.00	12.00
Si	2.98	3.00	2.99	3.01	3.00	2.99	2.99	3.00	3.00	3.01
Ti	0.00	0.00	0.00	0.00	0.00	0.00	0.00	0.00	0.00	0.00
Al	1.93	1.92	1.93	1.91	1.91	1.93	1.93	1.94	1.93	1.91
Cr	0.00	0.00	0.00	0.00	0.00	0.00	0.00	0.00	0.00	0.00
Fe3+	0.00	0.00	0.00	0.00	0.00	0.00	0.00	0.00	0.00	0.00
Fe2+	1.42	1.41	1.32	1.35	1.45	1.35	1.35	1.31	1.31	1.31
Mn	0.03	0.03	0.03	0.02	0.03	0.03	0.03	0.02	0.03	0.02
Mg	1.04	1.06	1.01	1.04	0.92	0.98	1.01	0.99	1.00	0.95
Ca	0.64	0.63	0.76	0.70	0.72	0.76	0.73	0.77	0.78	0.82
Na	0.00	0.01	0.00	0.00	0.00	0.00	0.00	0.00	0.00	0.00
K	0.00	0.00	0.00	0.00	0.00	0.00	0.00	0.00	0.00	0.00
Ni	0.00	0.00	0.00	0.00	0.00	0.00	0.00	0.00	0.00	0.00
Total	8.05	8.04	8.04	8.04	8.04	8.04	8.04	8.03	8.04	8.03
XAlm	0.45	0.45	0.43	0.43	0.47	0.43	0.43	0.42	0.42	0.42
XPyp	0.33	0.34	0.32	0.33	0.29	0.32	0.33	0.32	0.32	0.31
XGrs	0.21	0.20	0.24	0.23	0.23	0.24	0.23	0.25	0.25	0.26
XSps	0.01	0.01	0.01	0.01	0.01	0.01	0.01	0.01	0.01	0.01

Rocktype	omp-granulite									
Sample	1008A inclusion in grt corona	1008A inclusion in grt corona	1008A inclusion in grt corona	1008A inclusion in grt corona	1008A inclusion in grt corona	1008A inclusion in grt corona	1008A inclusion in grt corona	BS1008A grt corona 2 around cpx	BS1008A grt corona 2 around cpx	BS1008A grt corona 2 around cpx
SiO2	39.30	39.28	99.07	99.16	39.32	99.36	98.96	38.72	39.69	39.20
TiO2	0.07	0.05	0.01	0.00	0.04	0.00	0.02	0.04	0.06	0.04
Al2O3	21.44	21.50	0.02	0.02	21.40	0.03	0.20	21.21	21.65	21.26
Cr2O3	0.02	0.02	0.00	0.03	0.02	0.00	0.02	0.01	0.00	0.00
FeO	21.30	21.10	0.57	0.45	20.53	0.48	0.52	20.90	20.28	21.01
MnO	0.40	0.38	0.00	0.00	0.47	0.01	0.00	0.47	0.44	0.48
MgO	8.89	8.46	0.00	0.00	8.76	0.00	0.00	9.66	9.95	9.16
CaO	9.04	9.70	0.03	0.03	9.21	0.03	0.08	7.98	7.95	8.43
Na2O	0.01	0.03	0.00	0.00	0.02	0.00	0.04	0.01	0.03	0.02
K2O	0.00	0.01	0.01	0.00	0.01	0.01	0.01	0.03	0.00	0.02
Total	100.46	100.54	99.72	99.69	99.78	99.92	99.86	99.03	100.06	99.63
Num ox	12.00	12.00	12.00	12.00	12.00	12.00	12.00	12.00	12.00	12.00
Si	2.99	2.99	5.98	5.99	3.00	5.98	5.97	2.98	3.01	3.00
Ti	0.00	0.00	0.00	0.00	0.00	0.00	0.00	0.00	0.00	0.00
Al	1.92	1.93	0.00	0.00	1.93	0.00	0.01	1.92	1.93	1.92
Cr	0.00	0.00	0.00	0.00	0.00	0.00	0.00	0.00	0.00	0.00
Fe3+	0.00	0.00	0.00	0.00	0.00	0.00	0.00	0.00	0.00	0.00
Fe2+	1.36	1.34	0.03	0.02	1.31	0.02	0.03	1.35	1.28	1.35
Mn	0.03	0.02	0.00	0.00	0.03	0.00	0.00	0.03	0.03	0.03
Mg	1.01	0.96	0.00	0.00	1.00	0.00	0.00	1.11	1.12	1.04
Ca	0.74	0.79	0.00	0.00	0.75	0.00	0.01	0.66	0.65	0.69
Na	0.00	0.01	0.00	0.00	0.00	0.00	0.01	0.00	0.00	0.00
K	0.00	0.00	0.00	0.00	0.00	0.00	0.00	0.00	0.00	0.00
Ni	0.00	0.00	0.00	0.00	0.00	0.00	0.00	0.00	0.00	0.00
Total	8.04	8.05	6.02	6.01	8.03	6.01	6.02	8.06	8.03	8.04
XAlm	0.43	0.43						0.43	0.42	0.43
XPyp	0.32	0.31	quartz	quartz	quartz	quartz	quartz	0.35	0.36	0.34
XGrs	0.24	0.25						0.21	0.21	0.22
XSps	0.01	0.01						0.01	0.01	0.01

Rocktype	omp-granulite									
Sample	BS1008A grt corona 2 around cpx	BS1008A grt corona 2 around cpx	BS1008A grt corona 2 around cpx	BS1008A grt corona 2 around cpx	BS1008A grt corona 2 around cpx	BS1008A grt corona 2 around cpx	BS1008A grt corona 2 around cpx	BS1008A grt corona 2 around cpx	BS1008A grt corona 2 around cpx	BS1008A grt corona 2 around cpx
SiO2	39.24	39.08	39.33	39.22	39.28	39.40	39.31	38.92	38.75	39.09
TiO2	0.04	0.04	0.02	0.04	0.07	0.10	0.05	0.08	0.05	0.08
Al2O3	21.42	21.21	21.41	21.38	21.38	21.31	21.21	21.34	21.20	21.30
Cr2O3	0.00	0.00	0.02	0.02	0.00	0.01	0.00	0.00	0.00	0.00
FeO	19.95	20.03	21.46	20.80	20.87	21.28	21.19	21.45	22.02	22.92
MnO	0.42	0.40	0.55	0.45	0.54	0.54	0.49	0.51	0.53	0.52
MgO	9.66	9.98	9.41	9.88	9.74	10.32	9.20	9.74	9.22	9.11
CaO	8.41	8.10	7.86	7.86	7.83	7.19	8.53	7.54	7.47	6.98
Na2O	0.03	0.02	0.02	0.01	0.03	0.03	0.02	0.03	0.01	0.03
K2O	0.00	0.00	0.00	0.00	0.01	0.01	0.00	0.01	0.00	0.01
Total	**99.18**	**98.85**	**100.09**	**99.67**	**99.75**	**100.19**	**100.00**	**99.60**	**99.26**	**100.03**
Num ox	12.00	12.00	12.00	12.00	12.00	12.00	12.00	12.00	12.00	12.00
Si	3.00	3.00	3.00	2.99	3.00	2.99	3.00	2.98	2.99	2.99
Ti	0.00	0.00	0.00	0.00	0.00	0.01	0.00	0.00	0.00	0.00
Al	1.93	1.92	1.92	1.92	1.92	1.91	1.91	1.93	1.93	1.92
Cr	0.00	0.00	0.00	0.00	0.00	0.00	0.00	0.00	0.00	0.00
Fe3+	0.00	0.00	0.00	0.00	0.00	0.00	0.00	0.00	0.00	0.00
Fe2+	1.28	1.29	1.37	1.33	1.33	1.35	1.35	1.37	1.42	1.47
Mn	0.03	0.03	0.04	0.03	0.03	0.03	0.03	0.03	0.03	0.03
Mg	1.10	1.14	1.07	1.12	1.11	1.17	1.05	1.11	1.06	1.04
Ca	0.69	0.67	0.64	0.64	0.64	0.59	0.70	0.62	0.62	0.57
Na	0.00	0.00	0.00	0.00	0.00	0.00	0.00	0.00	0.00	0.00
K	0.00	0.00	0.00	0.00	0.00	0.00	0.00	0.00	0.00	0.00
Ni	0.00	0.00	0.00	0.00	0.00	0.00	0.00	0.00	0.00	0.00
Total	**8.03**	**8.04**	**8.04**	**8.04**	**8.04**	**8.05**	**8.04**	**8.05**	**8.05**	**8.04**
XAlm	0.41	0.41	0.44	0.43	0.43	0.43	0.43	0.44	0.45	0.47
XPyp	0.36	0.37	0.34	0.36	0.36	0.37	0.33	0.35	0.34	0.33
XGrs	0.22	0.21	0.21	0.21	0.21	0.19	0.22	0.20	0.20	0.18
XSps	0.01	0.01	0.01	0.01	0.01	0.01	0.01	0.01	0.01	0.01

Rocktype	omp-granulite									
Sample	BS1008A big single grt along vein	BS1008A big single grt along vein	BS1008A big single grt along vein	BS1008A big single grt along vein	BS1008A big single grt along vein	BS1008A big single grt along vein	BS1008A big single grt along vein	BS1008A big single grt along vein	BS1008A big single grt along vein	BS1008A big single grt along vein
SiO2	39.24	39.55	39.55	39.13	39.38	39.53	39.28	39.11	39.58	38.98
TiO2	0.07	0.06	0.06	0.03	0.07	0.04	0.05	0.04	0.04	0.04
Al2O3	21.34	21.52	21.46	21.39	21.46	21.65	21.53	21.38	21.45	21.43
Cr2O3	0.00	0.02	0.01	0.00	0.00	0.02	0.00	0.03	0.00	0.02
FeO	21.48	21.50	21.78	21.90	21.79	21.95	21.77	21.85	21.84	21.70
MnO	0.68	0.67	0.66	0.75	0.65	0.71	0.70	0.68	0.67	0.69
MgO	10.25	10.35	10.39	10.33	10.51	10.41	10.63	10.35	10.39	10.09
CaO	6.95	6.72	6.62	6.36	6.36	6.31	6.45	6.38	6.34	6.89
Na2O	0.03	0.03	0.03	0.04	0.02	0.02	0.01	0.02	0.03	0.02
K2O	0.01	0.00	0.00	0.01	0.01	0.01	0.00	0.00	0.00	0.01
Total	**100.06**	**100.42**	**100.55**	**99.95**	**100.27**	**100.65**	**100.42**	**99.85**	**100.35**	**99.86**
Num ox	12.00	12.00	12.00	12.00	12.00	12.00	12.00	12.00	12.00	12.00
Si	2.99	3.00	2.99	2.98	2.99	2.99	2.98	2.98	3.00	2.98
Ti	0.00	0.00	0.00	0.00	0.00	0.00	0.00	0.00	0.00	0.00
Al	1.91	1.92	1.91	1.92	1.92	1.93	1.92	1.92	1.92	1.93
Cr	0.00	0.00	0.00	0.00	0.00	0.00	0.00	0.00	0.00	0.00
Fe3+	0.00	0.00	0.00	0.00	0.00	0.00	0.00	0.00	0.00	0.00
Fe2+	1.37	1.36	1.38	1.40	1.38	1.39	1.38	1.39	1.38	1.39
Mn	0.04	0.04	0.04	0.05	0.04	0.05	0.04	0.04	0.04	0.04
Mg	1.16	1.17	1.17	1.17	1.19	1.17	1.20	1.18	1.17	1.15
Ca	0.57	0.55	0.54	0.52	0.52	0.51	0.52	0.52	0.52	0.56
Na	0.00	0.00	0.00	0.01	0.00	0.00	0.00	0.00	0.01	0.00
K	0.00	0.00	0.00	0.00	0.00	0.00	0.00	0.00	0.00	0.00
Ni	0.00	0.00	0.00	0.00	0.00	0.00	0.00	0.00	0.00	0.00
Total	**8.05**	**8.04**	**8.05**	**8.06**	**8.05**	**8.05**	**8.06**	**8.05**	**8.04**	**8.06**
XAlm	0.44	0.44	0.44	0.45	0.44	0.45	0.44	0.44	0.44	0.44
XPyp	0.37	0.37	0.37	0.37	0.38	0.38	0.38	0.38	0.38	0.37
XGrs	0.18	0.18	0.17	0.17	0.17	0.16	0.17	0.17	0.17	0.18
XSps	0.01	0.01	0.01	0.02	0.01	0.01	0.01	0.01	0.01	0.01

Rocktype	omp-granulite									
Sample	BS1008A big single grt along vein	BS1008A big single grt along vein	BS1008A big single grt along vein	BS1008A big single grt along vein	BS1008A big single grt along vein	BS1008A big single grt along vein	BS1008A big single grt along vein	BS1008A big single grt along vein	BS1008A big single grt along vein	BS1008B grt in cluster with omp 1
SiO2	39.04	38.89	39.09	38.73	38.79	38.99	39.10	38.85	38.94	38.69
TiO2	0.06	0.16	0.07	0.07	0.03	0.02	0.02	0.03	0.02	0.06
Al2O3	21.39	21.20	21.36	21.02	21.11	21.22	21.18	21.25	21.31	21.09
Cr2O3	0.00	0.02	0.00	0.01	0.02	0.00	0.00	0.01	0.00	0.03
FeO	21.66	21.89	22.21	21.77	21.04	21.64	21.40	21.81	21.87	22.10
MnO	0.65	0.73	0.74	0.69	0.70	0.74	0.67	0.75	0.71	0.48
MgO	10.06	10.33	10.34	10.67	9.88	9.88	10.63	9.89	10.31	10.36
CaO	6.77	6.15	6.27	6.08	7.39	6.98	6.58	6.88	6.51	6.28
Na2O	0.04	0.04	0.02	0.03	0.02	0.00	0.00	0.01	0.00	0.04
K2O	0.01	0.00	0.00	0.00	0.00	0.00	0.00	0.01	0.00	0.02
Total	**99.69**	**99.41**	**100.11**	**99.06**	**98.97**	**99.49**	**99.58**	**99.50**	**99.67**	**99.15**
Num ox	12.00	12.00	12.00	12.00	12.00	12.00	12.00	12.00	12.00	12.00
Si	2.98	2.98	2.98	2.98	2.99	2.99	2.99	2.98	2.98	2.98
Ti	0.00	0.01	0.00	0.00	0.00	0.00	0.00	0.00	0.00	0.00
Al	1.93	1.92	1.92	1.91	1.92	1.92	1.91	1.92	1.92	1.91
Cr	0.00	0.00	0.00	0.00	0.00	0.00	0.00	0.00	0.00	0.00
Fe3+	0.00	0.00	0.00	0.00	0.00	0.00	0.00	0.00	0.00	0.00
Fe2+	1.39	1.40	1.42	1.40	1.36	1.39	1.37	1.40	1.40	1.42
Mn	0.04	0.05	0.05	0.05	0.05	0.05	0.04	0.05	0.05	0.03
Mg	1.15	1.18	1.18	1.22	1.13	1.13	1.21	1.13	1.18	1.19
Ca	0.55	0.51	0.51	0.50	0.61	0.57	0.54	0.57	0.53	0.52
Na	0.01	0.01	0.00	0.00	0.00	0.00	0.00	0.00	0.00	0.01
K	0.00	0.00	0.00	0.00	0.00	0.00	0.00	0.00	0.00	0.00
Ni	0.00	0.00	0.00	0.00	0.00	0.00	0.00	0.00	0.00	0.00
Total	**8.05**	**8.05**	**8.06**	**8.06**	**8.05**	**8.05**	**8.06**	**8.06**	**8.06**	**8.06**
XAlm	0.44	0.45	0.45	0.44	0.43	0.44	0.43	0.44	0.44	0.45
XPyp	0.37	0.38	0.37	0.39	0.36	0.36	0.38	0.36	0.37	0.38
XGrs	0.18	0.16	0.16	0.16	0.19	0.18	0.17	0.18	0.17	0.16
XSps	0.01	0.02	0.02	0.01	0.01	0.02	0.01	0.02	0.01	0.01

Rocktype	omp-granulite									
Sample	BS1008B grt in cluster with omp 1	BS1008B grt in cluster with omp 1	BS1008B grt in cluster with omp 1	BS1008B grt in cluster with omp 1	BS1008B grt in cluster with omp 1	BS1008B grt in cluster with omp 1	BS1008B grt in cluster with omp 1	BS1008B grt in cluster with omp 1	BS1008B grt in cluster with omp 1	BS1008B grt in cluster with omp 2 traverse
SiO2	39.08	39.27	39.43	39.12	39.18	39.29	39.05	39.39	39.20	38.88
TiO2	0.06	0.05	0.04	0.00	0.05	0.08	0.06	0.05	0.03	0.08
Al2O3	21.28	21.18	21.31	21.32	21.44	21.40	21.45	21.19	21.53	20.90
Cr2O3	0.03	0.01	0.01	0.00	0.03	0.00	0.02	0.02	0.00	0.06
FeO	22.05	22.48	22.46	22.14	22.16	22.03	22.17	22.09	22.45	22.24
MnO	0.49	0.46	0.51	0.54	0.53	0.53	0.50	0.44	0.47	0.51
MgO	10.24	10.28	10.26	10.50	10.28	10.32	10.41	10.39	10.41	10.20
CaO	6.14	6.17	6.09	6.13	6.05	6.24	6.10	6.15	6.09	6.24
Na2O	0.02	0.02	0.03	0.02	0.02	0.02	0.03	0.08	0.04	0.07
K2O	0.02	0.01	0.01	0.01	0.01	0.01	0.01	0.05	0.01	0.01
Total	**99.40**	**99.93**	**100.14**	**99.79**	**99.76**	**99.93**	**99.79**	**99.85**	**100.23**	**99.19**
Num ox	12.00	12.00	12.00	12.00	12.00	12.00	12.00	12.00	12.00	12.00
Si	2.99	3.00	3.00	2.99	2.99	2.99	2.98	3.00	2.98	2.99
Ti	0.00	0.00	0.00	0.00	0.00	0.00	0.00	0.00	0.00	0.00
Al	1.92	1.91	1.91	1.92	1.93	1.92	1.93	1.90	1.93	1.90
Cr	0.00	0.00	0.00	0.00	0.00	0.00	0.00	0.00	0.00	0.00
Fe3+	0.00	0.00	0.00	0.00	0.00	0.00	0.00	0.00	0.00	0.00
Fe2+	1.41	1.43	1.43	1.41	1.41	1.40	1.42	1.41	1.43	1.43
Mn	0.03	0.03	0.03	0.04	0.03	0.03	0.03	0.03	0.03	0.03
Mg	1.17	1.17	1.16	1.19	1.17	1.17	1.18	1.18	1.18	1.17
Ca	0.50	0.50	0.50	0.50	0.49	0.51	0.50	0.50	0.50	0.51
Na	0.00	0.00	0.00	0.00	0.00	0.00	0.00	0.01	0.01	0.01
K	0.00	0.00	0.00	0.00	0.00	0.00	0.00	0.00	0.00	0.00
Ni	0.00	0.00	0.00	0.00	0.00	0.00	0.00	0.00	0.00	0.00
Total	**8.04**	**8.05**	**8.04**	**8.06**	**8.04**	**8.04**	**8.05**	**8.05**	**8.05**	**8.06**
XAlm	0.45	0.46	0.46	0.45	0.45	0.45	0.45	0.45	0.46	0.45
XPyp	0.38	0.37	0.37	0.38	0.38	0.38	0.38	0.38	0.38	0.37
XGrs	0.16	0.16	0.16	0.16	0.16	0.16	0.16	0.16	0.16	0.16
XSps	0.01	0.01	0.01	0.01	0.01	0.01	0.01	0.01	0.01	0.01

Rocktype	omp-granulite									
Sample	BS1008B grt in cluster with omp 2 traverse	BS1008B grt in cluster with omp 2 traverse	BS1008B grt in cluster with omp 2 traverse	BS1008B grt in cluster with omp 2 traverse	BS1008B grt in cluster with omp 2 traverse	BS1008B grt in cluster with omp 2 traverse	BS1008B grt in cluster with omp 2 traverse	BS1008B grt in cluster with omp 2 traverse	BS1008B grt in cluster with omp 2 traverse	BS1008B grt in cluster with omp 2 traverse
SiO2	38.53	39.27	38.84	38.59	38.68	39.03	38.64	38.56	39.13	38.90
TiO2	0.11	0.15	0.15	0.13	0.11	0.15	0.14	0.10	0.12	0.17
Al2O3	21.03	21.14	21.08	20.97	21.01	21.16	21.40	21.16	21.30	21.15
Cr2O3	0.01	0.00	0.02	0.00	0.00	0.01	0.00	0.00	0.01	0.03
FeO	21.83	22.22	21.98	22.10	21.79	22.02	21.86	21.89	21.91	21.64
MnO	0.44	0.45	0.44	0.46	0.48	0.41	0.48	0.39	0.42	0.41
MgO	10.55	10.54	10.55	10.72	10.67	10.72	10.61	10.65	10.49	10.48
CaO	6.18	5.91	6.03	5.90	5.99	5.92	5.93	6.05	6.13	6.36
Na2O	0.05	0.04	0.06	0.04	0.05	0.06	0.06	0.04	0.04	0.04
K2O	0.01	0.02	0.01	0.01	0.02	0.00	0.00	0.01	0.00	0.00
Total	**98.76**	**99.75**	**99.16**	**98.92**	**98.81**	**99.48**	**99.12**	**98.84**	**99.55**	**99.18**
Num ox	12.00	12.00	12.00	12.00	12.00	12.00	12.00	12.00	12.00	12.00
Si	2.97	3.00	2.98	2.97	2.98	2.99	2.97	2.97	2.99	2.98
Ti	0.01	0.01	0.01	0.01	0.01	0.01	0.01	0.01	0.01	0.01
Al	1.91	1.90	1.91	1.91	1.91	1.91	1.94	1.92	1.92	1.91
Cr	0.00	0.00	0.00	0.00	0.00	0.00	0.00	0.00	0.00	0.00
Fe3+	0.00	0.00	0.00	0.00	0.00	0.00	0.00	0.00	0.00	0.00
Fe2+	1.41	1.42	1.41	1.43	1.40	1.41	1.40	1.41	1.40	1.39
Mn	0.03	0.03	0.03	0.03	0.03	0.03	0.03	0.03	0.03	0.03
Mg	1.21	1.20	1.21	1.23	1.23	1.22	1.21	1.22	1.19	1.20
Ca	0.51	0.48	0.50	0.49	0.49	0.49	0.49	0.50	0.50	0.52
Na	0.01	0.01	0.01	0.01	0.01	0.01	0.01	0.01	0.01	0.01
K	0.00	0.00	0.00	0.00	0.00	0.00	0.00	0.00	0.00	0.00
Ni	0.00	0.00	0.00	0.00	0.00	0.00	0.00	0.00	0.00	0.00
Total	**8.07**	**8.05**	**8.06**	**8.07**	**8.06**	**8.06**	**8.06**	**8.06**	**8.05**	**8.05**
XAlm	0.45	0.45	0.45	0.45	0.44	0.45	0.45	0.45	0.45	0.44
XPyp	0.38	0.38	0.38	0.39	0.39	0.39	0.39	0.39	0.38	0.38
XGrs	0.16	0.15	0.16	0.15	0.16	0.15	0.16	0.16	0.16	0.17
XSps	0.01	0.01	0.01	0.01	0.01	0.01	0.01	0.01	0.01	0.01

Rocktype	omp-granulite									
Sample	BS1008B grt in cluster with omp 2 traverse	BS1008B grt in cluster with omp 3	BS1008B grt in cluster with omp 3	BS1008B grt in cluster with omp 3	BS1008B grt in cluster with omp 3	BS1008B grt in cluster with omp 3	BS1008B grt in cluster with omp 3	BS1008B grt in cluster with omp 3	BS1008B grt in cluster with omp 3	BS1008B grt in cluster with omp 3
SiO2	38.41	38.80	38.76	38.70	38.73	38.42	38.44	38.79	38.88	38.95
TiO2	0.07	0.04	0.02	0.04	0.03	0.02	0.04	0.03	0.03	0.03
Al2O3	20.91	21.29	21.13	20.97	21.28	21.06	21.27	21.38	21.30	20.92
Cr2O3	0.00	0.02	0.01	0.01	0.00	0.02	0.01	0.02	0.00	0.00
FeO	21.83	21.28	21.13	20.99	21.09	21.20	21.27	20.96	21.58	21.63
MnO	0.48	0.51	0.48	0.47	0.47	0.47	0.46	0.47	0.52	0.49
MgO	9.24	9.54	9.73	9.47	9.78	10.12	9.94	9.84	9.97	9.12
CaO	7.77	8.01	7.86	8.25	7.60	7.26	7.26	7.61	7.68	8.10
Na2O	0.04	0.02	0.02	0.00	0.01	0.02	0.02	0.00	0.02	0.04
K2O	0.01	0.02	0.02	0.00	0.01	0.01	0.01	0.00	0.01	0.00
Total	**98.76**	**99.52**	**99.15**	**98.92**	**99.00**	**98.59**	**98.72**	**99.11**	**100.01**	**99.29**
Num ox	12.00	12.00	12.00	12.00	12.00	12.00	12.00	12.00	12.00	12.00
Si	2.98	2.98	2.98	2.99	2.98	2.97	2.97	2.98	2.97	3.00
Ti	0.00	0.00	0.00	0.00	0.00	0.00	0.00	0.00	0.00	0.00
Al	1.91	1.93	1.92	1.91	1.93	1.92	1.94	1.94	1.92	1.90
Cr	0.00	0.00	0.00	0.00	0.00	0.00	0.00	0.00	0.00	0.00
Fe3+	0.00	0.00	0.00	0.00	0.00	0.00	0.00	0.00	0.00	0.00
Fe2+	1.42	1.37	1.36	1.35	1.36	1.37	1.37	1.35	1.38	1.39
Mn	0.03	0.03	0.03	0.03	0.03	0.03	0.03	0.03	0.03	0.03
Mg	1.07	1.09	1.12	1.09	1.12	1.17	1.14	1.13	1.14	1.05
Ca	0.65	0.66	0.65	0.68	0.63	0.60	0.60	0.63	0.63	0.67
Na	0.01	0.00	0.00	0.00	0.00	0.00	0.00	0.00	0.00	0.01
K	0.00	0.00	0.00	0.00	0.00	0.00	0.00	0.00	0.00	0.00
Ni	0.00	0.00	0.00	0.00	0.00	0.00	0.00	0.00	0.00	0.00
Total	**8.06**	**8.06**	**8.06**	**8.06**	**8.05**	**8.07**	**8.06**	**8.05**	**8.07**	**8.05**
XAlm	0.45	0.43	0.43	0.43	0.43	0.43	0.44	0.43	0.43	0.44
XPyp	0.34	0.35	0.35	0.34	0.36	0.37	0.36	0.36	0.36	0.33
XGrs	0.20	0.21	0.21	0.22	0.20	0.19	0.19	0.20	0.20	0.21
XSps	0.01	0.01	0.01	0.01	0.01	0.01	0.01	0.01	0.01	0.01

Rocktype	omp-granulite									eclogite
Sample	BS1008B grt in cluster with omp 3	BS1008B grt in cluster with omp 3	BS1008B grt in cluster with omp 3	BS1008B grt in cluster with omp 3	BS1008B grt in cluster with omp 3	BS1008B grt in cluster with omp 3	BS1008B grt in cluster with omp 3	BS1008B grt in cluster with omp 3	BS1008B grt in cluster with omp 3	BS1003B grt
SiO2	38.82	38.45	38.67	38.53	38.67	38.43	38.49	38.54	38.56	40.10
TiO2	0.12	0.10	0.10	0.06	0.12	0.14	0.12	0.12	0.07	0.10
Al2O3	21.10	21.06	21.08	21.13	20.94	20.93	20.79	20.88	21.07	22.03
Cr2O3	0.02	0.00	0.02	0.03	0.02	0.03	0.06	0.03	0.03	0.13
FeO	22.24	22.17	22.01	21.87	21.99	22.06	22.28	22.75	22.42	19.59
MnO	0.51	0.51	0.52	0.46	0.51	0.49	0.55	0.54	0.50	0.47
MgO	9.72	10.15	10.26	10.13	10.13	10.16	10.14	9.20	9.62	10.93
CaO	6.47	6.28	6.48	6.49	6.60	6.43	6.62	7.32	6.87	7.72
Na2O	0.06	0.04	0.03	0.03	0.04	0.04	0.04	0.04	0.03	0.03
K2O	0.00	0.01	0.01	0.00	0.00	0.00	0.01	0.01	0.00	0.01
Total	**99.06**	**98.76**	**99.19**	**98.74**	**99.02**	**98.71**	**99.10**	**99.41**	**99.20**	**101.11**
Num ox	12.00	12.00	12.00	12.00	12.00	12.00	12.00	12.00	12.00	12.00
Si	2.99	2.97	2.98	2.98	2.98	2.97	2.97	2.98	2.98	2.99
Ti	0.01	0.01	0.01	0.00	0.01	0.01	0.01	0.01	0.00	0.01
Al	1.92	1.92	1.91	1.92	1.90	1.91	1.89	1.90	1.92	1.94
Cr	0.00	0.00	0.00	0.00	0.00	0.00	0.00	0.00	0.00	0.01
Fe3+	0.00	0.00	0.00	0.00	0.00	0.00	0.00	0.00	0.00	0.00
Fe2+	1.43	1.43	1.42	1.41	1.42	1.43	1.44	1.47	1.45	1.22
Mn	0.03	0.03	0.03	0.03	0.03	0.03	0.04	0.04	0.03	0.03
Mg	1.12	1.17	1.18	1.17	1.16	1.17	1.17	1.06	1.11	1.22
Ca	0.53	0.52	0.53	0.54	0.55	0.53	0.55	0.61	0.57	0.62
Na	0.01	0.01	0.00	0.01	0.01	0.01	0.01	0.01	0.00	0.00
K	0.00	0.00	0.00	0.00	0.00	0.00	0.00	0.00	0.00	0.00
Ni	0.00	0.00	0.00	0.00	0.00	0.00	0.00	0.00	0.00	0.00
Total	**8.05**	**8.06**	**8.06**	**8.06**	**8.06**	**8.07**	**8.07**	**8.07**	**8.06**	**8.03**
XAlm	0.46	0.45	0.45	0.45	0.45	0.45	0.45	0.46	0.46	0.40
XPyp	0.36	0.37	0.37	0.37	0.37	0.37	0.37	0.33	0.35	0.39
XGrs	0.17	0.16	0.17	0.17	0.17	0.17	0.17	0.19	0.18	0.20
XSps	0.01	0.01	0.01	0.01	0.01	0.01	0.01	0.01	0.01	0.01

Rocktype	eclogite									pyroxenite
Sample	BS1003B grt	BS1003B grt	BS1003B grt	BS1003B grt	BS1003B grt	BS1003B grt	BS1003B grt	BS1003B grt	BS1003B grt	BS1010A grt-inclusion
SiO2	40.37	40.18	40.19	40.20	40.17	40.37	40.03	40.17	40.25	39.80
TiO2	0.09	0.08	0.08	0.04	0.04	0.07	0.09	0.08	0.10	0.05
Al2O3	22.08	21.99	21.95	22.04	22.21	22.15	22.16	22.05	22.04	21.84
Cr2O3	0.09	0.13	0.09	0.11	0.12	0.09	0.10	0.15	0.13	0.02
FeO	19.36	19.15	19.11	18.82	19.18	19.50	19.38	19.16	19.40	21.30
MnO	0.51	0.51	0.52	0.52	0.46	0.49	0.48	0.49	0.49	0.71
MgO	10.93	10.92	11.09	11.06	10.96	10.77	11.04	10.79	10.77	8.98
CaO	7.82	7.92	8.01	7.88	7.88	8.01	7.80	7.72	7.70	8.20
Na2O	0.01	0.03	0.03	0.02	0.04	0.02	0.02	0.03	0.04	0.03
K2O	0.01	0.01	0.00	0.01	0.01	0.00	0.00	0.00	0.00	0.00
Total	**101.27**	**100.93**	**101.08**	**100.70**	**101.06**	**101.47**	**101.11**	**100.64**	**100.90**	**100.93**
Num ox	12.00	12.00	12.00	12.00	12.00	12.00	12.00	12.00	12.00	12.00
Si	3.00	3.00	3.00	3.00	2.99	3.00	2.98	3.00	3.00	3.01
Ti	0.00	0.00	0.00	0.00	0.00	0.00	0.01	0.00	0.01	0.00
Al	1.94	1.94	1.93	1.94	1.95	1.94	1.95	1.94	1.94	1.94
Cr	0.01	0.01	0.01	0.01	0.01	0.01	0.01	0.01	0.01	0.00
Fe3+	0.00	0.00	0.00	0.00	0.00	0.00	0.00	0.00	0.00	0.00
Fe2+	1.20	1.20	1.19	1.18	1.19	1.21	1.21	1.20	1.21	1.35
Mn	0.03	0.03	0.03	0.03	0.03	0.03	0.03	0.03	0.03	0.05
Mg	1.21	1.21	1.23	1.23	1.22	1.19	1.23	1.20	1.20	1.01
Ca	0.62	0.63	0.64	0.63	0.63	0.64	0.62	0.62	0.62	0.66
Na	0.00	0.00	0.00	0.00	0.01	0.00	0.00	0.00	0.01	0.00
K	0.00	0.00	0.00	0.00	0.00	0.00	0.00	0.00	0.00	0.00
Ni	0.00	0.00	0.00	0.00	0.00	0.00	0.00	0.00	0.00	0.00
Total	**8.02**	**8.03**	**8.04**	**8.02**	**8.03**	**8.02**	**8.04**	**8.02**	**8.02**	**8.02**
XAlm	0.39	0.39	0.38	0.38	0.39	0.39	0.39	0.39	0.40	0.44
XPyp	0.39	0.39	0.40	0.40	0.40	0.39	0.40	0.39	0.39	0.33
XGrs	0.20	0.21	0.21	0.21	0.21	0.21	0.20	0.20	0.20	0.22
XSps	0.01	0.01	0.01	0.01	0.01	0.01	0.01	0.01	0.01	0.01

Rocktype	pyroxenite									
Sample	BS1010A grt-inclusion	BS1010A grt-inclusion	BS1010A grt-inclusion	BS1010A grt-inclusion	BS1010B grt-inclusion	BS1010B grt-inclusion	BS1010B grt-inclusion	BS1010B grt-inclusion	BS1010B grt-inclusion	BS1010B grt-inclusion
SiO2	39.37	39.92	39.82	45.34	38.88	39.60	39.34	39.69	39.69	39.37
TiO2	0.07	0.10	0.10	0.05	0.07	0.06	0.09	0.08	0.08	0.03
Al2O3	21.95	22.00	21.95	19.76	21.63	21.79	21.85	21.79	21.79	21.61
Cr2O3	0.06	0.03	0.00	0.01	0.00	0.04	0.03	0.01	0.01	0.05
FeO	21.55	20.91	21.06	14.41	21.58	21.91	21.71	22.07	22.07	21.67
MnO	0.68	0.61	0.63	0.38	0.61	0.68	0.62	0.61	0.61	0.63
MgO	9.34	9.53	9.72	7.63	7.94	7.84	7.92	7.93	7.93	7.77
CaO	7.61	7.84	7.76	4.34	9.65	9.64	9.56	9.73	9.73	9.81
Na2O	0.01	0.03	0.03	3.18	0.02	0.02	0.02	0.03	0.03	0.01
K2O	0.00	0.00	0.00	0.17	0.00	0.00	0.00	0.01	0.01	0.02
Total	**100.64**	**100.97**	**101.08**	**95.28**	**100.37**	**101.59**	**101.14**	**101.94**	**101.94**	**100.97**
Num ox	12.00	12.00	12.00	12.00	12.00	12.00	12.00	12.00	12.00	12.00
Si	2.98	3.00	2.99	3.46	2.97	2.99	2.98	2.99	2.99	2.99
Ti	0.00	0.01	0.01	0.00	0.00	0.00	0.01	0.00	0.00	0.00
Al	1.96	1.95	1.95	1.78	1.95	1.94	1.95	1.94	1.94	1.94
Cr	0.00	0.00	0.00	0.00	0.00	0.00	0.00	0.00	0.00	0.00
Fe3+	0.00	0.00	0.00	0.00	0.00	0.00	0.00	0.00	0.00	0.00
Fe2+	1.37	1.32	1.32	0.92	1.38	1.38	1.38	1.39	1.39	1.38
Mn	0.04	0.04	0.04	0.02	0.04	0.04	0.04	0.04	0.04	0.04
Mg	1.05	1.07	1.09	0.87	0.91	0.88	0.89	0.89	0.89	0.88
Ca	0.62	0.63	0.63	0.35	0.79	0.78	0.78	0.79	0.79	0.80
Na	0.00	0.00	0.00	0.47	0.00	0.00	0.00	0.00	0.00	0.00
K	0.00	0.00	0.00	0.02	0.00	0.00	0.00	0.00	0.00	0.00
Ni	0.00	0.00	0.00	0.00	0.00	0.00	0.00	0.00	0.00	0.00
Total	**8.03**	**8.02**	**8.03**	**7.89**	**8.05**	**8.03**	**8.04**	**8.04**	**8.04**	**8.04**
XAlm	0.44	0.43	0.43	0.42	0.44	0.45	0.45	0.45	0.45	0.44
XPyp	0.34	0.35	0.35	0.40	0.29	0.29	0.29	0.29	0.29	0.28
XGrs	0.20	0.21	0.20	0.16	0.25	0.25	0.25	0.25	0.25	0.26
XSps	0.01	0.01	0.01	0.01	0.01	0.01	0.01	0.01	0.01	0.01

Rocktype	pyroxenite									
Sample	BS1010B grt film	BS1010B grt film	BS1010B grt film	BS1010B grt film	BS1010B grt film	BS1010B grt film	BS1010B grt film	BS1010B grt film	BS1010B grt film	BS1010B grt film
SiO2	39.41	39.43	39.03	39.38	39.39	39.17	39.00	39.20	39.25	39.19
TiO2	0.09	0.10	0.10	0.07	0.09	0.07	0.09	0.11	0.12	0.06
Al2O3	21.76	21.68	21.71	21.74	21.72	21.74	21.75	21.80	21.85	21.70
Cr2O3	0.03	0.00	0.01	0.00	0.02	0.03	0.00	0.01	0.03	0.00
FeO	21.97	22.04	22.04	21.85	22.06	21.83	21.95	22.22	21.95	22.09
MnO	0.60	0.60	0.58	0.59	0.63	0.61	0.62	0.61	0.67	0.61
MgO	7.94	7.87	7.86	7.92	7.72	7.96	8.01	8.02	8.04	7.86
CaO	9.21	9.26	8.84	9.10	9.41	9.27	8.97	9.04	8.85	9.13
Na2O	0.03	0.03	0.05	0.04	0.01	0.03	0.02	0.01	0.04	0.03
K2O	0.00	0.01	0.00	0.01	0.01	0.00	0.00	0.01	0.00	0.01
Total	**101.03**	**101.01**	**100.23**	**100.69**	**101.06**	**100.71**	**100.43**	**101.02**	**100.81**	**100.68**
Num ox	12.00	12.00	12.00	12.00	12.00	12.00	12.00	12.00	12.00	12.00
Si	2.99	2.99	2.99	3.00	2.99	2.98	2.98	2.98	2.99	2.99
Ti	0.01	0.01	0.01	0.00	0.01	0.00	0.01	0.01	0.01	0.00
Al	1.95	1.94	1.96	1.95	1.95	1.95	1.96	1.95	1.96	1.95
Cr	0.00	0.00	0.00	0.00	0.00	0.00	0.00	0.00	0.00	0.00
Fe3+	0.00	0.00	0.00	0.00	0.00	0.00	0.00	0.00	0.00	0.00
Fe2+	1.40	1.40	1.41	1.39	1.40	1.39	1.40	1.41	1.40	1.41
Mn	0.04	0.04	0.04	0.04	0.04	0.04	0.04	0.04	0.04	0.04
Mg	0.90	0.89	0.90	0.90	0.87	0.90	0.91	0.91	0.91	0.89
Ca	0.75	0.75	0.72	0.74	0.77	0.76	0.73	0.74	0.72	0.75
Na	0.00	0.00	0.01	0.01	0.00	0.00	0.00	0.00	0.01	0.00
K	0.00	0.00	0.00	0.00	0.00	0.00	0.00	0.00	0.00	0.00
Ni	0.00	0.00	0.00	0.00	0.00	0.00	0.00	0.00	0.00	0.00
Total	**8.03**	**8.03**	**8.03**	**8.03**	**8.03**	**8.04**	**8.04**	**8.04**	**8.03**	**8.04**
XAlm	0.45	0.45	0.46	0.45	0.45	0.45	0.45	0.46	0.45	0.46
XPyp	0.29	0.29	0.29	0.29	0.28	0.29	0.30	0.29	0.30	0.29
XGrs	0.24	0.24	0.24	0.24	0.25	0.24	0.24	0.24	0.23	0.24
XSps	0.01	0.01	0.01	0.01	0.01	0.01	0.01	0.01	0.01	0.01

Rocktype	pyroxenite									
Sample	BS1010B grt film	BS1010B grt film	BS1010B grt film	BS1010B grt film	BS1010B grt film	BS1010B grt film	BS1010B grt film	BS1010B grt film	BS1010B grt film	BS1010B grt film
SiO2	38.95	38.98	39.40	39.30	39.44	39.03	39.07	39.29	39.24	38.96
TiO2	0.06	0.06	0.11	0.12	0.10	0.11	0.07	0.07	0.05	0.06
Al2O3	21.69	21.59	21.84	21.79	21.74	21.68	21.68	21.65	21.75	21.56
Cr2O3	0.00	0.03	0.03	0.02	0.03	0.03	0.02	0.02	0.03	0.04
FeO	22.03	21.78	22.17	22.32	22.18	21.79	21.43	21.59	21.73	22.01
MnO	0.61	0.62	0.64	0.63	0.63	0.61	0.59	0.63	0.59	0.61
MgO	7.79	7.72	8.12	8.14	7.98	7.93	7.76	7.78	7.49	7.40
CaO	9.28	9.41	8.88	8.74	8.89	8.97	9.52	9.36	9.67	9.77
Na2O	0.04	0.01	0.04	0.03	0.03	0.03	0.03	0.03	0.02	0.04
K2O	0.00	0.00	0.00	0.00	0.01	0.01	0.00	0.01	0.00	0.00
Total	**100.46**	**100.20**	**101.25**	**101.08**	**101.03**	**100.19**	**100.18**	**100.44**	**100.58**	**100.44**
Num ox	12.00	12.00	12.00	12.00	12.00	12.00	12.00	12.00	12.00	12.00
Si	2.98	2.99	2.99	2.98	2.99	2.99	2.99	3.00	2.99	2.98
Ti	0.00	0.00	0.01	0.01	0.01	0.01	0.00	0.00	0.00	0.00
Al	1.96	1.95	1.95	1.95	1.95	1.96	1.96	1.95	1.96	1.95
Cr	0.00	0.00	0.00	0.00	0.00	0.00	0.00	0.00	0.00	0.00
Fe3+	0.00	0.00	0.00	0.00	0.00	0.00	0.00	0.00	0.00	0.00
Fe2+	1.41	1.40	1.41	1.42	1.41	1.39	1.37	1.38	1.39	1.41
Mn	0.04	0.04	0.04	0.04	0.04	0.04	0.04	0.04	0.04	0.04
Mg	0.89	0.88	0.92	0.92	0.90	0.90	0.88	0.88	0.85	0.85
Ca	0.76	0.77	0.72	0.71	0.72	0.74	0.78	0.77	0.79	0.80
Na	0.01	0.00	0.01	0.00	0.00	0.00	0.00	0.01	0.00	0.01
K	0.00	0.00	0.00	0.00	0.00	0.00	0.00	0.00	0.00	0.00
Ni	0.00	0.00	0.00	0.00	0.00	0.00	0.00	0.00	0.00	0.00
Total	**8.04**	**8.03**	**8.03**	**8.04**	**8.03**	**8.03**	**8.03**	**8.03**	**8.03**	**8.04**
XAlm	0.45	0.45	0.46	0.46	0.46	0.45	0.45	0.45	0.45	0.46
XPyp	0.29	0.29	0.30	0.30	0.29	0.29	0.29	0.29	0.28	0.27
XGrs	0.25	0.25	0.23	0.23	0.24	0.24	0.25	0.25	0.26	0.26
XSps	0.01	0.01	0.01	0.01	0.01	0.01	0.01	0.01	0.01	0.01

Rocktype	garnetite									
Sample	BS1010A grt	BS1010A grt	BS1010A grt	BS1010A grt	BS1010A grt	BS1010A grt	BS1010A grt	BS1010A grt	BS1010A grt	BS1010A grt
SiO2	41.41	39.68	36.67	37.15	33.83	39.94	39.97	40.66	40.14	40.00
TiO2	0.03	0.06	0.03	0.02	0.04	0.05	0.04	0.06	0.04	0.03
Al2O3	23.67	21.97	21.17	18.52	21.82	22.07	22.17	22.95	22.26	22.24
Cr2O3	0.01	0.01	0.00	0.02	0.00	0.01	0.00	0.02	0.01	0.04
FeO	20.02	19.48	19.07	19.30	19.23	19.51	19.85	19.60	19.77	19.56
MnO	0.63	0.64	0.61	0.64	0.64	0.64	0.62	0.65	0.66	0.66
MgO	10.82	10.73	9.74	10.12	8.64	11.09	10.70	11.14	11.07	11.01
CaO	7.77	7.69	7.77	7.38	7.29	7.46	7.76	7.35	7.27	7.36
Na2O	0.02	0.01	0.00	0.02	0.03	0.02	0.03	0.02	0.01	0.02
K2O	0.00	0.00	0.02	0.00	0.00	0.00	0.01	0.00	0.00	0.00
Total	**104.38**	**100.26**	**95.07**	**93.18**	**91.53**	**100.81**	**101.16**	**102.45**	**101.22**	**100.92**
Num ox	12.00	12.00	12.00	12.00	12.00	12.00	12.00	12.00	12.00	12.00
Si	2.98	2.99	2.93	3.04	2.83	2.99	2.99	2.99	2.99	2.99
Ti	0.00	0.00	0.00	0.00	0.00	0.00	0.00	0.00	0.00	0.00
Al	2.01	1.95	1.99	1.79	2.15	1.95	1.95	1.99	1.95	1.96
Cr	0.00	0.00	0.00	0.00	0.00	0.00	0.00	0.00	0.00	0.00
Fe3+	0.00	0.00	0.00	0.00	0.00	0.00	0.00	0.00	0.00	0.00
Fe2+	1.21	1.23	1.27	1.32	1.34	1.22	1.24	1.20	1.23	1.22
Mn	0.04	0.04	0.04	0.04	0.05	0.04	0.04	0.04	0.04	0.04
Mg	1.16	1.20	1.16	1.23	1.08	1.24	1.19	1.22	1.23	1.23
Ca	0.60	0.62	0.67	0.65	0.65	0.60	0.62	0.58	0.58	0.59
Na	0.00	0.00	0.00	0.00	0.01	0.00	0.00	0.00	0.00	0.00
K	0.00	0.00	0.00	0.00	0.00	0.00	0.00	0.00	0.00	0.00
Ni	0.00	0.00	0.00	0.00	0.00	0.00	0.00	0.00	0.00	0.00
Total	**8.01**	**8.03**	**8.07**	**8.07**	**8.10**	**8.04**	**8.04**	**8.02**	**8.03**	**8.03**
XAlm	0.40	0.40	0.41	0.41	0.43	0.39	0.40	0.40	0.40	0.40
XPyp	0.39	0.39	0.37	0.38	0.35	0.40	0.39	0.40	0.40	0.40
XGrs	0.20	0.20	0.21	0.20	0.21	0.19	0.20	0.19	0.19	0.19
XSps	0.01	0.01	0.01	0.01	0.01	0.01	0.01	0.01	0.01	0.01

Rocktype	garnetite									
Sample	BS1010A grt	BS1010A grt	BS1010A grt	BS1010A grt	BS1010A grt	BS1010A grt	BS1010A grt	BS1010A grt	BS1010A grt	BS1010C grt
SiO2	37.30	40.84	40.32	40.36	40.02	40.24	40.69	40.40	39.69	39.98
TiO2	0.05	0.07	0.03	0.01	0.02	0.03	0.02	0.01	0.04	0.05
Al2O3	22.14	22.54	22.28	22.17	22.30	22.19	22.32	22.33	21.69	21.95
Cr2O3	0.00	0.00	0.00	0.00	0.00	0.00	0.00	0.00	0.00	0.02
FeO	19.41	19.97	19.41	19.51	19.50	19.50	19.81	19.59	20.03	19.81
MnO	0.64	0.62	0.65	0.62	0.64	0.70	0.64	0.63	0.65	0.67
MgO	9.83	11.50	11.20	10.96	10.96	11.30	10.79	11.08	10.96	10.61
CaO	7.54	7.29	7.22	7.38	7.34	7.32	7.19	7.53	7.46	7.54
Na2O	0.02	0.01	0.02	0.02	0.01	0.01	0.03	0.01	0.02	0.04
K2O	0.01	0.00	0.01	0.01	0.00	0.00	0.00	0.01	0.01	0.01
Total	**96.92**	**102.83**	**101.14**	**101.07**	**100.80**	**101.31**	**101.49**	**101.59**	**100.56**	**98.89**
Num ox	12.00	12.00	12.00	12.00	12.00	12.00	12.00	12.00	12.00	12.00
Si	2.92	2.99	3.00	3.01	2.99	2.99	3.02	3.00	2.99	3.00
Ti	0.00	0.00	0.00	0.00	0.00	0.00	0.00	0.00	0.00	0.00
Al	2.04	1.95	1.95	1.95	1.96	1.95	1.95	1.95	1.92	1.94
Cr	0.00	0.00	0.00	0.00	0.00	0.00	0.00	0.00	0.00	0.00
Fe3+	0.00	0.00	0.00	0.00	0.00	0.00	0.00	0.00	0.00	0.00
Fe2+	1.27	1.22	1.21	1.22	1.22	1.21	1.23	1.21	1.26	1.24
Mn	0.04	0.04	0.04	0.04	0.04	0.04	0.04	0.04	0.04	0.04
Mg	1.15	1.26	1.24	1.22	1.22	1.25	1.19	1.22	1.23	1.19
Ca	0.63	0.57	0.58	0.59	0.59	0.58	0.57	0.60	0.60	0.61
Na	0.00	0.00	0.00	0.00	0.00	0.00	0.00	0.00	0.00	0.01
K	0.00	0.00	0.00	0.00	0.00	0.00	0.00	0.00	0.00	0.00
Ni	0.00	0.00	0.00	0.00	0.00	0.00	0.00	0.00	0.00	0.00
Total	**8.06**	**8.03**	**8.02**	**8.02**	**8.03**	**8.03**	**8.01**	**8.03**	**8.05**	**8.03**
XAlm	0.41	0.40	0.39	0.40	0.40	0.39	0.41	0.39	0.40	0.40
XPyp	0.37	0.41	0.41	0.40	0.40	0.40	0.39	0.40	0.39	0.39
XGrs	0.20	0.19	0.19	0.19	0.19	0.19	0.19	0.19	0.19	0.20
XSps	0.01	0.01	0.01	0.01	0.01	0.01	0.01	0.01	0.01	0.01

Rocktype	garnetite									
Sample	BS1010C grt	BS1010C grt	BS1010C grt	BS1010C grt	BS1010C grt	BS1010C grt	BS1010C grt	BS1010C grt	BS1010C grt	BS1010C grt
SiO2	39.88	39.71	39.92	39.94	40.15	39.93	39.90	39.42	39.51	40.06
TiO2	0.05	0.04	0.05	0.04	0.01	0.02	0.05	0.10	0.12	0.03
Al2O3	22.19	22.15	22.25	22.23	22.29	22.14	22.09	22.10	22.11	22.17
Cr2O3	0.02	0.01	0.04	0.02	0.00	0.01	0.01	0.03	0.01	0.00
FeO	19.88	19.65	19.55	19.85	19.38	19.87	19.54	19.78	19.93	20.17
MnO	0.62	0.62	0.57	0.59	0.55	0.59	0.59	0.59	0.63	0.62
MgO	11.12	10.80	10.84	10.87	10.87	10.76	10.73	10.68	10.59	10.50
CaO	7.42	7.36	7.37	7.11	7.45	7.56	7.53	7.63	7.54	7.61
Na2O	0.02	0.02	0.03	0.02	0.02	0.00	0.04	0.03	0.05	0.02
K2O	0.01	0.00	0.00	0.01	0.00	0.00	0.01	0.00	0.00	0.01
Total	**98.75**	**99.06**	**98.41**	**98.57**	**98.95**	**99.09**	**99.38**	**98.75**	**98.85**	**99.13**
Num ox	12.00	12.00	12.00	12.00	12.00	12.00	12.00	12.00	12.00	12.00
Si	2.98	2.99	2.99	2.99	3.00	2.99	2.99	2.97	2.97	2.99
Ti	0.00	0.00	0.00	0.00	0.00	0.00	0.00	0.01	0.01	0.00
Al	1.95	1.96	1.96	1.96	1.96	1.95	1.95	1.96	1.96	1.95
Cr	0.00	0.00	0.00	0.00	0.00	0.00	0.00	0.00	0.00	0.00
Fe3+	0.00	0.00	0.00	0.00	0.00	0.00	0.00	0.00	0.00	0.00
Fe2+	1.24	1.24	1.22	1.24	1.21	1.24	1.23	1.25	1.25	1.26
Mn	0.04	0.04	0.04	0.04	0.04	0.04	0.04	0.04	0.04	0.04
Mg	1.24	1.21	1.21	1.21	1.21	1.20	1.20	1.20	1.19	1.17
Ca	0.59	0.59	0.59	0.57	0.60	0.61	0.61	0.62	0.61	0.61
Na	0.00	0.00	0.00	0.00	0.00	0.00	0.01	0.01	0.01	0.00
K	0.00	0.00	0.00	0.00	0.00	0.00	0.00	0.00	0.00	0.00
Ni	0.00	0.00	0.00	0.00	0.00	0.00	0.00	0.00	0.00	0.00
Total	**8.05**	**8.03**	**8.03**	**8.03**	**8.02**	**8.03**	**8.03**	**8.04**	**8.04**	**8.03**
XAlm	0.40	0.40	0.40	0.41	0.40	0.40	0.40	0.40	0.41	0.41
XPyp	0.40	0.39	0.40	0.40	0.40	0.39	0.39	0.39	0.38	0.38
XGrs	0.19	0.19	0.19	0.19	0.20	0.20	0.20	0.20	0.20	0.20
XSps	0.01	0.01	0.01	0.01	0.01	0.01	0.01	0.01	0.01	0.01

Rocktype	garnetite									
Sample	BS1010C grt	BS1010C grt	BS1010C grt	BS1010C grt	BS1010C grt	BS1010C grt	BS1010C grt	BS1010C grt	BS1010C grt	BS1010C grt
SiO2	39.50	40.02	39.63	39.84	39.66	39.66	40.05	39.84	40.07	40.22
TiO2	0.05	0.08	0.02	0.04	0.09	0.10	0.01	0.01	0.02	0.06
Al2O3	22.14	22.03	22.14	22.20	22.09	22.26	22.21	22.16	22.16	22.05
Cr2O3	0.01	0.01	0.00	0.02	0.02	0.03	0.02	0.03	0.00	0.00
FeO	20.07	19.65	20.01	19.85	19.96	19.76	19.82	19.87	19.95	19.91
MnO	0.63	0.67	0.60	0.64	0.61	0.58	0.61	0.61	0.60	0.61
MgO	10.32	10.60	10.67	10.73	10.73	10.91	10.70	10.64	10.44	10.32
CaO	7.74	7.72	7.58	7.54	7.44	7.65	7.38	7.39	7.48	7.69
Na2O	0.02	0.03	0.01	0.03	0.06	0.06	0.01	0.02	0.03	0.02
K2O	0.00	0.01	0.00	0.01	0.00	0.00	0.00	0.00	0.02	0.00
Total	**98.67**	**98.92**	**98.41**	**98.41**	**99.19**	**99.12**	**99.08**	**99.48**	**98.86**	**99.18**
Num ox	12.00	12.00	12.00	12.00	12.00	12.00	12.00	12.00	12.00	12.00
Si	2.98	3.00	2.98	2.98	2.98	2.97	3.00	2.99	3.00	3.01
Ti	0.00	0.00	0.00	0.00	0.00	0.01	0.00	0.00	0.00	0.00
Al	1.97	1.95	1.96	1.96	1.96	1.96	1.96	1.96	1.96	1.95
Cr	0.00	0.00	0.00	0.00	0.00	0.00	0.00	0.00	0.00	0.00
Fe3+	0.00	0.00	0.00	0.00	0.00	0.00	0.00	0.00	0.00	0.00
Fe2+	1.26	1.23	1.26	1.24	1.25	1.24	1.24	1.25	1.25	1.25
Mn	0.04	0.04	0.04	0.04	0.04	0.04	0.04	0.04	0.04	0.04
Mg	1.16	1.18	1.20	1.20	1.20	1.22	1.19	1.19	1.17	1.15
Ca	0.62	0.62	0.61	0.60	0.60	0.61	0.59	0.59	0.60	0.62
Na	0.00	0.00	0.00	0.00	0.01	0.01	0.00	0.00	0.00	0.00
K	0.00	0.00	0.00	0.00	0.00	0.00	0.00	0.00	0.00	0.00
Ni	0.00	0.00	0.00	0.00	0.00	0.00	0.00	0.00	0.00	0.00
Total	**8.04**	**8.03**	**8.04**	**8.04**	**8.04**	**8.05**	**8.02**	**8.03**	**8.02**	**8.02**
XAlm	0.41	0.40	0.41	0.40	0.41	0.40	0.40	0.41	0.41	0.41
XPyp	0.38	0.38	0.39	0.39	0.39	0.39	0.39	0.39	0.38	0.38
XGrs	0.20	0.20	0.20	0.20	0.19	0.20	0.19	0.19	0.20	0.20
XSps	0.01	0.01	0.01	0.01	0.01	0.01	0.01	0.01	0.01	0.01

Rocktype	garnetite									
Sample	BS1010C grt	BS1010C grt	BS1010C grt	BS1010C grt	BS1010C grt	BS1010E grt	BS1010E grt	BS1010E grt	BS1010E grt	BS1010E grt
SiO2	39.65	39.82	39.94	39.51	39.50	39.02	39.42	38.87	38.54	39.01
TiO2	0.02	0.04	0.04	0.02	0.08	0.03	0.03	0.05	0.01	0.05
Al2O3	22.22	22.19	22.10	22.19	22.21	21.55	21.68	21.54	21.32	21.55
Cr2O3	0.01	0.02	0.04	0.02	0.01	0.01	0.03	0.05	0.01	0.02
FeO	19.77	19.63	20.40	20.21	19.53	19.94	20.08	19.50	19.89	19.61
MnO	0.65	0.66	0.72	0.65	0.58	0.63	0.58	0.61	0.60	0.58
MgO	10.95	10.95	10.44	10.58	10.79	10.81	10.82	10.69	10.77	10.61
CaO	7.35	7.58	7.38	7.46	7.51	7.58	7.45	7.48	7.35	7.55
Na2O	0.03	0.01	0.01	0.03	0.02	0.03	0.02	0.03	0.02	0.03
K2O	0.00	0.00	0.00	0.00	0.01	0.01	0.01	0.00	0.00	0.02
Total	**98.33**	**98.58**	**99.38**	**100.66**	**100.25**	**99.61**	**100.12**	**98.82**	**98.53**	**99.05**
Num ox	12.00	12.00	12.00	12.00	12.00	12.00	12.00	12.00	12.00	12.00
Si	2.97	2.98	2.99	2.97	2.97	2.97	2.98	2.98	2.97	2.98
Ti	0.00	0.00	0.00	0.00	0.00	0.00	0.00	0.00	0.00	0.00
Al	1.97	1.96	1.95	1.97	1.97	1.93	1.93	1.94	1.93	1.94
Cr	0.00	0.00	0.00	0.00	0.00	0.00	0.00	0.00	0.00	0.00
Fe3+	0.00	0.00	0.00	0.00	0.00	0.00	0.00	0.00	0.00	0.00
Fe2+	1.24	1.23	1.28	1.27	1.23	1.27	1.27	1.25	1.28	1.25
Mn	0.04	0.04	0.05	0.04	0.04	0.04	0.04	0.04	0.04	0.04
Mg	1.22	1.22	1.16	1.19	1.21	1.23	1.22	1.22	1.24	1.21
Ca	0.59	0.61	0.59	0.60	0.61	0.62	0.60	0.61	0.61	0.62
Na	0.00	0.00	0.00	0.00	0.00	0.00	0.00	0.00	0.00	0.00
K	0.00	0.00	0.00	0.00	0.00	0.00	0.00	0.00	0.00	0.00
Ni	0.00	0.00	0.00	0.00	0.00	0.00	0.00	0.00	0.00	0.00
Total	**8.04**	**8.04**	**8.03**	**8.04**	**8.04**	**8.06**	**8.05**	**8.05**	**8.07**	**8.05**
XAlm	0.40	0.40	0.41	0.41	0.40	0.40	0.41	0.40	0.41	0.40
XPyp	0.40	0.39	0.38	0.38	0.39	0.39	0.39	0.39	0.39	0.39
XGrs	0.19	0.20	0.19	0.19	0.20	0.20	0.19	0.20	0.19	0.20
XSps	0.01	0.01	0.01	0.01	0.01	0.01	0.01	0.01	0.01	0.01

Rocktype	garnetite									
Sample	BS1010E grt	BS1010E grt	BS1010E grt	BS1010E grt	BS1010E grt	BS1010E grt	BS1010E grt	BS1010E grt	BS1010E grt	BS1010E grt
SiO2	38.35	38.73	38.52	39.03	38.34	38.74	38.65	38.81	39.61	38.82
TiO2	0.03	0.05	0.02	0.03	0.03	0.03	0.03	0.03	0.02	0.05
Al2O3	21.28	21.31	21.11	21.45	21.21	21.52	21.37	21.59	21.81	21.55
Cr2O3	0.03	0.05	0.02	0.02	0.05	0.01	0.03	0.03	0.03	0.03
FeO	20.13	19.97	19.75	19.86	19.82	20.13	20.08	19.86	20.04	20.12
MnO	0.66	0.57	0.56	0.60	0.59	0.59	0.59	0.59	0.61	0.64
MgO	10.65	10.79	10.72	10.84	10.88	10.72	10.81	10.83	10.72	10.83
CaO	7.49	7.33	7.33	7.29	7.51	7.42	7.27	7.27	7.31	7.35
Na2O	0.02	0.01	0.01	0.03	0.02	0.00	0.02	0.01	0.01	0.04
K2O	0.00	0.00	0.00	0.01	0.00	0.00	0.00	0.00	0.00	0.02
Total	**98.63**	**98.81**	**98.06**	**99.15**	**98.45**	**99.16**	**98.86**	**99.02**	**100.18**	**99.45**
Num ox	12.00	12.00	12.00	12.00	12.00	12.00	12.00	12.00	12.00	12.00
Si	2.96	2.97	2.98	2.98	2.96	2.96	2.97	2.97	2.99	2.96
Ti	0.00	0.00	0.00	0.00	0.00	0.00	0.00	0.00	0.00	0.00
Al	1.93	1.93	1.92	1.93	1.93	1.94	1.93	1.95	1.94	1.94
Cr	0.00	0.00	0.00	0.00	0.00	0.00	0.00	0.00	0.00	0.00
Fe3+	0.00	0.00	0.00	0.00	0.00	0.00	0.00	0.00	0.00	0.00
Fe2+	1.30	1.28	1.28	1.27	1.28	1.29	1.29	1.27	1.27	1.28
Mn	0.04	0.04	0.04	0.04	0.04	0.04	0.04	0.04	0.04	0.04
Mg	1.22	1.23	1.24	1.23	1.25	1.22	1.24	1.23	1.21	1.23
Ca	0.62	0.60	0.61	0.60	0.62	0.61	0.60	0.60	0.59	0.60
Na	0.00	0.00	0.00	0.00	0.00	0.00	0.00	0.00	0.00	0.01
K	0.00	0.00	0.00	0.00	0.00	0.00	0.00	0.00	0.00	0.00
Ni	0.00	0.00	0.00	0.00	0.00	0.00	0.00	0.00	0.00	0.00
Total	**8.08**	**8.06**	**8.06**	**8.05**	**8.08**	**8.06**	**8.07**	**8.06**	**8.04**	**8.07**
XAlm	0.41	0.41	0.40	0.40	0.40	0.41	0.41	0.40	0.41	0.41
XPyp	0.38	0.39	0.39	0.39	0.39	0.39	0.39	0.39	0.39	0.39
XGrs	0.19	0.19	0.19	0.19	0.19	0.19	0.19	0.19	0.19	0.19
XSps	0.01	0.01	0.01	0.01	0.01	0.01	0.01	0.01	0.01	0.01

Rocktype	garnetite				
Sample	BS1010E grt	BS1010E grt	BS1010E grt	BS1010E grt	BS1010E grt
SiO2	39.32	38.71	38.75	39.10	38.94
TiO2	0.05	0.05	0.03	0.07	0.05
Al2O3	21.52	21.41	21.45	21.63	21.45
Cr2O3	0.03	0.00	0.01	0.05	0.00
FeO	20.16	19.77	20.09	19.84	19.88
MnO	0.63	0.57	0.60	0.59	0.58
MgO	10.79	10.86	10.92	10.73	10.85
CaO	7.33	7.26	7.43	7.42	7.36
Na2O	0.02	0.02	0.00	0.03	0.02
K2O	0.01	0.00	0.00	0.01	0.00
Total	**99.87**	**98.66**	**99.28**	**99.47**	**99.13**
Num ox	12.00	12.00	12.00	12.00	12.00
Si	2.98	2.97	2.96	2.98	2.97
Ti	0.00	0.00	0.00	0.00	0.00
Al	1.93	1.94	1.93	1.94	1.93
Cr	0.00	0.00	0.00	0.00	0.00
Fe3+	0.00	0.00	0.00	0.00	0.00
Fe2+	1.28	1.27	1.28	1.26	1.27
Mn	0.04	0.04	0.04	0.04	0.04
Mg	1.22	1.24	1.24	1.22	1.24
Ca	0.60	0.60	0.61	0.61	0.60
Na	0.00	0.00	0.00	0.01	0.00
K	0.00	0.00	0.00	0.00	0.00
Ni	0.00	0.00	0.00	0.00	0.00
Total	**8.05**	**8.06**	**8.07**	**8.05**	**8.06**
XAlm	0.41	0.40	0.40	0.40	0.40
XPyp	0.39	0.39	0.39	0.39	0.39
XGrs	0.19	0.19	0.19	0.19	0.19
XSps	0.01	0.01	0.01	0.01	0.01

Appendix 2 – EMP pyroxene

Rocktype	eclogite									
Sample	BS1003B cpx incl in grt	BS1003B cpx incl in grt	BS1003B cpx incl in grt	BS1003B cpx	BS1003B cpx	BS1003B cpx	BS1003B cpx	BS1003B cpx	BS1003B cpx	BS1003B cpx
SiO2	52.93	53.87	53.54	51.59	52.17	51.60	51.14	51.32	51.12	51.46
TiO2	0.19	0.18	0.19	0.44	0.33	0.54	0.55	0.53	0.53	0.43
Al2O3	4.73	4.94	4.73	7.36	6.41	8.83	8.96	8.85	8.80	8.82
FeO	5.77	5.56	5.86	6.38	6.24	6.19	6.11	6.29	6.33	6.37
MnO	0.02	0.06	0.01	0.02	0.02	0.05	0.03	0.04	0.04	0.01
MgO	12.84	12.95	12.88	11.23	11.51	10.45	10.36	10.49	10.49	10.58
CaO	20.45	20.73	20.33	19.65	19.97	19.15	19.15	19.12	19.24	19.28
K2O	0.00	0.02	0.00	0.02	0.01	0.01	0.01	0.00	0.00	0.01
Na2O	2.61	2.38	2.40	2.84	2.60	3.03	3.09	3.07	3.13	3.17
Cr2O3	0.11	0.12	0.12	0.09	0.07	0.11	0.10	0.08	0.07	0.14
Total	**99.66**	**100.82**	**100.06**	**99.61**	**99.32**	**99.95**	**99.51**	**99.81**	**99.75**	**100.28**
Si Calc	1.95	1.95	1.96	1.90	1.93	1.89	1.88	1.88	1.88	1.88
Ti Calc	0.01	0.00	0.01	0.01	0.01	0.01	0.02	0.01	0.01	0.01
Al Calc	0.21	0.21	0.20	0.32	0.28	0.38	0.39	0.38	0.38	0.38
Fe Calc	0.18	0.17	0.18	0.20	0.19	0.19	0.19	0.19	0.19	0.19
Mn Calc	0.00	0.00	0.00	0.00	0.00	0.00	0.00	0.00	0.00	0.00
Mg Calc	0.70	0.70	0.70	0.62	0.63	0.57	0.57	0.57	0.57	0.58
Ca Calc	0.81	0.81	0.80	0.78	0.79	0.75	0.75	0.75	0.76	0.76
K Calc	0.00	0.00	0.00	0.00	0.00	0.00	0.00	0.00	0.00	0.00
Na Calc	0.19	0.17	0.17	0.20	0.19	0.21	0.22	0.22	0.22	0.22
Ni Calc	0.00	0.00	0.00	0.00	0.00	0.00	0.00	0.00	0.00	0.00
Cr Calc	0.00	0.00	0.00	0.00	0.00	0.00	0.00	0.00	0.00	0.00
Fe 3+ Droop	0.11	0.05	0.06	0.08	0.05	0.04	0.06	0.06	0.08	0.08
Total Calc	**4.04**	**4.02**	**4.02**	**4.03**	**4.02**	**4.01**	**4.02**	**4.02**	**4.03**	**4.03**
J	0.37	0.33	0.34	0.40	0.37	0.43	0.44	0.43	0.44	0.45
Q	1.57	1.61	1.61	1.49	1.55	1.47	1.45	1.45	1.44	1.43
group	Quad	Quad	Quad	Ca-Na	Quad	Ca-Na	Ca-Na	Ca-Na	Ca-Na	Ca-Na
adjective	aluminian	faluminian	aluminian		aluminian					
pyroxene	diopside	diopside	diopside	omphacite	diopside	omphacite	omphacite	omphacite	omphacite	omphacite
enstatite	41.70	41.77	41.84	----------	39.18	----------	----------	----------	----------	----------
ferrosillite	10.55	10.17	10.70	----------	11.95	----------	----------	----------	----------	----------
wollastonite	47.75	48.06	47.46	----------	48.87	----------	----------	----------	----------	----------
jadeite	----------	----------	----------	15.11	----------	19.66	19.07	18.67	17.73	17.71
aegirine	----------	----------	----------	6.10	----------	2.95	4.18	4.37	5.86	6.04
Ca-Mg-Fe	----------	----------	----------	78.79	----------	77.39	76.75	76.97	76.41	76.25

Rocktype	eclogite			pyroxenite						
Sample	BS1003B cpx	BS1003B cpx	BS1003B cpx	BS1010A cpx-layer	BS1010A cpx-layer	BS1010A cpx-layer	BS1010A cpx-layer	BS1010A cpx-layer	BS1010A cpx-layer	BS1010A cpx-layer
SiO2	51.82	51.30	50.93	49.60	49.82	48.18	49.92	49.91	49.03	50.00
TiO2	0.34	0.42	0.51	0.74	0.71	0.70	0.80	0.66	0.88	0.89
Al2O3	8.19	8.46	8.84	9.73	9.76	9.10	9.90	9.48	10.07	8.98
FeO	6.30	6.54	6.38	7.39	7.49	9.77	7.33	7.48	7.94	7.22
MnO	0.04	0.06	0.06	0.07	0.04	0.03	0.07	0.09	0.09	0.06
MgO	10.79	10.57	10.54	10.11	10.05	12.85	9.83	9.97	10.47	10.35
CaO	19.09	19.25	19.55	19.62	19.73	16.03	19.69	19.55	18.66	19.78
K2O	0.00	0.01	0.00	0.01	0.02	0.19	0.00	0.01	0.03	0.02
Na2O	3.06	2.99	2.86	2.78	2.52	1.90	2.47	2.46	2.44	2.38
Cr2O3	0.09	0.09	0.07	0.01	0.04	0.03	0.01	0.01	0.03	0.00
Total	**99.72**	**99.70**	**99.75**	**100.06**	**100.19**	**98.78**	**100.03**	**99.62**	**99.63**	**99.69**
Si Calc	1.90	1.89	1.87	1.83	1.84	1.81	1.84	1.85	1.82	1.85
Ti Calc	0.01	0.01	0.01	0.02	0.02	0.02	0.02	0.02	0.02	0.02
Al Calc	0.35	0.37	0.38	0.42	0.42	0.40	0.43	0.41	0.44	0.39
Fe Calc	0.19	0.20	0.20	0.23	0.23	0.31	0.23	0.23	0.25	0.22
Mn Calc	0.00	0.00	0.00	0.00	0.00	0.00	0.00	0.00	0.00	0.00
Mg Calc	0.59	0.58	0.58	0.56	0.55	0.72	0.54	0.55	0.58	0.57
Ca Calc	0.75	0.76	0.77	0.78	0.78	0.64	0.78	0.78	0.74	0.78
K Calc	0.00	0.00	0.00	0.00	0.00	0.01	0.00	0.00	0.00	0.00
Na Calc	0.22	0.21	0.20	0.20	0.18	0.14	0.18	0.18	0.18	0.17
Ni Calc	0.00	0.00	0.00	0.00	0.00	0.00	0.00	0.00	0.00	0.00
Cr Calc	0.00	0.00	0.00	0.00	0.00	0.00	0.00	0.00	0.00	0.00
Fe 3+ Droop	0.06	0.07	0.07	0.11	0.07	0.14	0.04	0.05	0.08	0.05
Total Calc	**4.02**	**4.02**	**4.02**	**4.04**	**4.02**	**4.05**	**4.01**	**4.02**	**4.03**	**4.02**
J	0.43	0.42	0.41	0.39	0.36	0.27	0.35	0.35	0.35	0.34
Q	1.47	1.46	1.47	1.44	1.48	1.51	1.50	1.50	1.48	1.52
group	Ca-Na	Ca-Na	Ca-Na	Ca-Na	Quad	Quad	Quad	Quad	Quad	Quad
adjective					aluminian	aluminian	faluminian	aluminian	aluminian	aluminian
pyroxene	omphacite	omphacite	omphacite	omphacite	diopside	augite	wollastonite	diopside	diopside	diopside
enstatite	----------	----------	----------	----------	35.33	43.02	34.93	35.29	36.89	36.13
ferrosillite	----------	----------	----------	----------	14.84	18.41	14.76	15.01	15.86	14.26
wollastonite	----------	----------	----------	----------	49.83	38.56	50.31	49.71	47.24	49.61
jadeite	18.35	17.44	16.98	14.67	----------	----------	----------	----------	----------	----------
aegirine	4.46	5.05	4.69	6.88	----------	----------	----------	----------	----------	----------
Ca-Mg-Fe	77.19	77.50	78.34	78.45	----------	----------	----------	----------	----------	----------

Rocktype	pyroxenite									
Sample	BS1010A cpx-layer	BS1010A cpx-layer	BS1010A cpx-layer	BS1010A cpx-layer	BS1010A cpx-layer	BS1010A cpx-layer	BS1010A cpx-layer	BS1010A cpx-layer	BS1010A cpx-layer	1010B cpx1 surrounded by grt film
SiO2	49.01	36.79	50.00	29.81	49.93	49.72	44.95	51.54	49.68	51.66
TiO2	0.95	0.46	0.78	0.55	1.04	0.85	0.70	0.75	0.71	0.37
Al2O3	9.86	4.93	8.41	2.99	9.32	9.55	8.97	8.34	6.90	5.20
FeO	7.38	6.04	7.59	5.10	7.50	7.70	7.30	7.15	7.07	6.93
MnO	0.06	0.06	0.02	0.03	0.07	0.09	0.08	0.06	0.05	0.04
MgO	9.85	7.32	10.43	5.24	10.36	10.06	9.19	11.43	10.90	12.34
CaO	19.77	18.01	20.07	10.39	19.34	19.45	17.03	19.28	20.12	21.10
K2O	0.00	0.00	0.00	0.04	0.00	0.02	0.04	0.02	0.00	0.00
Na2O	2.50	1.45	2.37	0.56	2.41	2.48	2.23	2.30	2.22	1.96
Cr2O3	0.00	0.02	0.02	0.03	0.03	0.03	0.00	0.05	0.06	0.04
Total	**99.39**	**75.08**	**99.69**	**54.76**	**100.01**	**99.94**	**90.51**	**100.92**	**97.72**	**99.66**
Si Calc	1.82	1.84	1.85	2.00	1.84	1.84	1.83	1.87	1.88	1.91
Ti Calc	0.03	0.02	0.02	0.03	0.03	0.02	0.02	0.02	0.02	0.01
Al Calc	0.43	0.29	0.37	0.24	0.40	0.42	0.43	0.36	0.31	0.23
Fe Calc	0.23	0.25	0.24	0.29	0.23	0.24	0.25	0.22	0.22	0.21
Mn Calc	0.00	0.00	0.00	0.00	0.00	0.00	0.00	0.00	0.00	0.00
Mg Calc	0.55	0.55	0.58	0.52	0.57	0.55	0.56	0.62	0.61	0.68
Ca Calc	0.79	0.97	0.80	0.75	0.76	0.77	0.74	0.75	0.82	0.84
K Calc	0.00	0.00	0.00	0.00	0.00	0.00	0.00	0.00	0.00	0.00
Na Calc	0.18	0.14	0.17	0.07	0.17	0.18	0.18	0.16	0.16	0.14
Ni Calc	0.00	0.00	0.00	0.00	0.00	0.00	0.00	0.00	0.00	0.00
Cr Calc	0.00	0.00	0.00	0.00	0.00	0.00	0.00	0.00	0.00	0.00
Fe 3+ Droop	0.08	0.19	0.07	0.00	0.04	0.06	0.06	0.02	0.08	0.09
Total Calc	**4.03**	**4.06**	**4.03**	**3.90**	**4.01**	**4.02**	**4.02**	**4.01**	**4.03**	**4.03**
J	0.36	0.28	0.34	0.15	0.34	0.35	0.35	0.32	0.32	0.28
Q	1.48	1.55	1.52	1.60	1.52	1.49	1.49	1.56	1.56	1.63
group	Quad	Quad	Quad	Quad	Quad	Quad	Quad	Quad	Quad	Quad
adjective	aluminian	aluminian	f aluminian	aluminian	aluminian	aluminian	aluminian	aluminian	aluminian	aluminian
pyroxene	wollastonite	wollastonite	diopside	diopside	diopside	diopside	diopside	diopside	diopside	diopside
enstatite	34.90	30.92	35.80	33.62	36.35	35.42	35.94	38.98	37.13	39.29
ferrosillite	14.79	14.45	14.66	18.47	14.90	15.39	16.20	13.78	13.61	12.45
wollastonite	50.31	54.63	49.53	47.90	48.76	49.19	47.86	47.24	49.27	48.26
jadeite	----------	----------	----------	----------	----------	----------	----------	----------	----------	----------
aegirine	----------	----------	----------	----------	----------	----------	----------	----------	----------	----------
Ca-Mg-Fe	----------	----------	----------	----------	----------	----------	----------	----------	----------	----------

Rocktype	pyroxenite									
Sample	1010B cpx1 surrounded by grt film	1010B cpx1 surrounded by grt film	1010B cpx1 surrounded by grt film	1010B cpx1 surrounded by grt film	1010B cpx1 surrounded by grt film	1010B cpx1 surrounded by grt film	1010B cpx1 surrounded by grt film	1010B cpx1 surrounded by grt film	1010B cpx1 surrounded by grt film	1010B cpx1 surrounded by grt film
SiO2	51.43	50.46	50.49	50.51	50.76	49.19	48.90	48.87	49.17	49.49
TiO2	0.38	0.59	0.61	0.59	0.78	1.03	1.12	1.22	1.24	0.84
Al2O3	5.05	6.40	6.40	6.34	7.96	9.04	9.25	9.49	9.67	7.89
FeO	6.86	7.33	7.12	7.45	7.24	7.20	7.35	7.58	7.54	6.97
MnO	0.01	0.07	0.06	0.06	0.06	0.05	0.05	0.03	0.04	0.05
MgO	12.38	11.50	11.58	11.59	10.79	10.14	10.06	10.16	10.09	10.94
CaO	21.26	21.01	20.81	20.99	20.09	20.03	19.91	19.90	19.90	20.24
K2O	0.00	0.01	0.01	0.01	0.00	0.01	0.01	0.01	0.00	0.03
Na2O	1.87	2.02	1.98	1.92	2.44	2.45	2.44	2.48	2.44	2.47
Cr2O3	0.01	0.00	0.05	0.03	0.04	0.05	0.00	0.05	0.02	0.06
Total	**99.24**	**99.38**	**99.12**	**99.50**	**100.14**	**99.18**	**99.10**	**99.79**	**100.11**	**98.99**
Si Calc	1.91	1.88	1.88	1.88	1.87	1.83	1.83	1.81	1.82	1.85
Ti Calc	0.01	0.02	0.02	0.02	0.02	0.03	0.03	0.03	0.03	0.02
Al Calc	0.22	0.28	0.28	0.28	0.35	0.40	0.41	0.42	0.42	0.35
Fe Calc	0.21	0.23	0.22	0.23	0.22	0.22	0.23	0.24	0.23	0.22
Mn Calc	0.00	0.00	0.00	0.00	0.00	0.00	0.00	0.00	0.00	0.00
Mg Calc	0.69	0.64	0.64	0.64	0.59	0.56	0.56	0.56	0.56	0.61
Ca Calc	0.85	0.84	0.83	0.84	0.79	0.80	0.80	0.79	0.79	0.81
K Calc	0.00	0.00	0.00	0.00	0.00	0.00	0.00	0.00	0.00	0.00
Na Calc	0.13	0.15	0.14	0.14	0.17	0.18	0.18	0.18	0.18	0.18
Ni Calc	0.00	0.00	0.00	0.00	0.00	0.00	0.00	0.00	0.00	0.00
Cr Calc	0.00	0.00	0.00	0.00	0.00	0.00	0.00	0.00	0.00	0.00
Fe 3+ Droop	0.09	0.10	0.09	0.09	0.07	0.08	0.08	0.10	0.08	0.13
Total Calc	**4.03**	**4.03**	**4.03**	**4.03**	**4.02**	**4.03**	**4.03**	**4.03**	**4.03**	**4.04**
J	0.27	0.29	0.28	0.28	0.35	0.35	0.35	0.35	0.35	0.35
Q	1.64	1.59	1.60	1.60	1.53	1.50	1.49	1.48	1.49	1.49
group	Quad	Quad	Quad	Quad	Quad	Quad	Quad	Quad	Quad	Quad
adjective	aluminian	aluminian	f aluminian	aluminian	aluminian	aluminian	aluminian	aluminian	aluminian	aluminian f
pyroxene	diopside	diopside	diopside	diopside	diopside	wollastonite	wollastonite	diopside	diopside	diopside
enstatite	39.28	37.40	37.87	37.53	36.79	35.44	35.27	35.36	35.21	37.17
ferrosillite	12.23	13.50	13.18	13.64	13.96	14.21	14.56	14.85	14.86	13.39
wollastonite	48.49	49.10	48.94	48.83	49.24	50.35	50.17	49.78	49.92	49.44
jadeite	----------	----------	----------	----------	----------	----------	----------	----------	----------	----------
aegirine	----------	----------	----------	----------	----------	----------	----------	----------	----------	----------
Ca-Mg-Fe	----------	----------	----------	----------	----------	----------	----------	----------	----------	----------

Rocktype	pyroxenite									
Sample	1010B cpx1 surrounded by grt film	1010B cpx3	1010B cpx3	1010B cpx3	1010B cpx3	1010B cpx3	1010B cpx3	1010B cpx3	1010B cpx3	1010B cpx3
SiO2	48.75	49.14	48.23	48.75	48.25	48.89	48.71	48.59	48.47	48.85
TiO2	1.13	1.07	1.25	1.17	1.04	0.99	0.98	0.95	0.95	0.81
Al2O3	9.19	9.03	9.89	9.79	9.80	9.69	9.96	9.73	9.90	9.67
FeO	7.33	7.15	7.64	7.64	7.71	7.81	8.01	7.68	7.94	8.02
MnO	0.04	0.05	0.06	0.01	0.04	0.07	0.08	0.07	0.09	0.10
MgO	10.25	10.32	9.85	10.11	10.10	10.12	10.01	10.06	10.13	10.13
CaO	19.88	19.90	19.81	19.34	19.49	19.27	19.14	19.63	18.84	19.32
K2O	0.01	0.01	0.01	0.00	0.02	0.01	0.00	0.00	0.02	0.01
Na2O	2.47	2.44	2.47	2.44	2.40	2.46	2.33	2.32	2.35	2.39
Cr2O3	0.02	0.02	0.00	0.01	0.03	0.04	0.00	0.04	0.02	0.04
Total	99.07	99.15	99.21	99.26	98.89	99.34	99.21	99.06	98.71	99.34
Si Calc	1.82	1.83	1.80	1.82	1.81	1.82	1.82	1.82	1.82	1.82
Ti Calc	0.03	0.03	0.04	0.03	0.03	0.03	0.03	0.03	0.03	0.02
Al Calc	0.40	0.40	0.44	0.43	0.43	0.43	0.44	0.43	0.44	0.42
Fe Calc	0.23	0.22	0.24	0.24	0.24	0.24	0.25	0.24	0.25	0.25
Mn Calc	0.00	0.00	0.00	0.00	0.00	0.00	0.00	0.00	0.00	0.00
Mg Calc	0.57	0.57	0.55	0.56	0.56	0.56	0.56	0.56	0.57	0.56
Ca Calc	0.80	0.79	0.79	0.77	0.78	0.77	0.76	0.79	0.76	0.77
K Calc	0.00	0.00	0.00	0.00	0.00	0.00	0.00	0.00	0.00	0.00
Na Calc	0.18	0.18	0.18	0.18	0.17	0.18	0.17	0.17	0.17	0.17
Ni Calc	0.00	0.00	0.00	0.00	0.00	0.00	0.00	0.00	0.00	0.00
Cr Calc	0.00	0.00	0.00	0.00	0.00	0.00	0.00	0.00	0.00	0.00
Fe 3+ Droop	0.10	0.08	0.10	0.08	0.10	0.08	0.07	0.08	0.07	0.09
Total Calc	4.03	4.03	4.03	4.03	4.03	4.03	4.02	4.03	4.02	4.03
J	0.35	0.35	0.35	0.35	0.35	0.35	0.33	0.33	0.34	0.34
Q	1.48	1.50	1.46	1.49	1.47	1.48	1.50	1.49	1.49	1.48
group	Quad	Quad	Quad	Quad	Quad	Quad	Quad	Quad	Quad	Quad
adjective	aluminian	faluminian	aluminian	faluminian	aluminian	faluminian	aluminian	aluminian	aluminian	aluminian
pyroxene	diopside	diopside	wollastonite	diopside	diopside	diopside	diopside	diopside	diopside	diopside
enstatite	35.75	36.01	34.68	35.72	35.50	35.65	35.35	35.29	35.95	35.43
ferrosillite	14.41	14.10	15.20	15.17	15.28	15.56	16.04	15.24	15.98	15.96
wollastonite	49.84	49.89	50.12	49.11	49.22	48.79	48.60	49.47	48.07	48.60
jadeite	----------	----------	----------	----------	----------	----------	----------	----------	----------	----------
aegirine	----------	----------	----------	----------	----------	----------	----------	----------	----------	----------
Ca-Mg-Fe	----------	----------	----------	----------	----------	----------	----------	----------	----------	----------

Rocktype	pyroxenite									
Sample	1010B cpx3	1010B cpx3	1010B cpx3	1010B cpx3	1010B cpx3	1010B cpx3	BS1010D	BS1010D	BS1010D	BS1010D
SiO2	49.79	49.24	49.91	49.28	50.05	47.28	48.31	48.41	48.40	47.95
TiO2	0.82	0.83	0.74	0.99	1.03	1.47	1.03	1.00	1.00	1.04
Al2O3	9.14	9.89	8.81	9.63	8.91	11.29	9.85	9.67	9.72	10.09
FeO	7.71	7.84	7.84	7.84	7.47	10.06	7.53	7.80	7.58	8.40
MnO	0.10	0.10	0.08	0.09	0.08	0.07	0.08	0.06	0.13	0.10
MgO	10.26	10.16	10.46	9.99	10.40	11.14	9.90	10.15	9.96	10.62
CaO	19.61	19.55	20.14	19.61	20.04	15.81	19.71	19.21	19.89	17.78
K2O	0.02	0.00	0.00	0.01	0.00	0.02	0.02	0.01	0.02	0.01
Na2O	2.24	2.24	2.11	2.27	2.30	2.36	2.44	2.40	2.36	2.40
Cr2O3	0.04	0.04	0.00	0.02	0.00	0.04	0.02	0.05	0.01	0.02
Total	99.73	99.88	100.09	99.72	100.28	99.55	98.89	98.75	99.06	98.41
Si Calc	1.84	1.82	1.84	1.83	1.84	1.76	1.81	1.81	1.81	1.80
Ti Calc	0.02	0.02	0.02	0.03	0.03	0.04	0.03	0.03	0.03	0.03
Al Calc	0.40	0.43	0.38	0.42	0.39	0.50	0.43	0.43	0.43	0.45
Fe Calc	0.24	0.24	0.24	0.24	0.23	0.31	0.24	0.24	0.24	0.26
Mn Calc	0.00	0.00	0.00	0.00	0.00	0.00	0.00	0.00	0.00	0.00
Mg Calc	0.57	0.56	0.58	0.55	0.57	0.62	0.55	0.57	0.56	0.59
Ca Calc	0.78	0.78	0.80	0.78	0.79	0.63	0.79	0.77	0.80	0.72
K Calc	0.00	0.00	0.00	0.00	0.00	0.00	0.00	0.00	0.00	0.00
Na Calc	0.16	0.16	0.15	0.16	0.16	0.17	0.18	0.17	0.17	0.17
Ni Calc	0.00	0.00	0.00	0.00	0.00	0.00	0.00	0.00	0.00	0.00
Cr Calc	0.00	0.00	0.00	0.00	0.00	0.00	0.00	0.00	0.00	0.00
Fe 3+ Droop	0.04	0.06	0.06	0.05	0.05	0.11	0.10	0.09	0.10	0.10
Total Calc	4.01	4.02	4.02	4.02	4.02	4.04	4.03	4.03	4.03	4.03
J	0.32	0.32	0.30	0.33	0.33	0.34	0.35	0.35	0.34	0.35
Q	1.53	1.51	1.55	1.52	1.53	1.44	1.47	1.48	1.48	1.47
group	Quad	Quad	Quad	Quad	Quad	Quad	Quad	Quad	Quad	Quad
adjective	aluminian	aluminian	aluminian	aluminian	aluminian	aluminian	faluminian	aluminian	aluminian	aluminian
pyroxene	diopside	diopside	diopside	diopside	diopside	augite	wollastonite	diopside	wollastonite	diopside
enstatite	35.71	35.45	35.62	35.01	35.83	39.53	34.93	35.78	34.84	37.70
ferrosillite	15.25	15.52	15.12	15.58	14.58	20.16	15.06	15.54	15.13	16.93
wollastonite	49.04	49.02	49.26	49.41	49.59	40.31	50.00	48.68	50.03	45.38
jadeite	----------	----------	----------	----------	----------	----------	----------	----------	----------	----------
aegirine	----------	----------	----------	----------	----------	----------	----------	----------	----------	----------
Ca-Mg-Fe	----------	----------	----------	----------	----------	----------	----------	----------	----------	----------

Rocktype	pyroxenite									
Sample	BS1010D	BS1010D	BS1010D	BS1010D	BS1010D	BS1010D	BS1010D	BS1010D	BS1010D	BS1010D
SiO2	48.41	48.59	49.41	51.49	48.63	50.35	49.38	48.56	48.44	48.66
TiO2	0.92	0.97	0.90	0.46	1.01	0.62	0.83	1.08	1.15	1.08
Al2O3	9.48	9.37	8.12	5.42	9.11	7.45	8.66	9.33	9.50	9.49
FeO	7.49	7.59	7.39	6.74	7.27	7.04	7.42	7.41	7.49	7.46
MnO	0.07	0.08	0.06	0.02	0.04	0.04	0.04	0.04	0.04	0.08
MgO	10.01	10.09	10.71	12.28	10.22	10.89	10.32	10.02	10.00	9.79
CaO	19.76	19.83	20.18	20.93	20.01	20.21	20.03	19.77	19.92	19.51
K2O	0.01	0.01	0.00	0.00	0.01	0.00	0.00	0.02	0.00	0.01
Na2O	2.39	2.38	2.28	2.03	2.43	2.23	2.40	2.39	2.36	2.33
Cr2O3	0.02	0.05	0.03	0.02	0.02	0.02	0.05	0.03	0.01	0.01
Total	**98.57**	**98.95**	**99.09**	**99.38**	**98.75**	**98.85**	**99.13**	**98.67**	**98.92**	**98.41**
Si Calc	1.82	1.82	1.85	1.91	1.82	1.88	1.84	1.82	1.81	1.83
Ti Calc	0.03	0.03	0.03	0.01	0.03	0.02	0.02	0.03	0.03	0.03
Al Calc	0.42	0.41	0.36	0.24	0.40	0.33	0.38	0.41	0.42	0.42
Fe Calc	0.24	0.24	0.23	0.21	0.23	0.22	0.23	0.23	0.23	0.23
Mn Calc	0.00	0.00	0.00	0.00	0.00	0.00	0.00	0.00	0.00	0.00
Mg Calc	0.56	0.56	0.60	0.68	0.57	0.61	0.57	0.56	0.56	0.55
Ca Calc	0.80	0.80	0.81	0.83	0.80	0.81	0.80	0.79	0.80	0.78
K Calc	0.00	0.00	0.00	0.00	0.00	0.00	0.00	0.00	0.00	0.00
Na Calc	0.17	0.17	0.17	0.15	0.18	0.16	0.17	0.17	0.17	0.17
Ni Calc	0.00	0.00	0.00	0.00	0.00	0.00	0.00	0.00	0.00	0.00
Cr Calc	0.00	0.00	0.00	0.00	0.00	0.00	0.00	0.00	0.00	0.00
Fe 3+ Droop	0.10	0.10	0.10	0.09	0.11	0.06	0.09	0.09	0.09	0.05
Total Calc	**4.03**	**4.03**	**4.03**	**4.03**	**4.04**	**4.02**	**4.03**	**4.03**	**4.03**	**4.02**
J	0.35	0.34	0.33	0.29	0.35	0.32	0.35	0.34	0.34	0.34
Q	1.48	1.48	1.53	1.62	1.48	1.56	1.51	1.49	1.49	1.51
group	Quad	Quad	Quad	Quad	Quad	Quad	Quad	Quad	Quad	Quad
adjective	aluminian	aluminian	aluminian	aluminian	aluminian	faluminian	aluminian	aluminian	aluminian	aluminian
pyroxene	diopside	diopside	diopside	diopside	wollastonite	diopside	diopside	wollastonite	wollastonite	wollastonite
enstatite	35.19	35.22	36.44	39.47	35.61	37.06	35.72	35.28	35.04	34.92
ferrosillite	14.90	15.02	14.22	12.18	14.28	13.51	14.48	14.71	14.80	15.08
wollastonite	49.91	49.76	49.34	48.36	50.11	49.43	49.80	50.02	50.16	50.00
jadeite	----------	----------	----------	----------	----------	----------	----------	----------	----------	----------
aegirine	----------	----------	----------	----------	----------	----------	----------	----------	----------	----------
Ca-Mg-Fe	----------	----------	----------	----------	----------	----------	----------	----------	----------	----------

Rocktype	pyroxenite									
Sample	BS1010D	BS1010D	BS1010D	BS1010D	BS1010D	BS1010D	BS1010D	BS1010D	BS1010D	BS1010D
SiO2	48.50	48.91	48.73	49.73	48.99	48.76	48.87	47.15	47.18	49.08
TiO2	1.01	0.95	1.09	0.90	1.15	1.03	1.16	1.20	1.11	0.79
Al2O3	9.49	9.35	9.74	8.31	9.50	8.91	9.53	10.73	10.95	9.37
FeO	7.65	7.73	7.66	7.21	7.50	7.53	7.72	9.33	8.96	7.94
MnO	0.06	0.09	0.07	0.05	0.07	0.06	0.05	0.10	0.14	0.07
MgO	9.97	10.09	10.11	10.46	10.01	10.23	9.94	10.56	10.33	9.96
CaO	19.23	19.63	19.18	19.90	19.69	19.90	19.50	16.85	17.50	19.78
K2O	0.02	0.00	0.02	0.01	0.00	0.00	0.00	0.01	0.01	0.00
Na2O	2.48	2.41	2.50	2.47	2.53	2.40	2.39	2.36	2.41	2.36
Cr2O3	0.01	0.03	0.01	0.05	0.05	0.04	0.02	0.03	0.00	0.04
Total	**98.41**	**99.19**	**99.12**	**99.08**	**99.48**	**98.86**	**99.18**	**98.33**	**98.58**	**99.38**
Si Calc	1.82	1.83	1.82	1.85	1.82	1.83	1.82	1.78	1.77	1.83
Ti Calc	0.03	0.03	0.03	0.03	0.03	0.03	0.03	0.03	0.03	0.02
Al Calc	0.42	0.41	0.43	0.36	0.42	0.39	0.42	0.48	0.49	0.41
Fe Calc	0.24	0.24	0.24	0.22	0.23	0.24	0.24	0.29	0.28	0.25
Mn Calc	0.00	0.00	0.00	0.00	0.00	0.00	0.00	0.00	0.00	0.00
Mg Calc	0.56	0.56	0.56	0.58	0.55	0.57	0.55	0.59	0.58	0.55
Ca Calc	0.77	0.79	0.77	0.79	0.78	0.80	0.78	0.68	0.71	0.79
K Calc	0.00	0.00	0.00	0.00	0.00	0.00	0.00	0.00	0.00	0.00
Na Calc	0.18	0.17	0.18	0.18	0.18	0.17	0.17	0.17	0.18	0.17
Ni Calc	0.00	0.00	0.00	0.00	0.00	0.00	0.00	0.00	0.00	0.00
Cr Calc	0.00	0.00	0.00	0.00	0.00	0.00	0.00	0.00	0.00	0.00
Fe 3+ Droop	0.09	0.09	0.08	0.08	0.09	0.10	0.06	0.11	0.12	0.08
Total Calc	**4.03**	**4.03**	**4.03**	**4.03**	**4.03**	**4.03**	**4.02**	**4.04**	**4.04**	**4.03**
J	0.36	0.35	0.36	0.35	0.36	0.35	0.34	0.34	0.35	0.34
Q	1.48	1.49	1.47	1.51	1.48	1.49	1.50	1.45	1.44	1.50
group	Quad	Quad	Quad	Quad	Quad	Quad	Quad	Quad	Quad	Quad
adjective	aluminian	aluminian	aluminian	aluminian	aluminian	aluminian	aluminian	aluminian	faluminian	faluminian
pyroxene	diopside	diopside	diopside	diopside	diopside	diopside	diopside	augite	augite	diopside
enstatite	35.45	35.29	35.82	36.28	35.24	35.52	35.10	37.76	36.88	34.74
ferrosillite	15.40	15.35	15.36	14.11	14.95	14.78	15.40	18.93	18.23	15.67
wollastonite	49.15	49.37	48.81	49.61	49.81	49.70	49.50	43.31	44.90	49.60
jadeite	----------	----------	----------	----------	----------	----------	----------	----------	----------	----------
aegirine	----------	----------	----------	----------	----------	----------	----------	----------	----------	----------
Ca-Mg-Fe	----------	----------	----------	----------	----------	----------	----------	----------	----------	----------

Rocktype	pyroxenite									
Sample	BS1010F	BS1010F	BS1010F	BS1010F	BS1010F	BS1010F	BS1010F	BS1010F	BS1010F	BS1010F
SiO2	49.48	50.16	50.14	50.33	49.77	50.73	49.41	49.63	50.16	50.13
TiO2	0.79	0.81	0.93	0.73	0.75	0.67	0.84	0.74	0.68	0.71
Al2O3	8.11	8.50	8.44	8.84	9.25	8.80	9.51	9.14	8.61	8.65
FeO	7.54	7.42	7.52	7.44	7.97	7.41	8.33	7.61	7.58	7.11
MnO	0.06	0.05	0.04	0.03	0.05	0.06	0.03	0.05	0.04	0.03
MgO	10.21	10.36	10.06	9.97	10.19	9.98	10.19	10.11	10.09	10.16
CaO	18.98	18.95	19.28	18.86	18.27	19.23	18.04	18.44	19.05	19.62
K2O	0.00	0.00	0.01	0.01	0.03	0.01	0.01	0.03	0.00	0.01
Na2O	2.71	2.75	2.70	2.67	2.60	2.61	2.56	2.68	2.63	2.39
Cr2O3	0.02	0.00	0.00	0.03	0.00	0.03	0.01	0.08	0.03	0.04
Total	**97.89**	**99.02**	**99.12**	**98.90**	**98.87**	**99.52**	**98.94**	**98.52**	**98.86**	**98.84**
Si Calc	1.87	1.87	1.87	1.87	1.85	1.88	1.84	1.86	1.87	1.87
Ti Calc	0.02	0.02	0.03	0.02	0.02	0.02	0.02	0.02	0.02	0.02
Al Calc	0.36	0.37	0.37	0.39	0.41	0.38	0.42	0.40	0.38	0.38
Fe Calc	0.24	0.23	0.23	0.23	0.25	0.23	0.26	0.24	0.24	0.22
Mn Calc	0.00	0.00	0.00	0.00	0.00	0.00	0.00	0.00	0.00	0.00
Mg Calc	0.57	0.57	0.56	0.55	0.57	0.55	0.57	0.56	0.56	0.56
Ca Calc	0.77	0.76	0.77	0.75	0.73	0.76	0.72	0.74	0.76	0.78
K Calc	0.00	0.00	0.00	0.00	0.00	0.00	0.00	0.00	0.00	0.00
Na Calc	0.20	0.20	0.19	0.19	0.19	0.19	0.18	0.19	0.19	0.17
Ni Calc	0.00	0.00	0.00	0.00	0.00	0.00	0.00	0.00	0.00	0.00
Cr Calc	0.00	0.00	0.00	0.00	0.00	0.00	0.00	0.00	0.00	0.00
Fe 3+ Droop	0.09	0.07	0.06	0.03	0.05	0.02	0.05	0.06	0.05	0.03
Total Calc	**4.03**	**4.02**	**4.02**	**4.01**	**4.02**	**4.01**	**4.02**	**4.02**	**4.02**	**4.01**
J	0.39	0.40	0.39	0.38	0.37	0.37	0.37	0.39	0.38	0.34
Q	1.48	1.48	1.49	1.50	1.49	1.51	1.49	1.48	1.50	1.54
group	Ca-Na	Ca-Na	Ca-Na	Ca-Na	Ca-Na	Quad	Quad	Ca-Na	Ca-Na	Quad
adjective						aluminian	aluminian			aluminian
pyroxene	omphacite	omphacite	omphacite	omphacite	omphacite	diopside	diopside	omphacite	omphacite	diopside
enstatite	----------	----------	----------	----------	----------	35.66	36.60	----------	----------	35.94
ferrosillite	----------	----------	----------	----------	----------	14.96	16.85	----------	----------	14.17
wollastonite	----------	----------	----------	----------	----------	49.37	46.54	----------	----------	49.89
jadeite	14.81	16.02	16.26	18.17	16.88	----------	----------	16.92	16.64	----------
aegirine	6.22	5.04	4.33	2.18	3.17	----------	----------	3.83	3.48	----------
Ca-Mg-Fe	78.98	78.94	79.42	79.65	79.95	----------	----------	79.24	79.88	----------

Rocktype	pyroxenite									
Sample	BS1010F	BS1010F	BS1010F	BS1010F	BS1010F	BS1010F	BS1010F	BS1010F	BS1010F	BS1010F
SiO2	49.68	50.39	48.44	50.31	51.00	50.56	49.50	51.07	50.77	51.31
TiO2	0.68	0.64	0.97	0.58	0.70	1.92	0.73	0.59	0.65	0.68
Al2O3	8.64	8.40	9.82	8.00	8.00	8.11	8.79	8.14	8.13	8.05
FeO	7.85	7.51	8.83	7.67	7.30	7.43	8.31	7.43	7.32	7.37
MnO	0.08	0.05	0.08	0.09	0.07	0.07	0.07	0.06	0.02	0.07
MgO	10.06	10.06	10.62	10.18	10.49	10.06	10.46	10.29	10.19	10.18
CaO	18.72	19.34	17.07	19.09	19.76	19.09	17.78	19.25	19.42	19.17
K2O	0.01	0.01	0.02	0.00	0.00	0.01	0.02	0.01	0.02	0.01
Na2O	2.66	2.61	2.50	2.60	2.54	2.60	2.54	2.58	2.63	2.76
Cr2O3	0.03	0.04	0.03	0.04	0.04	0.08	0.02	0.01	0.04	0.05
Total	**98.40**	**99.05**	**98.39**	**98.56**	**99.91**	**99.94**	**98.22**	**99.43**	**99.20**	**99.64**
Si Calc	1.86	1.88	1.82	1.88	1.88	1.86	1.86	1.89	1.88	1.89
Ti Calc	0.02	0.02	0.03	0.02	0.02	0.05	0.02	0.02	0.02	0.02
Al Calc	0.38	0.37	0.43	0.35	0.35	0.35	0.39	0.36	0.36	0.35
Fe Calc	0.25	0.23	0.28	0.24	0.23	0.23	0.26	0.23	0.23	0.23
Mn Calc	0.00	0.00	0.00	0.00	0.00	0.00	0.00	0.00	0.00	0.00
Mg Calc	0.56	0.56	0.59	0.57	0.58	0.55	0.59	0.57	0.56	0.56
Ca Calc	0.75	0.77	0.69	0.77	0.78	0.75	0.72	0.76	0.77	0.76
K Calc	0.00	0.00	0.00	0.00	0.00	0.00	0.00	0.00	0.00	0.00
Na Calc	0.19	0.19	0.18	0.19	0.18	0.19	0.18	0.18	0.19	0.20
Ni Calc	0.00	0.00	0.00	0.00	0.00	0.00	0.00	0.00	0.00	0.00
Cr Calc	0.00	0.00	0.00	0.00	0.00	0.00	0.00	0.00	0.00	0.00
Fe 3+ Droop	0.07	0.05	0.08	0.05	0.05	0.00	0.06	0.03	0.04	0.03
Total Calc	**4.02**	**4.02**	**4.03**	**4.02**	**4.02**	**4.00**	**4.02**	**4.01**	**4.01**	**4.01**
J	0.38	0.38	0.36	0.38	0.36	0.37	0.37	0.37	0.38	0.39
Q	1.48	1.51	1.47	1.51	1.53	1.54	1.50	1.53	1.52	1.51
group	Ca-Na	Quad	Quad	Quad	Quad	Quad	Quad	Quad	Quad	Ca-Na
adjective		aluminian	aluminian	aluminian	aluminian	aluminian	aluminian	aluminian	aluminian	
pyroxene	omphacite	diopside	augite	diopside	diopside	diopside	diopside	diopside	diopside	omphacite
enstatite	----------	35.66	38.09	36.04	36.39	35.96	37.44	36.34	36.05	----------
ferrosillite	----------	15.05	17.93	15.40	14.35	15.03	16.83	14.83	14.57	----------
wollastonite	----------	49.29	43.98	48.56	49.26	49.01	45.74	48.83	49.38	----------
jadeite	15.93	----------	----------	----------	----------	----------	----------	----------	----------	18.30
aegirine	4.64	----------	----------	----------	----------	----------	----------	----------	----------	2.36
Ca-Mg-Fe	79.43	----------	----------	----------	----------	----------	----------	----------	----------	79.34

Rocktype	garnetite								
Sample	BS1010A cpx1 incl in grt	BS1010A cpx1 incl in grt	BS1010A cpx1 incl in grt	BS1010A cpx2 incl in grt	BS1010A cpx2 in cl in grt	BS1010A cpx2 incl in grt	BS1010A cpx3 incl in grt	BS1010A cpx3 incl in grt	BS1010A cpx3 incl in grt
SiO2	42.90	48.64	39.83	51.89	52.70	52.23	51.85	52.23	53.42
TiO2	0.52	0.42	0.50	0.54	0.46	0.54	0.51	0.42	0.31
Al2O3	5.48	4.19	3.73	5.52	4.87	5.47	5.64	5.38	4.65
FeO	8.08	5.99	7.41	6.94	6.07	6.64	6.58	6.43	6.20
MnO	0.04	0.06	0.04	0.04	0.04	0.05	0.03	0.06	0.02
MgO	9.55	11.44	8.95	12.30	12.96	12.32	12.14	12.21	13.13
CaO	14.93	20.89	15.60	20.43	21.00	20.55	20.57	20.75	21.06
K2O	0.03	0.00	0.04	0.00	0.00	0.01	0.01	0.01	0.03
Na2O	1.57	1.69	1.19	1.94	2.12	2.27	2.17	2.14	1.97
Cr2O3	0.05	0.03	0.04	0.02	0.03	0.00	0.03	0.02	0.03
Total	**83.14**	**93.35**	**77.32**	**99.62**	**100.25**	**100.08**	**99.53**	**99.65**	**100.84**
Si Calc	1.91	1.93	1.92	1.92	1.93	1.92	1.92	1.93	1.94
Ti Calc	0.02	0.01	0.02	0.01	0.01	0.01	0.01	0.01	0.01
Al Calc	0.29	0.20	0.21	0.24	0.21	0.24	0.25	0.23	0.20
Fe Calc	0.30	0.20	0.30	0.21	0.19	0.20	0.20	0.20	0.19
Mn Calc	0.00	0.00	0.00	0.00	0.00	0.00	0.00	0.00	0.00
Mg Calc	0.63	0.68	0.64	0.68	0.71	0.68	0.67	0.67	0.71
Ca Calc	0.71	0.89	0.81	0.81	0.82	0.81	0.81	0.82	0.82
K Calc	0.00	0.00	0.00	0.00	0.00	0.00	0.00	0.00	0.00
Na Calc	0.14	0.13	0.11	0.14	0.15	0.16	0.16	0.15	0.14
Ni Calc	0.00	0.00	0.00	0.00	0.00	0.00	0.00	0.00	0.00
Cr Calc	0.00	0.00	0.00	0.00	0.00	0.00	0.00	0.00	0.00
Fe 3+ Droop	0.00	0.08	0.04	0.05	0.08	0.08	0.07	0.06	0.05
Total Calc	**4.00**	**4.03**	**4.01**	**4.02**	**4.03**	**4.03**	**4.02**	**4.02**	**4.02**
J	0.27	0.26	0.22	0.28	0.30	0.32	0.31	0.30	0.28
Q	1.65	1.67	1.70	1.65	1.63	1.60	1.61	1.62	1.66
group	Quad	Quad	Quad	Quad	Quad	Quad	Quad	Quad	Quad
adjective	aluminian	aluminian	aluminian	aluminian	aluminian	aluminian	aluminian	aluminian	aluminian
pyroxene	augite	wollastonite	diopside	diopside	diopside	diopside	diopside	diopside	diopside
enstatite	38.45	38.33	36.76	39.81	41.17	39.94	39.64	39.70	41.34
ferrosillite	18.34	11.38	17.18	12.67	10.88	12.17	12.10	11.82	11.00
wollastonite	43.22	50.29	46.06	47.52	47.95	47.89	48.26	48.48	47.66
jadeite	----------	----------	----------	----------	----------	----------	----------	----------	----------
aegirine	----------	----------	----------	----------	----------	----------	----------	----------	----------
Ca-Mg-Fe	----------	----------	----------	----------	----------	----------	----------	----------	----------

Appendix 3 – rock densities of BOG

Scale: Mettler Toledo AG 204 Delta Range equiped with density determination kit
Date: 01/02/2010 and 02/02/2010

Density = [(A x DL)/(A-B)]+C

Sample No	Rock-Type	Density [g/cm^3]	Average [g/cm^3]	Stdev	A (dry-wt) [g]	DL (Liqiud Den	B (wet-wt) [g]	Constant
P78754	Omp Granulite	2.9806	3.0173	0.034	20.5335	0.99662	13.6649	0.0012
(0907)		2.9909			4.4122	0.99654	2.9415	0.0012
		3.0846			10.8793	0.99654	7.3632	0.0012
		2.9828			10.9483	0.99651	7.2892	0.0012
		2.9893			11.3677	0.99651	7.5767	0.0012
		3.0237			13.8972	0.99651	9.3153	0.0012
		3.0123			9.3865	0.99648	6.2802	0.0012
		3.0297			5.4059	0.99648	3.6272	0.0012
		3.0541			8.8875	0.99646	5.9866	0.0012
		3.0253			4.0179	0.99643	2.694	0.0012
		2.9717			7.3062	0.99626	4.8558	0.0012
		3.0065			5.2437	0.99626	3.5054	0.0012
		3.0725			12.0779	0.99657	8.1589	0.0012
		2.9864			9.2156	0.99657	6.1391	0.0012
		2.9438			3.9381	0.99657	2.6044	0.0012
P78760	Omp Granulite	3.2692	3.1311	0.109	10.958	0.99643	7.6168	0.0012
(0901C)		3.1588			10.6215	0.9964	7.2698	0.0012
		3.0437			9.9325	0.9964	6.6797	0.0012
		3.2322			3.433	0.9964	2.3743	0.0012
		3.1202			13.9452	0.9964	9.4903	0.0012
		3.0310			7.5659	0.99637	5.0778	0.0012
		2.9924			6.4555	0.99637	4.3052	0.0012
		3.2988			6.805	0.99637	4.7489	0.0012
		3.1372			5.5435	0.99637	3.7822	0.0012
		3.0272			4.998	0.99637	3.3523	0.0012
P73831	retrogr. Omp Granulite w	2.9248	2.8812	0.065	14.6535	0.99634	9.6597	0.0012
		2.8307			28.1141	0.99632	18.2146	0.0012
		2.9065			11.3137	0.99629	7.434	0.0012
		2.7965			4.9829	0.99629	3.2069	0.0012
		2.9477			21.8818	0.99626	14.4832	0.0012
0901A	Omp Granulite	2.9768	3.0486		15.5145	0.99614	10.3208	0.0012
		3.1204			26.2297	0.99614	17.853	0.0012
0901B	Omp Granulite	2.9722	2.9769		15.3956	0.99648	10.2319	0.0012
		2.9760			16.6568	0.99648	11.0773	0.0012
		2.9975			15.0996	0.99648	10.078	0.0012
		3.0329			22.4106	0.99648	15.0445	0.0012
		2.8841			9.2545	0.99648	6.0557	0.0012
		2.9986			36.8215	0.99648	24.5802	0.0012
0901D	Omp Granulite	2.7567	2.7657		10.8014	0.99646	6.8953	0.0012
0902A	Omp Granulite	3.0133	3.0133		19.2959	0.99617	12.9144	0.0012
0904D	Omp Granulite	3.0507	3.0325		29.6898	0.9962	19.9909	0.0012
		3.0531			21.375	0.9962	14.3977	0.0012
		2.9939			5.3851	0.9962	3.5925	0.0012
0904G	Omp Granulite	2.9574	2.9868		34.4333	0.99626	22.8292	0.0012
		3.0161			28.3399	0.99626	18.975	0.0012
0905A	Omp Granulite	2.9782	2.9590		31.7593	0.99617	21.132	0.0012
		2.9019			31.2369	0.99617	20.5095	0.0012
		2.9511			13.8834	0.99617	9.195	0.0012
		2.9887			5.3839	0.99654	3.588	0.0012
		2.9751			41.1868	0.99654	27.3852	0.0012
0905B	Omp Granulite	3.0891	3.0657		18.2832	0.99623	12.3847	0.0012
		3.0423			19.3895	0.99623	13.0378	0.0012

Sample No	Rock-Type	Density [g/cm^3]	Average [g/cm^3]	Stdev	A (dry-wt) [g]	DL (Liqiud Den	B (wet-wt) [g]	Constant
0908A	Omp Granulite (not typic	3.1502	3.1262		37.4856	0.99614	25.6277	0.0012
		3.1019			6.2356	0.99651	4.2316	0.0012
		3.1325			2.7743	0.99651	1.8914	0.0012
		3.1422			4.6354	0.99651	3.1648	0.0012
		3.1043			16.3376	0.99648	11.0912	0.0012
0908B	Omp-Granulite	2.8495	2.8272		6.8548	0.99646	4.4567	0.0012
		2.8260			5.5467	0.99646	3.5901	0.0012
		2.8060			6.3837	0.99646	4.1158	0.0012
0909	Omp Granulite	3.0557	3.0557		49.6732	0.9967	33.4645	0.0012
0905C	2-Pyroxene Granulite	2.9405	2.9394		19.7675	0.99626	13.0673	0.0012
		2.9383			55.1922	0.99623	36.4719	0.0012
P78753	Eclogite	3.5707	3.5602	0.024	16.0549	0.99654	11.5727	0.0012
(0904C)		3.5439			10.7782	0.99654	7.7464	0.0012
		3.5604			10.0731	0.99654	7.2527	0.0012
		3.5736			9.8108	0.99648	7.0742	0.0012
		3.5776			10.4217	0.99648	7.5179	0.0012
		3.5881			10.5243	0.99648	7.6005	0.0012
		3.5648			19.2322	0.99648	13.8543	0.0012
		3.5795			7.3011	0.99643	5.268	0.0012
		3.5133			5.4297	0.99643	3.8892	0.0012
		3.5302			15.3602	0.99643	11.0232	0.0012
0901C	Eclogite	3.1350	3.135		26.2907	0.99617	17.9334	0.0012
0901E	Eclogite (pyx-rich)	3.4321	3.3994		69.025	0.99681	48.9705	0.0012
		3.3667			39.9578	0.99659	28.1256	0.0012
0902B	Eclogite	3.3205	3.2847		31.9247	0.99662	22.3394	0.0012
		3.2440			2.9544	0.99654	2.0465	0.0012
		3.2600			4.2198	0.99654	2.9294	0.0012
		3.3142			31.2567	0.99654	21.8549	0.0012
0902C	Eclogite	3.3016	3.3188		8.8721	0.99651	6.1933	0.0012
		3.3341			40.4046	0.99651	28.3241	0.0012
		3.3205			13.5057	0.99614	9.4526	0.0012
0902D	Eclogite	3.3660	3.366		30.383	0.99668	21.3832	0.0012
0903C	Eclogite	3.5790	3.5512		19.3668	0.99654	13.9725	0.0012
		3.5312			10.2123	0.99654	7.3293	0.0012
		3.5435			11.1853	0.99654	8.0386	0.0012
0904A	Eclogite	3.5009	3.4560		54.3617	0.99614	38.8882	0.0012
		3.4283			81.041	0.99614	57.4852	0.0012
		3.4387			50.1044	0.99662	35.5779	0.0012
0904C	Eclogite	3.5135	3.5459		10.8848	0.99668	7.796	0.0012
		3.5783			16.8106	0.99668	12.1267	0.0012
0904E	Eclogite	3.6081	3.6081		13.3063	0.9967	9.6293	0.0012
0904F	Eclogite	3.5493	3.5406		26.4876	0.99617	19.0509	0.0012
		3.5311			77.462	0.99617	55.6015	0.0012
		3.5413			10.8695	0.99617	7.8109	0.0012
0910A	Eclogite	3.4591	3.2410		6.0952	0.99648	4.3387	0.0012
		3.2692			4.2867	0.99648	2.9796	0.0012
		3.3446			2.4201	0.99648	1.6988	0.0012
		3.1691			2.5515	0.99648	1.7489	0.0012
		2.9629			31.5725	0.99665	20.9479	0.0012
0904B	Eclogite (grt-rich)	3.6481	3.6094		21.3787	0.99614	15.5391	0.0012
		3.5708			39.3666	0.99614	28.381	0.0012
0906B	Garnetite	3.6943	3.6357		5.0035	0.99651	3.6534	0.0012
		3.5727			2.4866	0.99651	1.7928	0.0012
		3.6712			17.1797	0.99651	12.5149	0.0012
		3.6045			68.954	0.99617	49.8911	0.0012
0910B	Garnetite	3.6945	3.6404		76.233	0.99614	55.672	0.0012
		3.5862			90.632	0.99614	65.449	0.0012
0910D	Pyroxenite/Garnetite	3.2761	3.2500		3.4126	0.99651	2.3742	0.0012
		3.2239			57.3512	0.99651	39.6171	0.0012
0910C	Pyroxenite	3.4431	3.4378		7.9821	0.99646	5.6712	0.0012
		3.4564			2.8336	0.99646	2.0164	0.0012
		3.3696			3.6309	0.99646	2.5568	0.0012
		3.4821			20.8315	0.99646	14.8682	0.0012
0906A	Pyroxenite	3.3662	3.3662		66.519	0.99678	46.8146	0.0012
0903A	Hbl Peridotite	3.2651	3.2651		15.0958	0.99678	10.4856	0.0012
0903B	Hbl Peridotite	3.2922	3.2922		43.8366	0.99668	30.5607	0.0012

Appendix 4 – pictures of zircon minerals

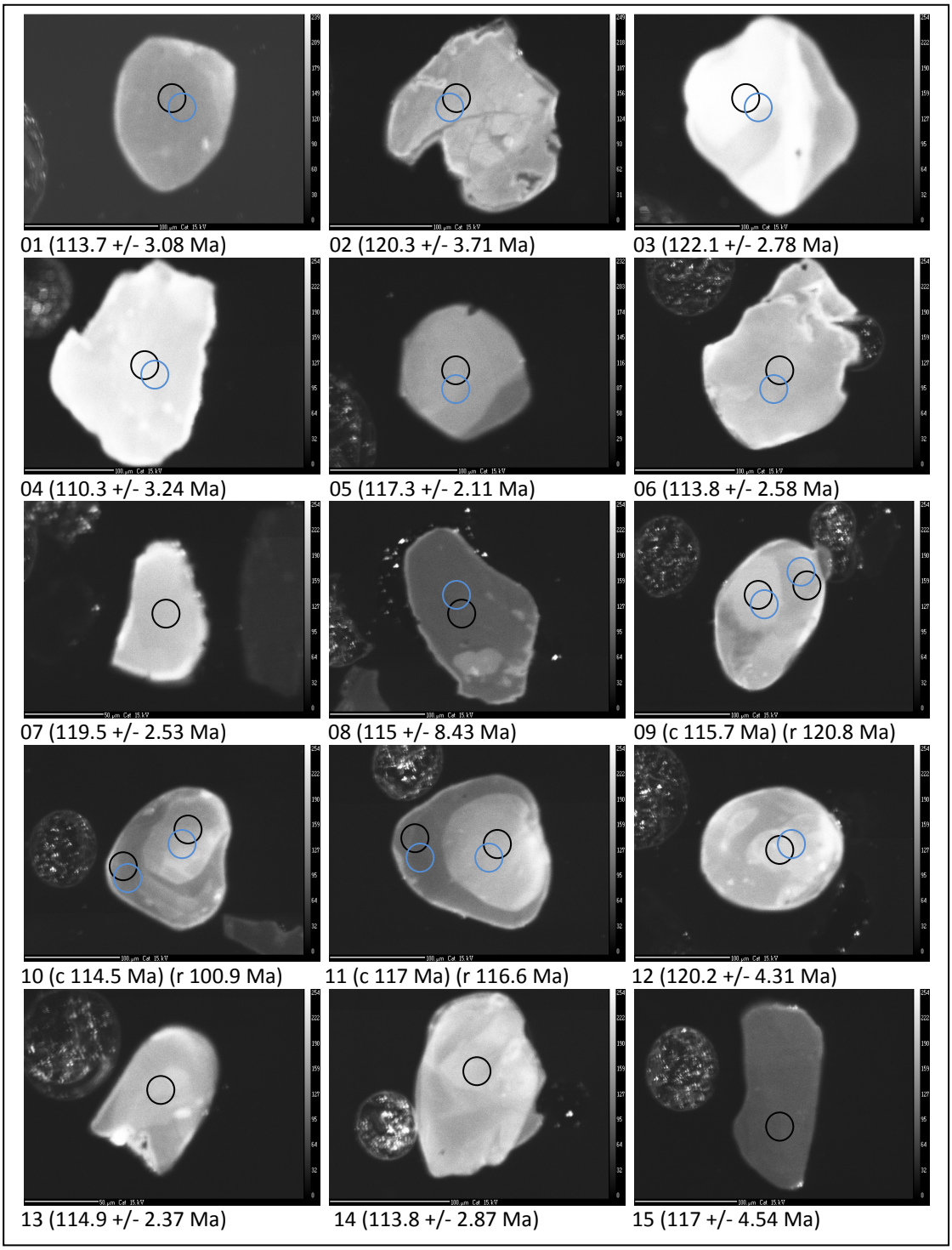

Sample P78760 (mount b): black circles location of Pb/U, blue circles locations of Hf measurement

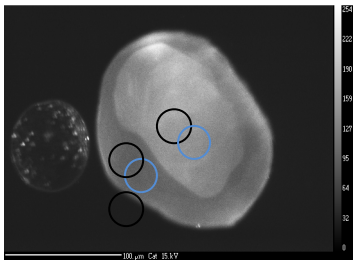
16 (c 119 Ma) (r 114.4 Ma)

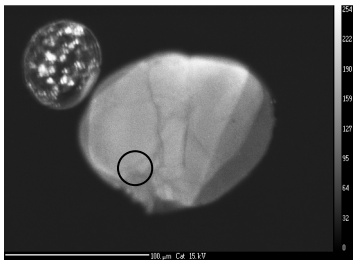
17 (113.8 1/- 2.54 Ma)

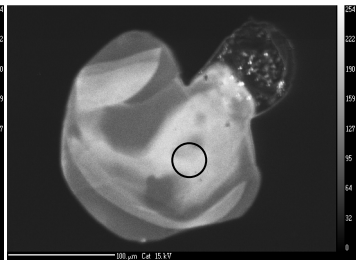
18 (114.4 +/- 3.89 Ma)

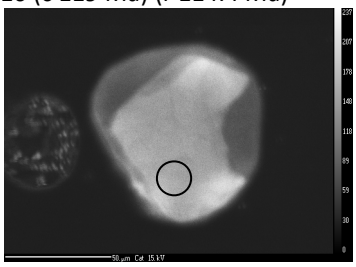
19 (87.6 +/- 3.97 Ma)

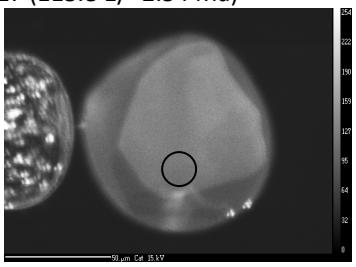
20 (112.2 +/- 2.42 Ma)

21 (110.6 +/- 3.09 Ma)

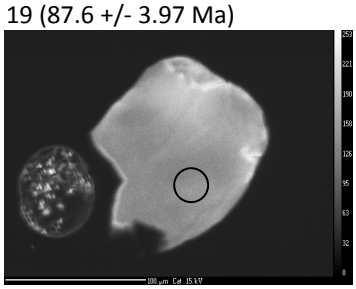
22 (112.3 +/- 2.64 Ma)

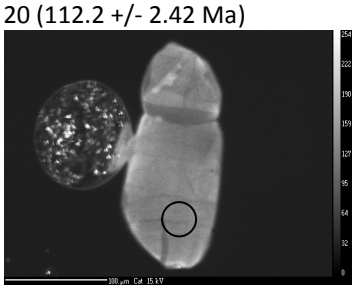
23 (116 +/- 3.97 Ma)

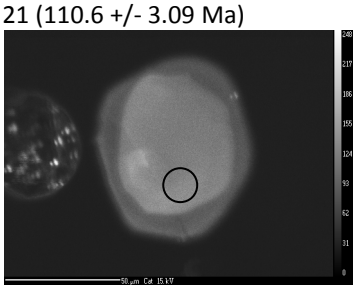
24 (112.1 +/- 3.64 Ma)

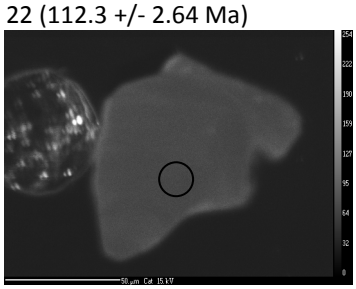
25 (106.9 +/- 4.63 Ma)

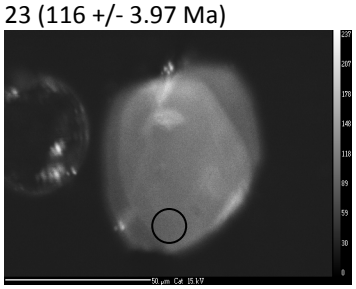
26 (116.2 +/- 2.78 Ma)

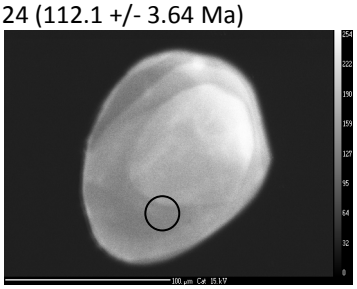
27 (118 +/- 2.72 Ma)

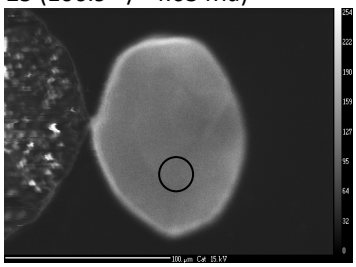
28 (102.7 +/- 3.36 Ma)

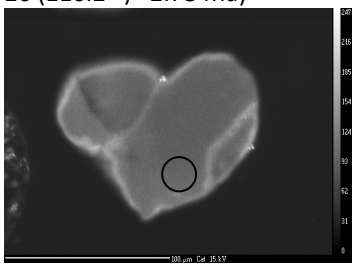
29 (112.1 +/- 2.98 Ma)

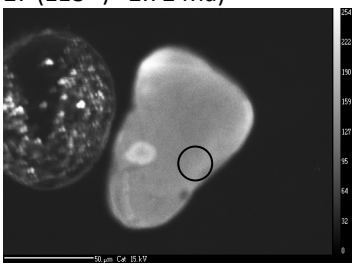
30 (115 +/- 4.42 Ma)

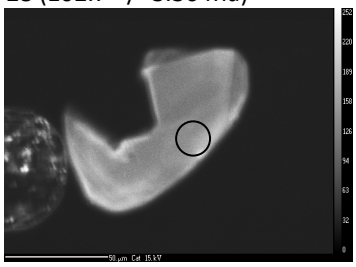
31 (122.2 +/- 2.49 Ma)

Sample 78760 (mount b) continued: black circles location of Pb/U, blue circles locations of Hf measurement

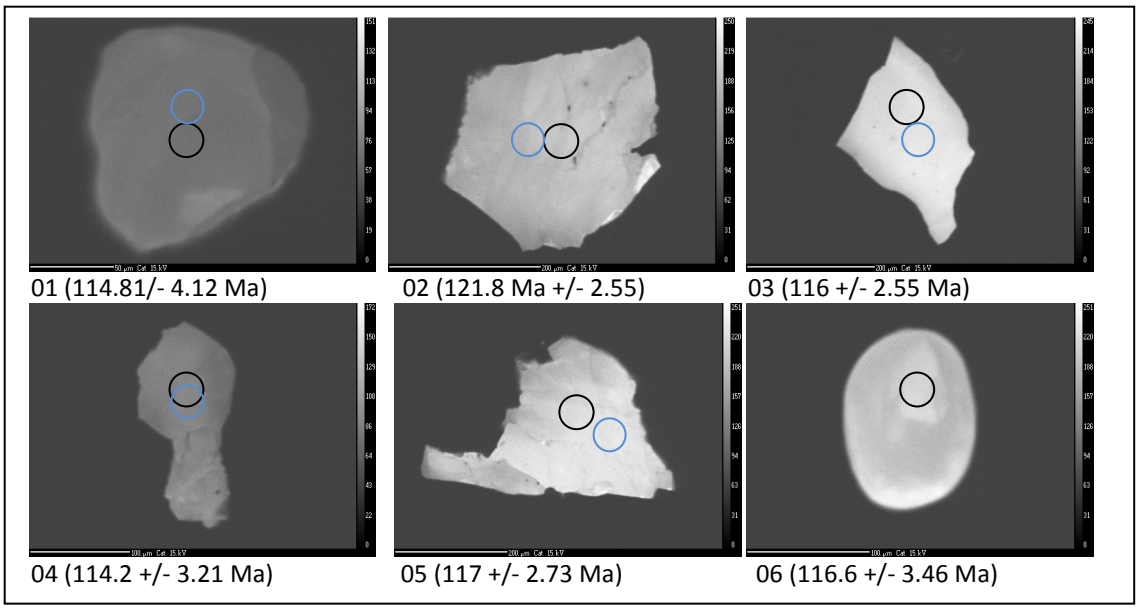

Sample 78760 (mount a): black circles location of Pb/U, blue circles locations of Hf measurement.

Appendix 5 – U/Pb data

GLITTER! 4.4 revision 525: Laser Ablation Analysis Results

Z:\Daniel\run1
Created: Tue Apr 27 11:24:53 2010

GLITTER!: Isotope ratios.

Analysis_#	Pb207/Pb206	Pb206/U238	Pb207/U235	Pb208/Th232		
STDGJ-01	0.06035292	0.09666232	0.8040415	0.03130166		
STDGJ-02	0.06169122	0.09717686	0.82627022	0.0293684		
91500-1	0.07633008	0.17898691	1.88286412	0.05648741		
MT-1	0.06457114	0.12093329	1.07627952	0.03853992		
STDGJ-03	0.05940876	0.09857848	0.80721694	0.0327063		
P78760B-01	0.05454176	0.01779193	0.1337585	0.0057729		
P78760B-02	0.04757214	0.01882958	0.12348374	0.00633203		
P78760B-03	0.04915043	0.01911675	0.12950784	0.00658522		
P78760B-04	0.04632553	0.01725697	0.11020177	0.0054857		
P78760B-05	0.04776761	0.01835986	0.12089254	0.00574959		
P78760B-06	0.05119781	0.01781106	0.12570412	0.00623543		
P78760B-07	0.05129026	0.01870646	0.13226089	0.00582178		
P78760B-08	-0.05084451	0.01799689	-0.12614039	0.00840725		
P78760B-09 core	0.0482086	0.01811246	0.12037211	0.00586547		
P78760B-09 rim	0.04791747	0.01891861	0.12497939	0.006404		
STDGJ-04	0.06050843	0.09792533	0.81690025	0.0300482		
STDGJ-05	0.05919113	0.09676772	0.7897982	0.03179593		

GLITTER!: Isotopic ratios: 1 sigma uncertainty.

Analysis_#	Pb207/Pb206	Pb206/U238	Pb207/U235	Pb208/Th232		
STDGJ-01	0.00107076	0.00116922	0.01436418	0.00191199		
STDGJ-02	0.00105198	0.0011452	0.01409133	0.00176425		
91500-1	0.00155522	0.00228623	0.03802896	0.00260327		
MT-1	0.00133339	0.00153149	0.02212541	0.00166133		
STDGJ-03	0.00186512	0.00150364	0.02475875	0.00356673		
P78760B-01	0.00827132	0.00048602	0.02001815	0.00049021		
P78760B-02	0.00876216	0.0005865	0.02248926	0.00058115		
P78760B-03	0.00569151	0.00043911	0.01480252	0.00051488		
P78760B-04	0.00787974	0.00051154	0.01852628	0.00048036		
P78760B-05	0.00426545	0.00033401	0.01067102	0.00034508		
P78760B-06	0.00529311	0.00040803	0.01276439	0.0005028		
P78760B-07	0.00567319	0.00039984	0.01445562	0.00049841		
P78760B-08	0.03472389	0.00133189	0.08566317	0.00177358		
P78760B-09 core	0.00521447	0.00037306	0.01286922	0.00043085		
P78760B-09 rim	0.0069782	0.00046703	0.01800841	0.00055948		
STDGJ-04	0.00127159	0.00123643	0.01710073	0.00231634		
STDGJ-05	0.00155728	0.00129667	0.02032247	0.00295345		

GLITTER!: Age estimates (ma).

Analysis_#	Pb207/Pb206	Pb206/U238	Pb207/U235	Pb208/Th232		
STDGJ-01	616.2	594.8	599.1	623		
STDGJ-02	663.4	597.8	611.5	585.1		
91500-1	1103.7	1061.4	1075.1	1110.7		
MT-1	760.4	735.9	741.8	764.3		
STDGJ-03	582.1	606.1	600.9	650.5		
P78760B-01	393.4	113.7	127.5	116.3		
P78760B-02	77.3	120.3	118.2	127.6		
P78760B-03	155	122.1	123.7	132.7		
P78760B-04	14.6	110.3	106.1	110.6		
P78760B-05	86.8	117.3	115.9	115.9		
P78760B-06	249.7	113.8	120.2	125.6		
P78760B-07	253.9	119.5	126.1	117.3		
P78760B-08	0.1	115	-136.9	169.2		
P78760B-09 core	109.5	115.7	115.4	118.2		
P78760B-09 rim	94.1	120.8	119.6	129		
STDGJ-04	621.8	602.2	606.3	598.4		
STDGJ-05	574.1	595.4	591.1	632.7		

GLITTER!: Age estimates: 1 sigma uncertainty (ma).

Analysis_#	Pb207/Pb206	Pb206/U238	Pb207/U235	Pb208/Th232		
STDGJ-01	37.85	6.87	8.08	37.47		
STDGJ-02	36.12	6.73	7.83	34.64		
91500-1	40.21	12.5	13.39	49.8		
MT-1	42.95	8.81	10.82	32.33		
STDGJ-03	66.75	8.82	13.91	69.81		
P78760B-01	308.46	3.08	17.93	9.85		
P78760B-02	387.52	3.71	20.33	11.67		
P78760B-03	250.74	2.78	13.31	10.34		
P78760B-04	364.85	3.24	16.94	9.66		
P78760B-05	200.03	2.11	9.67	6.93		
P78760B-06	221.23	2.58	11.51	10.1		
P78760B-07	235.61	2.53	12.96	10.02		
P78760B-08	0	8.43	99.54	35.55		
P78760B-09 core	237.22	2.36	11.66	8.66		
P78760B-09 rim	313.84	2.95	16.25	11.24		
STDGJ-04	44.7	7.26	9.56	45.45		
STDGJ-05	56.2	7.62	11.53	57.86		

GLITTER!: Mean Raw CPS background subtracted.

Analysis_#	Pb204	Pb206	Pb207	Pb208	Th232	U238
STDGJ-01	136	7025	427	107	3679	81004
STDGJ-02	162	7065	442	100	3534	79081
91500-1	290	4251	326	476	9016	26407
MT-1	235	4467	290	1172	32573	41371
STDGJ-03	180	7135	425	120	4158	84773
P78760B-01	151	240	13	68	12160	14435
P78760B-02	183	296	14	112	20501	18893
P78760B-03	120	381	18	93	16152	23144
P78760B-04	179	304	14	125	26734	21058
P78760B-05	71	440	21	128	23558	26328
P78760B-06	103	351	18	87	14804	21289
P78760B-07	87	318	16	60	11430	19247
P78760B-08	76	49	0	17	2350	3210
P78760B-09 core	94	364	17	108	19873	22188
P78760B-09 rim	51	275	13	76	12911	16106
STDGJ-04	191	7421	450	108	3949	84415
STDGJ-05	156	6882	408	111	3587	76732

GLITTER! 4.4 revision 525: Laser Ablation Analysis Results

Z:\Daniel\run2
Created: Tue Apr 27 12:42:12 2010

GLITTER!: Isotope ratios.

Analysis_#	Pb207/Pb206	Pb206/U238	Pb207/U235	Pb208/Th232
STDGJ-04	0.06046927	0.09817331	0.81846857	0.03037038
STDGJ-05	0.059235	0.09675035	0.79022735	0.03141543
MT-02	0.06662764	0.12222526	1.12278295	0.03842035
91500-02	0.07489362	0.17922635	1.85069811	0.05524866
P78760B-10 rim	0.00151463	0.01577723	0.00329463	0.00610559
P78760B-10 core	0.04922412	0.01792342	0.12164223	0.00592925
P78760B-11 rim	0.0480299	0.01831939	0.12131072	0.00494473
P78760B-11core	0.05693406	0.01825938	0.14332753	0.00610751
P78760B-12	0.01955217	0.01882425	0.05074267	0.00540009
P78760B-13	0.04923273	0.0179814	0.12205009	0.00580402
P78760B-14	0.05139234	0.01780213	0.12613735	0.00625814
P78760B-15	0.0398851	0.01831678	0.10072498	0.00509408
P78760B-16 rim	0.03716249	0.01789785	0.09170283	0.00596183
P78760B-16 core	0.05028563	0.01862732	0.12914084	0.00539132
STDGJ-06	0.05518333	0.09661387	0.73504931	0.02610962
STDGJ-07	0.05960331	0.09724277	0.79911309	0.03019371
STDGJ-08	0.06020742	0.09833777	0.81624812	0.03197815

GLITTER!: Isotopic ratios: 1 sigma uncertainty.

Analysis_#	Pb207/Pb206	Pb206/U238	Pb207/U235	Pb208/Th232
STDGJ-04	0.00100833	0.00117594	0.01386172	0.00166128
STDGJ-05	0.00120236	0.00118259	0.01582134	0.00204326
MT-02	0.00129001	0.00151011	0.02165759	0.0013734
91500-02	0.00155443	0.00231806	0.03819343	0.00239525
P78760B-10 rim	0.02261605	0.00082883	0.04919443	0.00126429
P78760B-10 core	0.0054926	0.00042495	0.01335968	0.00036447
P78760B-10 rim	0.02425989	0.0010206	0.06092459	0.00120516
P78760B-11core	0.00561482	0.00038636	0.01392314	0.0003674
P78760B-12	0.01340983	0.00068083	0.03476094	0.00069026
P78760B-13	0.00480807	0.00037458	0.01175444	0.00032775
P78760B-14	0.00783956	0.00045391	0.01904008	0.00041185
P78760B-15	0.01535146	0.00071698	0.0385916	0.00073722
P78760B-16 rim	0.01174431	0.00057963	0.02885341	0.00069133
P78760B-16 core	0.00767319	0.00059975	0.01935957	0.00060921
STDGJ-06	0.00213801	0.00167141	0.02774391	0.00337366
STDGJ-07	0.00648642	0.00365309	0.08295892	0.009996
STDGJ-08	0.00126807	0.00124103	0.01704222	0.00220159

GLITTER!: Age estimates (ma).

Analysis_#	Pb207/Pb206	Pb206/U238	Pb207/U235	Pb208/Th232
STDGJ-04	620.4	603.7	607.2	604.7
STDGJ-05	575.7	595.3	591.3	625.2
MT-02	826.2	743.4	764.3	762
91500-02	1065.6	1062.7	1063.7	1086.9
P78760B-10 rim	0.1	100.9	3.3	123
P78760B-10 core	158.5	114.5	116.6	119.5
P78760B-10 rim	100.7	117	116.3	99.7
P78760B-11core	488.3	116.6	136	123.1
P78760B-12	0.1	120.2	50.3	108.9
P78760B-13	158.9	114.9	116.9	117
P78760B-14	258.5	113.8	120.6	126.1
P78760B-15	0.1	117	97.4	102.7
P78760B-16 rim	0.1	114.4	89.1	120.1
P78760B-16 core	208.2	119	123.3	108.7
STDGJ-06	419.5	594.5	559.5	521
STDGJ-07	589.2	598.2	596.3	601.3
STDGJ-08	611	604.7	606	636.2

GLITTER!: Age estimates: 1 sigma uncertainty (ma).

Analysis_#	Pb207/Pb206	Pb206/U238	Pb207/U235	Pb208/Th232
STDGJ-04	35.58	6.9	7.74	32.59
STDGJ-05	43.52	6.95	8.97	40.04
MT-02	39.89	8.67	10.36	26.73
91500-02	41.18	12.67	13.6	45.88
P78760B-10 rim	0	5.26	49.79	25.4
P78760B-10 core	241.58	2.69	12.09	7.32
P78760B-10 rim	893.37	6.46	55.17	24.24
P78760B-11core	204.59	2.45	12.37	7.38
P78760B-12	0	4.31	33.59	13.88
P78760B-13	213.67	2.37	10.64	6.59
P78760B-14	317.18	2.87	17.17	8.27
P78760B-15	421.53	4.54	35.6	14.83
P78760B-16 rim	143.26	3.67	26.84	13.89
P78760B-16 core	319.65	3.8	17.41	12.25
STDGJ-06	83.95	9.83	16.24	66.45
STDGJ-07	220.01	21.46	46.82	196.12
STDGJ-08	44.87	7.28	9.53	43.12

GLITTER!: Mean Raw CPS background subtracted.

Analysis_#	Pb204	Pb206	Pb207	Pb208	Th232	U238
STDGJ-04	186	7421	450	109	3950	84415
STDGJ-05	150	6881	408	111	3587	76725
MT-02	208	4192	280	1075	29780	37907
91500-02	209	4293	322	459	8908	26914
P78760B-10 rim	117	71	0	15	2675	5063
P78760B-10 core	133	384	18	150	27637	24442
P78760B-10 rim	115	65	3	13	2912	3960
P78760B-11core	107	313	17	95	16240	19159
P78760B-12	124	121	2	29	5837	7585
P78760B-13	94	394	19	171	31296	25148
P78760B-14	48	209	10	87	14370	13206
P78760B-15	92	110	4	26	5329	6748
P78760B-16 rim	110	133	4	31	5501	8340
P78760B-16 core	96	309	15	75	14162	20316
STDGJ-06	247	6009	334	87	3448	76989
STDGJ-07	240	7322	434	125	3621	83203
STDGJ-08	119	6419	386	106	3269	72516

GLITTER! 4.4 revision 525: Laser Ablation Analysis Results

Z:\Daniel\run3
Created: Tue Apr 27 14:56:33 2010

GLITTER!: Isotope ratios.

Analysis_#	Pb207/Pb206	Pb206/U238	Pb207/U235	Pb208/Th232		
STDGJ-07	0.05911755	0.09759897	0.79509985	0.0369741		
STDGJ-08	0.06003951	0.09939077	0.82233578	0.03186462		
MT-03	0.06514516	0.12099238	1.08625507	0.03474544		
91500-03	0.0761777	0.17741872	1.86267877	0.04911335		
P78760B-17	0.04376695	0.01780749	0.10741497	0.00538148		
P78760B-18	0.05056945	0.01790312	0.1248571	0.00550833		
STDGJ-09	0.05945744	0.0996499	0.8163321	0.03319822		
STDGJ-10	0.06061392	0.09349181	0.78095835	0.03136922		
P78760B-19	0.04683382	0.01368414	0.08832796	0.00499152		
P78760B-20	0.04816824	0.01756439	0.11660895	0.00561382		
P78760B-21	0.05317084	0.01730089	0.12679011	0.00653578		
P78760B-22	0.05513365	0.01756546	0.1334722	0.00550024		
P78760B-23	0.0496145	0.01815559	0.12414178	0.00661339		
P78760B-24	0.04993053	0.0175385	0.1207533	0.00602616		
P78760B-25	0.01923193	0.01672263	0.04432995	0.00647169		
P78760B-26	0.05043231	0.01818377	0.12639993	0.0057991		
P78760B-27	0.04662777	0.01846823	0.11870079	0.00620702		
STDGJ-11	0.06252656	0.09941205	0.8574208	0.02930704		
STDGJ-12	0.05763943	0.09722856	0.77272493	0.03248852		

GLITTER!: Isotopic ratios: 1 sigma uncertainty.

Analysis_#	Pb207/Pb206	Pb206/U238	Pb207/U235	Pb208/Th232		
STDGJ-07	0.00480451	0.00285028	0.06178395	0.01006387		
STDGJ-08	0.00102444	0.00120265	0.0142493	0.00166248		
MT-03	0.00131417	0.00154564	0.02196023	0.00117881		
91500-03	0.00145802	0.00227699	0.03584035	0.00185571		
P78760B-17	0.00584646	0.00040112	0.01421189	0.00025248		
P78760B-18	0.00869446	0.00061372	0.02112126	0.00057498		
STDGJ-09	0.00114627	0.00124763	0.01579403	0.00197877		
STDGJ-10	0.00126855	0.00118006	0.01620378	0.002086		
P78760B-19	0.01557588	0.00062444	0.02912127	0.00049574		
P78760B-20	0.00543012	0.00038159	0.01298199	0.00038132		
P78760B-21	0.00808171	0.00048698	0.01901774	0.00055705		
P78760B-22	0.00747192	0.00041735	0.01788508	0.00033606		
P78760B-23	0.00945483	0.00062747	0.02331765	0.00059869		
P78760B-24	0.00771568	0.0005738	0.01833465	0.0007203		
P78760B-25	0.01767292	0.00072984	0.04069473	0.00056344		
P78760B-26	0.00572158	0.00043849	0.01409099	0.00055139		
P78760B-27	0.00516726	0.00043017	0.01296104	0.00051745		
STDGJ-11	0.0020037	0.00143158	0.02635977	0.00334758		
STDGJ-12	0.00188629	0.00142029	0.02423838	0.00368125		

GLITTER!: Age estimates (ma).

Analysis_#	Pb207/Pb206	Pb206/U238	Pb207/U235	Pb208/Th232		
STDGJ-07	571.4	600.3	594.1	733.8		
STDGJ-08	605	610.8	609.4	634		
MT-03	779	736.3	746.7	690.4		
91500-03	1099.7	1052.9	1067.9	969.1		
P78760B-17	0.1	113.8	103.6	108.5		
P78760B-18	221.2	114.4	119.5	111		
STDGJ-09	583.9	612.4	606	660.1		
STDGJ-10	625.6	576.2	586	624.3		
P78760B-19	40.5	87.6	85.9	100.6		
P78760B-20	107.5	112.2	112	113.2		
P78760B-21	336	110.6	121.2	131.7		
P78760B-22	417.5	112.3	127.2	110.9		
P78760B-23	177	116	118.8	133.2		
P78760B-24	191.8	112.1	115.8	121.4		
P78760B-25	0.1	106.9	44	130.4		
P78760B-26	215	116.2	120.9	116.9		
P78760B-27	30.1	118	113.9	125.1		
STDGJ-11	692.2	611	628.7	583.8		
STDGJ-12	515.8	598.1	581.3	646.2		

GLITTER!: Age estimates: 1 sigma uncertainty (ma).

Analysis_#	Pb207/Pb206	Pb206/U238	Pb207/U235	Pb208/Th232		
STDGJ-07	167.63	16.74	34.95	196.16		
STDGJ-08	36.49	7.05	7.94	32.56		
MT-03	41.85	8.89	10.69	23.03		
91500-03	37.82	12.47	12.71	35.75		
P78760B-17	176.82	2.54	13.03	5.08		
P78760B-18	355.56	3.89	19.07	11.56		
STDGJ-09	41.31	7.31	8.83	38.71		
STDGJ-10	44.49	6.96	9.24	40.88		
P78760B-19	647.64	3.97	27.17	9.97		
P78760B-20	246.57	2.42	11.81	7.66		
P78760B-21	312.07	3.09	17.14	11.19		
P78760B-22	277.35	2.64	16.02	6.76		
P78760B-23	392.68	3.97	21.06	12.02		
P78760B-24	324.29	3.64	16.61	14.47		
P78760B-25	0	4.63	39.57	11.32		
P78760B-26	243.14	2.78	12.7	11.08		
P78760B-27	246.28	2.72	11.76	10.39		
STDGJ-11	66.89	8.39	14.41	65.74		
STDGJ-12	70.59	8.34	13.88	72.06		

GLITTER!: Mean Raw CPS background subtracted.

Analysis_#	Pb204	Pb206	Pb207	Pb208	Th232	U238
STDGJ-07	242	7318	434	125	3619	83158
STDGJ-08	119	6419	386	106	3269	72516
MT-03	181	4401	287	1196	34219	41366
91500-03	173	4093	312	422	8659	26311
P78760B-17	60	295	13	155	29208	18883
P78760B-18	108	258	13	64	12221	17717
STDGJ-09	117	7726	460	130	4091	87505
STDGJ-10	120	5689	346	99	3244	67528
P78760B-19	53	113	5	42	8805	9296
P78760B-20	76	273	13	70	12921	17313
P78760B-21	86	243	13	64	10826	16328
P78760B-22	141	227	12	95	18097	14232
P78760B-23	57	229	11	100	15491	13432
P78760B-24	125	325	16	78	15168	23077
P78760B-25	130	87	1	48	8058	5791
P78760B-26	99	371	19	67	12213	21521
P78760B-27	109	383	18	100	18683	24100
STDGJ-11	146	6412	406	101	3407	65000
STDGJ-12	186	6449	376	114	3622	68653

GLITTER! 4.4 revision 525: Laser Ablation Analysis Results						
Z:\Daniel\run4						
Created: Tue Apr 27 16:05:12 2010						
GLITTER!: Isotope ratios.						
Analysis_#	Pb207/Pb206	Pb206/U238	Pb207/U235	Pb208/Th232		
STDGJ-11	0.06257428	0.09839121	0.84943944	0.02901882		
STDGJ-12	0.05794792	0.09683324	0.7739439	0.03191771		
91500-04	0.07524633	0.16605711	1.72258663	0.05396851		
MT-04	0.06203704	0.11869439	1.0151962	0.03823864		
P78760B-28	0.0525667	0.01605452	0.11631785	0.00441978		
P78760B-29	0.06883014	0.01753991	0.16646792	0.00554087		
P78760B-30	0.03695346	0.01799222	0.09167039	0.00570862		
P78760B-31	0.04513014	0.01914275	0.11909498	0.00610621		
P78760A-01	0.04943913	0.01797173	0.12248265	0.0046382		
P78760A-02	0.08652212	0.01907742	0.22753686	0.00721091		
P78760A-03	0.05193809	0.01816276	0.13004407	0.00606133		
P78760A-04	0.04987394	0.01786686	0.12284421	0.00592749		
P78760A-05	0.05113447	0.01831826	0.12913251	0.00570911		
P78760A-06	0.04980325	0.01824475	0.12525715	0.00605862		
STDGJ-13	0.06106057	0.09723151	0.81841165	0.03237005		
STDGJ-14	0.05985129	0.09874328	0.81467807	0.03260041		
GLITTER!: Isotopic ratios: 1 sigma uncertainty.						
Analysis_#	Pb207/Pb206	Pb206/U238	Pb207/U235	Pb208/Th232		
STDGJ-11	0.00163417	0.00126727	0.02125788	0.00254763		
STDGJ-12	0.00154366	0.00127048	0.01990917	0.00269636		
91500-04	0.00158994	0.00215056	0.03596542	0.00232659		
MT-04	0.00174911	0.00175542	0.02832235	0.00194185		
P78760B-28	0.00825162	0.00053033	0.01791327	0.00053299		
P78760B-29	0.0066797	0.00047072	0.01564785	0.00039383		
P78760B-30	0.01024694	0.00069759	0.02520784	0.00054787		
P78760B-31	0.00488342	0.00039292	0.01274517	0.00044427		
P78760A-01	0.0141919	0.00065002	0.03492002	0.00077283		
P78760A-02	0.00595959	0.00040343	0.01522243	0.00040455		
P78760A-03	0.00537548	0.00040349	0.01325292	0.00036005		
P78760A-04	0.00749905	0.00050693	0.0182105	0.00046625		
P78760A-05	0.00659936	0.0004312	0.01647612	0.00038262		
P78760A-06	0.00830419	0.00054718	0.02062053	0.00056566		
STDGJ-13	0.00203234	0.00149727	0.02681508	0.00363359		
STDGJ-14	0.00200329	0.00155109	0.0267876	0.00342199		
GLITTER!: Age estimates (ma).						
Analysis_#	Pb207/Pb206	Pb206/U238	Pb207/U235	Pb208/Th232		
STDGJ-11	693.8	605	624.3	578.2		
STDGJ-12	527.5	595.8	582	635		
91500-04	1075.1	990.4	1017	1062.4		
MT-04	675.4	723	711.5	758.5		
P78760B-28	310.1	102.7	111.7	89.1		
P78760B-29	893.7	112.1	156.3	111.7		
P78760B-30	0.1	115	89.1	115.1		
P78760B-31	0.1	122.2	114.3	123		
P78760A-01	168.7	114.8	117.3	93.5		
P78760A-02	1349.9	121.8	208.2	145.2		
P78760A-03	282.7	116	124.1	122.1		
P78760A-04	189.1	114.2	117.6	119.5		
P78760A-05	246.9	117	123.3	115.1		
P78760A-06	185.8	116.6	119.8	122.1		
STDGJ-13	641.4	598.2	607.2	643.9		
STDGJ-14	598.2	607	605.1	648.4		
GLITTER!: Age estimates: 1 sigma uncertainty (ma).						
Analysis_#	Pb207/Pb206	Pb206/U238	Pb207/U235	Pb208/Th232		
STDGJ-11	54.71	7.44	11.67	50.04		
STDGJ-12	57.68	7.47	11.4	52.81		
91500-04	41.85	11.89	13.41	44.62		
MT-04	59.16	10.12	14.27	37.8		
P78760B-28	322.7	3.36	16.29	10.73		
P78760B-29	188.45	2.98	13.62	7.92		
P78760B-30	58.82	4.42	23.45	11.01		
P78760B-31	195.52	2.49	11.56	8.93		
P78760A-01	560.68	4.12	31.59	15.55		
P78760A-02	127.32	2.55	12.59	8.12		
P78760A-03	220.47	2.55	11.91	7.23		
P78760A-04	316.33	3.21	16.47	9.37		
P78760A-05	272.55	2.73	14.82	7.69		
P78760A-06	347.5	3.46	18.61	11.36		
STDGJ-13	70	8.8	14.97	71.14		
STDGJ-14	70.88	9.1	14.99	66.98		
GLITTER!: Mean Raw CPS background subtracted.						
Analysis_#	Pb204	Pb206	Pb207	Pb208	Th232	U238
STDGJ-11	146	6412	406	101	3407	65000
STDGJ-12	183	6453	376	114	3624	68684
91500-04	144	3773	287	405	8384	25244
MT-04	168	3381	212	889	27312	34313
P78760B-28	150	260	13	49	12596	17866
P78760B-29	96	352	24	136	24425	20707
P78760B-30	98	187	7	73	14637	12617
P78760B-31	119	377	17	72	12682	22208
P78760A-01	92	114	5	21	4945	7251
P78760A-02	133	345	30	154	23093	20852
P78760A-03	118	336	17	145	25260	20735
P78760A-04	52	319	15	160	27638	19267
P78760A-05	121	262	13	95	17515	16282
P78760A-06	92	260	12	78	13809	16396
STDGJ-13	123	7268	443	112	3560	82739
STDGJ-14	176	7166	427	126	3991	84007

Appendix 6 – Hf data

sample no.	$^{176}Hf/^{177}Hf$	1 se	$^{178}Hf/^{177}Hf$	1 se	$^{180}Hf/^{177}Hf$	1 se	total Hf beam	1 se
P78760b-01	0.282815	0.000026	1.46674	0.000048	1.88693	0.00011	1.27663	0.052
P78760b-02	0.282874	0.000025	1.46662	0.000043	1.88699	0.00012	1.46753	0.087
P78760b-03	0.282761	0.000026	1.46669	0.000063	1.88659	0.00011	0.969184	0.052
P78760b-04	0.283007	0.000022	1.46661	0.000035	1.88669	0.00012	1.21803	0.057
P78760b-05	0.282895	0.000025	1.46679	0.000053	1.88673	0.00011	1.17595	0.044
P78760b-06	0.282905	0.000027	1.46674	0.000054	1.88674	0.00015	1.17105	0.053
P78760b-08	0.282981	0.000027	1.46675	0.000033	1.88655	0.000089	1.05214	0.039
P78760b-09 core	0.282937	0.000029	1.46691	0.000042	1.88664	0.00012	0.977552	0.04
P78760b-09 rim	0.282807	0.000026	1.46682	0.00004	1.88674	0.00011	1.29109	0.053
MT-10-316	0.282521	0.000015	1.46693	0.000028	1.88666	0.00006	1.81527	0.09
P78760b-10 rim	0.283016	0.000028	1.46684	0.000036	1.88672	0.0001	1.10808	0.046
P78760b-10 core	0.282798	0.000021	1.46687	0.000053	1.88673	0.000096	1.05075	0.041
P78760b-11 rim	0.282984	0.000026	1.46674	0.00005	1.88663	0.00011	1.09194	0.041
P78760b-11 core	0.28284	0.000024	1.46684	0.00005	1.8868	0.00011	1.25159	0.061
P78760b-12	0.282862	0.000022	1.4669	0.000046	1.88641	0.00013	1.21285	0.072
MT-10-317	0.281458	0.000026	1.45746	0.000051	1.87852	0.00012	1.98415	0.06
MT-10-318	0.281685	0.000019	1.45724	0.000082	1.87727	0.000071	1.68597	0.08
P78760b-16 rim	0.282983	0.000028	1.46724	0.00005	1.88637	0.00013	0.996723	0.064
P78760b-16 core	0.28286	0.000025	1.46736	0.000049	1.88664	0.0001	1.0174	0.045
MT-10-319	0.282531	0.000028	1.46722	0.000037	1.88651	0.00011	1.46563	0.074
P78760a-01	0.282903	0.000019	1.46733	0.00003	1.88684	0.000078	1.51097	0.086
P78760a-02	0.282996	0.000024	1.46712	0.000034	1.88636	0.00012	1.03946	0.06
P78760a-03	0.282908	0.000028	1.46703	0.000036	1.88612	0.000081	0.835079	0.045
P78760a-04	0.282859	0.000027	1.46725	0.000041	1.8868	0.00011	1.03289	0.052
P78760a-05	0.282928	0.000016	1.46725	0.000034	1.88658	0.000081	1.80281	0.11
MT-10-320	0.282561	0.000015	1.46719	0.00003	1.88638	0.00008	1.80797	0.094

sample no.	exp. factor	1 se	$^{176}Lu/^{177}Hf$	1 se	$^{176}Yb/^{177}Hf$	1 se	$^{176}Hf/^{177}Hf$	1 se
P78760b-01	1.38423	0.005	6.5613E-05	0.0000098	0.00311526	0.00038	0.285981	0.0004
P78760b-02	1.34897	0.0039	0.00024631	0.0000015	0.0108814	0.000016	0.294007	0.000035
P78760b-03	1.35305	0.0051	0.00017144	0.0000038	0.00776531	0.00012	0.290636	0.00012
P78760b-04	1.32901	0.0039	0.00010743	0.0000006	0.0050546	0.000019	0.288201	0.000029
P78760b-05	1.34278	0.0053	0.00015273	0.0000011	0.00730281	0.000029	0.290396	0.00004
P78760b-06	1.32557	0.0049	0.00015879	0.0000034	0.00751447	0.000087	0.290509	0.000095
P78760b-08	1.36051	0.0052	2.8324E-05	0.00000058	0.00178735	0.000027	0.284813	0.000021
P78760b-09 core	1.3482	0.0049	0.0003395	0.0000027	0.0178413	0.00017	0.301101	0.00018
P78760b-09 rim	1.33295	0.003	0.00019684	0.0000027	0.0101306	0.0002	0.293117	0.00021
MT-10-316	1.34016	0.0044	5.5548E-05	0.00000042	0.00317548	0.000026	0.285768	0.000025
P78760b-10 rim	1.3458	0.0052	8.8177E-05	0.000003	0.00438129	0.000088	0.28748	0.00011
P78760b-10 core	1.33426	0.0043	0.00012957	0.00000079	0.00609777	0.000043	0.289039	0.000062
P78760b-11 rim	1.3328	0.0039	4.2332E-05	0.0000014	0.00218169	0.000042	0.285243	0.000041
P78760b-11 core	1.30817	0.0036	0.00020485	0.0000058	0.00967161	0.00019	0.292701	0.00021
P78760b-12	1.34702	0.006	0.00025057	0.000008	0.0112093	0.00029	0.294347	0.0003
MT-10-317	1.38855	0.0052	8.5352E-05	0.0000006	0.00510706	0.000031	0.286657	0.000037
MT-10-318	1.45297	0.0041	0.00012778	0.00000029	0.00738058	0.000066	0.289213	0.000065
P78760b-16 rim	1.40181	0.0065	3.5331E-05	0.0000011	0.00174011	0.00003	0.284781	0.000034
P78760b-16 core	1.33878	0.0056	0.00015617	0.0000044	0.00755379	0.00013	0.290551	0.00013
MT-10-319	1.36726	0.0035	0.00011207	0.00000045	0.00636254	0.000048	0.28902	0.000054
P78760a-01	1.45293	0.0031	3.9454E-05	0.0000011	0.00179819	0.000023	0.284736	0.000036
P78760a-02	1.43052	0.0047	0.0002448	0.0000025	0.0115982	0.00025	0.294838	0.00025
P78760a-03	1.43301	0.0034	0.00066543	0.0000047	0.0341247	0.00022	0.317678	0.00021
P78760a-04	1.38656	0.0035	8.5178E-05	0.0000017	0.00420259	0.000022	0.287175	0.00003
P78760a-05	1.4097	0.0025	0.00047472	0.0000018	0.0207264	0.00011	0.304117	0.00011
MT-10-320	1.39564	0.0057	0.00011869	0.00000043	0.00676623	0.000063	0.289446	0.000065

Appendix 7 – Zircon composition

hide column L after editing

Modelled rock type from zircon composition (Belousova et al. 2002, Fig. 8)

	Zircon electron microprobe data							Other data (*=MC-LAM-ICPMS; **=LAM-ICPMS; ***=electron microprobe)								
Analysis No.	ZrO_2	SiO_2	HfO_2	Y_2O_3	U_2O_3	ThO_2	Total	Hf***	Y***	Analysis No.	Th**	U**	Th/U**	Lu*	Yb*	modelled rock type
	(wt%)	(wt%)	(wt%)	(wt%)	(wt%)	(wt%)	(wt%)	(wt%)	(ppm)		(ppm)	(ppm)		(ppm)	(ppm)	
P78760a-1	67.5587	32.6495	1.07	0.0342			101.31	0.87		P78760a-01	20	115	0.92	2	23	Kimberlite
P78760a-2	66.8487	32.5228	1.1992	0.0389			100.61	1.01	135	P78760a-02	95	122	1.49	18	171	Carbonatite
P78760a-3	67.1327	32.4721	1.0555	0.1127			100.77	1.00	157	P78760a-03	104	116	1.64	48	498	Dolerite
P78760a-4	67.3669	32.491	1.0674	0.0302			100.96	0.88		P78760a-04	114	114	1.93	5	54	Carbonatite
P78760a-5	67.138	32.7258	1.0636	0.0569			100.98	0.96	112	P78760a-05	20	22	1	33	291	Dolerite
P78760a-6	67.1351	32.623	1.1101	0.0532			100.92	0.98	394		95	64	1			
P78760b-1	68.1963	32.7437	1.0301				101.97	0.94		P78760b-01	104	63	2	4	43	Carbonatite
P78760b-2	67.7072	32.7374	1.1861	0.0172			101.65	0.93	34	P78760b-02	114	59	2	16	148	Carbonatite
P78760b-3	67.3059	32.6273	1.1739	0.0199			101.13	0.94	662	P78760b-03	72	50	1	12	107	Carbonatite
P78760b-4	68.1682	32.7608	1.0357				101.96	0.92		P78760b-04	57	50	1	7	68	Carbonatite
P78760b-5	67.9459	32.5235	1.1307	0.0142			101.61	0.95	191	P78760b-05	48	41	1	10	101	Carbonatite
P78760b-6	67.1209	32.6881	1.1557	0.05			101.01	0.89	405	P78760b-06	81	54	2	10	98	Carbonatite
P78760b-7	67.4984	32.606	1.104				101.21	0.93	246		64	66	1			
P78760b-8	67.6759	32.7662	1.0942	0.0043			101.54	0.90		P78760b-08	106	60	2	2	24	Kimberlite
P78760b-09 C	67.597	32.6104	1.1131	0.084			101.40	0.96		P78760b-09 C	93	75	1	23	251	Dolerite
P78760b-09 R	67.597	32.6104	1.1131	0.084			101.40	0.96		P78760b-09 R	59	60	1	14	142	Carbonatite
P78760b-10 R	67.0812	32.6584	1.0895				100.83	0.99		P78760b-10 R	45	55	1	6	63	Carbonatite
P78760b-10 C	67.0812	32.6584	1.0895				100.83	0.99		P78760b-10 C	9	9	1	9	88	Carbonatite
P78760b-11 R	67.2855	32.5248	1.1179	0.0243			100.95	0.96	303	P78760b-11 R	79	63	1	3	31	Carbonatite
P78760b-11 C	67.2855	32.5248	1.1179	0.0243			100.95	0.96	303	P78760b-11 C	51	46	1	14	137	Carbonatite
P78760b-12	67.7903	32.5847	1.0488	0.0514			101.48	0.89	382	P78760b-12	11	15	1	16	146	Carbonatite
P78760b-13	67.7816	32.6705	1.0962	0.0313			101.58	1.05			116	71	2			
P78760b-14	67.397	32.5728	1.0668				101.04	0.88	494		12	12	1			
P78760b-15	67.1178	32.5849	1.1308				100.83	0.98	528		68	56	1			
P78760b-16 R	67.5211	32.6148	1.1655				101.30	0.88	157	P78760b-16 R	24	22	1	2	22	Kimberlite
P78760b-16 C	67.5211	32.6148	1.1655				101.30	0.88	157	P78760b-16 C	131	73	2	10	97	Carbonatite
P78760b-17	67.3769	32.5798	1.1378	0.0385			101.13	0.86	257		60	39	2			
P78760b-18	68.0472	32.6194	1.0511	0.0485			101.77	1.06	68		22	20	1			
P78760b-19	67.8039	32.6874	1.2389				101.73	0.94	259		23	24	1			
P78760b-20	68.3606	32.5025	1.0349	0.0627			101.96	1.00			59	59	1			
P78760b-21	66.7788	32.4574	1.151	0.067			100.45	0.98	383		124	59	2			
P78760b-22	68.1655	32.5259	1.0328	0.0199			101.74	0.91	258		52	55	1			
P78760b-23	67.8069	32.3196	1.0104	0.0326			101.17	0.89	372		37	29	1			
P78760b-24	67.2895	32.6345	1.2514	0.0086			101.18	0.93	213		55	54	1			
P78760b-25	67.0224	32.6404	1.1141	0.0329			100.81	0.87	405		46	51	1			
P78760b-26	67.5044	32.3055	1.1798				100.99	0.91	269		77	44	2			
P78760b-27	67.3657	32.6692	1.1514	0.0486			101.23	1.02	306		66	42	2			
P78760b-28	68.0191	32.535	1.0761	0.0327			101.66	0.90	888		64	72	1			
P78760b-29	66.779	32.6797	1.0452	0.0472			100.55	0.91	238		34	18	2			
P78760b-30	67.4269	32.509	1.0991	0.0271			101.06	0.90	448		52	67	1			
P78760b-31	67.3202	32.7121	1.0214	0.0514			101.11	0.94	419		79	75	1			

Appendix 8 – CIPW norms of Snake River basalt and BOG

Calculated mineral volume %

Breaksea Orthogneiss

Sample	MDP0611A	MDP0709A	MDP0613	B471-81-428	BS716B	MDP0737B	MDP0669	MDP0705H	0901A	0902A	0901C	907
Plagioclase	64.46	68.89	69.80	66.77	71.40	68.68	66.58	67.41	68.80	70.41	51.78	69.39
Orthoclase	4.79	10.58	6.68	6.79	7.29	9.27	11.28	6.76	9.29	7.59	8.99	7.41
Nepheline	0.91	0.00	0.00	0.00	0.00	0.00	0.00	0.00	0.00	0.00	0.00	0.00
Diopside	10.75	6.30	7.06	6.14	7.77	9.30	7.89	8.08	7.11	7.82	16.60	5.95
Hypersthene	0.00	2.57	5.78	3.86	1.74	1.59	3.95	1.61	2.80	0.77	1.16	8.24
Olivine	16.56	9.34	8.12	13.51	9.50	8.95	8.10	13.53	9.50	10.67	17.78	6.85
Ilmenite	1.66	1.49	1.50	1.66	1.26	1.38	1.38	1.77	1.59	1.61	2.35	1.38
Apatite	0.86	0.83	1.05	1.28	1.04	0.83	0.83	0.85	0.92	1.13	1.34	0.78
Total	99.99	100.00	99.99	100.01	100.00	100.00	100.01	100.01	100.01	100.00	100.00	100.00

Snake River basalt

Sample	96SRP-38-2	SRP 119	SRP 122	SRP 120	ML-3	DMI-18	DMK-2	DMK-4
Plagioclase	55.13	55.93	53.20	53.06	57.53	53.38	56.81	57.89
Orthoclase	8.95	9.10	7.68	8.51	7.92	11.88	9.45	13.29
Nepheline	1.11	0.00	1.23	1.49	0.72	2.34	0.87	1.13
Diopside	13.23	13.46	14.67	16.89	12.58	13.57	12.17	12.14
Hypersthene	0.00	3.83	0.00	0.00	0.00	0.00	0.00	0.00
Olivine	17.72	13.40	18.51	16.05	17.09	15.49	17.02	10.78
Ilmenite	2.63	2.74	3.20	2.63	2.96	2.31	2.49	2.98
Apatite	1.22	1.53	1.50	1.36	1.20	1.03	1.19	1.79
Total	99.99	99.99	99.99	99.99	100.00	100.00	100.00	100.00

Appendix 9 – List of abbreviations

Rock units

BOG	Break Sea Orthogneiss
WFO	Western Fjordland Orthogneiss

Minerals

alm	alamandine
bt	biotite
cpx	clinopyroxene
fs	feldspar
grs	grosular
grt	garnet
hbl	hornblende
omp	omphacite
plg	plagioclase
prg	pargasite
pyp	pyrope
qtz	quartz
rt	rutile
sps	spessartine

List of Figures and Tables

Figures

Fig. 1: Zealandia, restored position in Gondwana and Gravity anomaly map. 8
Fig. 2: Tectonic map of South Island New Zealand. 10
Fig. 3: Geologic map of the Western Fiordland Orthogneiss. 11
Fig. 4: P-T path of the Breaksea Orthogneiss. 12
Fig. 5: Typical outcrop of omphacite granulite and an ultramafic pod. 13
Fig. 6: Field aspect of layered xenolith. 16
Fig. 7: Garnet in different structural settings in outcrop. 18
Fig. 8: Field aspects of different modes of feldspar, pyroxene and garnet. 19
Fig. 9: Field aspect of ultramafic eclogite layers within omp-granulite. 20
Fig. 10: Thin section: Garnet corona around the omphacite. 21
Fig. 11: Thin section: single garnet grain along a feldspatic vein. 22
Fig. 12: Thin section: Garnet and omphacite in equi-granular cluster. 23
Fig. 13: Thin section: Two different types of clinopyroxene inclusions in garnet. 24
Fig. 14: Layered garnetite-pyroxenite (outcrop of samples BS1010A-F). 26
Fig. 15: The boulder of samples BS1010A-1010F, hand samples and thin sections. 27
Fig. 16: Thin section: Ovoid inclusions of cpx in grt close to a layer boundary. 29
Fig. 17: Thin section: Ovoid inclusions of cpx in grt close to a layer boundary. 30
Fig. 18: Thin section: euhedral grt inclusion in cpx within the pyroxenite layer. 31
Fig. 19: Thin section: garnet grt veins or films in the pyroxenite layer. 32
Fig. 20: Thin section: contact of garnetite and pyroxenite with symplectites. 33
Fig 21: TAS diagram of BOG. 34
Fig. 22: Ternaries of cpx, grt and fs in different rock types. 35
Fig. 24: Mg# vs Ca-Cations in clinopyroxene and garnet of different rock types. 36
Fig. 25: Ternary of garnet in different textural settings in the omp-granulite. 37
Fig. 26: Mg# vs Ca Cations of grt in omp-granulite, garnetite and pyroxenite. 38

Fig. 27: Traverse of a garnet grain in an equi-granular garnet-clinopyroxene cluster. 38
Fig. 28: Ternaries of cpx in different layers and textural settings in layered xenolith. 39
Fig. 29: Mg# vs Ca Cations of pyroxene in layered garnetite-pyroxenite. 39
Fig. 30: Mg# vs Ca Cations of grt in different textural settings in layered xenolith. 40
Fig. 31: Traverse over the boundary from the pyroxenite-layer to a garnetite layer. 41
Fig. 32: REE-pattern of grt in different rock types and aspect of thick sections. 42
Fig. 33: La/Yb versus Dy/Yb of garnet in different rock types. 43
Fig. 34: Chondrite normalized REE-pattern of cpx in different rock types. 44
Fig. 35: Chondrite normalized REE-pattern of plg in omp-granulite. 45
Fig. 36: Recalculated melts from partition coefficients. 46
Fig. 37: Concordia age on an inverse Concordia and distribution of measured data. 48
Fig. 38: Pb-206/U-238age vs 176-Hf/177-Hf initial of zircon. 49
Fig. 39: Densities of different rock types. 51
Fig. 40: P-T phase diagram for the melting of Snake River and comparison with BOG. 55
Fig. 41: Comparison of Breaksea layered garnetite-pyroxenite with other locations. 56
Fig. 42: Model for the formation of low- and high-MgO pyroxenites in a subduction. 57
Fig. 43: Model for the metamorphic origin of equi-granular grt-cpx clusters. 64
Fig. 44: Double diffusion model for the formation of layers in mafic layered intrusions. 65

Tables

Tab: 1: Compositions and mineral chemistry data of different lithologies of BOG 14
Tab. 2: Overview of evidence for igneous, cumulate or metamorphic character. 67

Statement of Originality

All the work submitted in this thesis is the original work of the author except where otherwise acknowledged. No part of this thesis has been previously submitted to any other university institution

Daniel Miescher Date